Review

From Fenton and ORR 2e−-Type Catalysts to Bifunctional Electrodes for Environmental Remediation Using the Electro-Fenton Process

Edgar Fajardo-Puerto, Abdelhakim Elmouwahidi [ID], Esther Bailón-García *, Agustín Francisco Pérez-Cadenas [ID] and Francisco Carrasco-Marín [ID]

Materiales Polifuncionales Basados en Carbono (UGR-Carbon), Departamento de Química Inorgánica, Universidad de Granada, 18071 Granada, Spain
* Correspondence: estherbg@ugr.es

Abstract: Currently, the presence of emerging contaminants in water sources has raised concerns worldwide due to low rates of mineralization, and in some cases, zero levels of degradation through conventional treatment methods. For these reasons, researchers in the field are focused on the use of advanced oxidation processes (AOPs) as a powerful tool for the degradation of persistent pollutants. These AOPs are based mainly on the in-situ production of hydroxyl radicals ($OH^{\bullet}$) generated from an oxidizing agent (H_2O_2 or O_2) in the presence of a catalyst. Among the most studied AOPs, the Fenton reaction stands out due to its operational simplicity and good levels of degradation for a wide range of emerging contaminants. However, it has some limitations such as the storage and handling of H_2O_2. Therefore, the use of the electro-Fenton (EF) process has been proposed in which H_2O_2 is generated in situ by the action of the oxygen reduction reaction (ORR). However, it is important to mention that the ORR is given by two routes, by two or four electrons, which results in the products of H_2O_2 and H_2O, respectively. For this reason, current efforts seek to increase the selectivity of ORR catalysts toward the 2e− route and thus improve the performance of the EF process. This work reviews catalysts for the Fenton reaction, ORR 2e− catalysts, and presents a short review of some proposed catalysts with bifunctional activity for ORR 2e− and Fenton processes. Finally, the most important factors for electro-Fenton dual catalysts to obtain high catalytic activity in both Fenton and ORR 2e− processes are summarized.

Keywords: Fenton; electro-Fenton; ORR; bifunctional catalysts

1. Environmental Problems

One of the largest problems facing society today is water pollution, so special interest has been aroused in knowing the main pollutants that affect it and their subsequent treatment. Currently, some pollutants considered conventional (metals, fats and oils, nitrates, etc.) are controlled and monitored; however, more and more attention has been paid in recent years to those termed today as emerging [1–3]. Emerging contaminants can be defined as substances and/or chemical compounds that are not normally monitored but nevertheless remain continuous and remain present in water bodies despite being treated by conventional wastewater treatment plants [4–7].

Pharmaceuticals, along with their metabolites and degradation products, are considered emerging contaminants [8]. Their continuous discharge, together with their toxic and harmful levels, makes them highly dangerous for human and aquatic organisms [9,10]; therefore, it explains the importance of exercising controls and monitoring the concentrations of these pollutants both in the ecosystem and in effluents [11,12]. Currently, the global pharmaceutical market exceeds one trillion US dollars [13], which demonstrates the strong growth of this industry and its impact on the environment.

Among pharmaceutical products, antibiotics are of special interest because they are made to affect microorganisms, so they are prone to affect microbial communities in aquatic systems, causing a possible disappearance of them, which may have key functions in the ecosystem [14]. An antibiotic is defined as a chemotherapeutic agent capable of stopping the growth of microorganisms through cell destruction [15]. Antibiotic use has grown steadily globally, mostly in low- and middle-income countries [16]. It has been found that the presence of antibiotics in the environment favors the proliferation of microorganisms resistant to this type of drug [17].

Aquatic environments have been considered large deposits of antibiotics since this type of contaminant can arrive through two main ways, wastewater discharge and agricultural activity [18]. An example of this was a study conducted in 165 rivers in 72 countries, where researchers detected the presence of antibiotics in more than 60% of the 711 sampling sites [19]. In addition to these bodies of water, groundwater has also been susceptible to contamination with antibiotics mainly through the leaching of soils fertilized with manure from livestock, since it contains high concentrations of veterinary drugs [20].

Currently, wastewater treatment processes are composed of three phases in a general way:

1. Primary treatment by physicochemical operations;
2. Secondary treatment by biological processes;
3. Tertiary treatment by additional processes.

However, these treatment technologies only achieve moderate to significant elimination of some antibiotics [21]. For this reason, other types of treatments have been explored to achieve almost total elimination of the antibiotics present in water. Currently, in this study, advanced oxidation processes (AOPs) are explored [22–24], such as Fenton, electro-Fenton, ozonation, photocatalysis, and electrocoagulation, among others [25–29], which are based on the in situ production of hydroxyl radicals (OH$^{\bullet}$) generated from an oxidizing agent (H_2O_2, O_2) in the presence of a catalyst. OH$^{\bullet}$ has strong oxidizing power and thus, a high capacity to degrade organic compounds to simpler and less toxic biodegradable substances, and in some cases, even reaching complete mineralization [30].

2. Fenton Reaction

The first report on the Fenton reaction dates from 1876, where a mixture of H_2O_2 and Fe^{2+} salt (Fenton reagent) was used to achieve the oxidation of tartaric acid [31]; from there, various investigations have been carried out to apply this reaction in multiple applications. It is currently mainly used in environmental remediation [32–36].

The Fenton reaction can be considered an AOP, where it is based on a mixture of ferrous ion (Fe^{2+}) (usually in a liquid state) with hydrogen peroxide (H_2O_2) [37], which, under the right reaction conditions, results in the formation of hydroxyl radicals [38] with high oxidative potential capable of degrading a wide range of contaminants (Figure 1) [39].
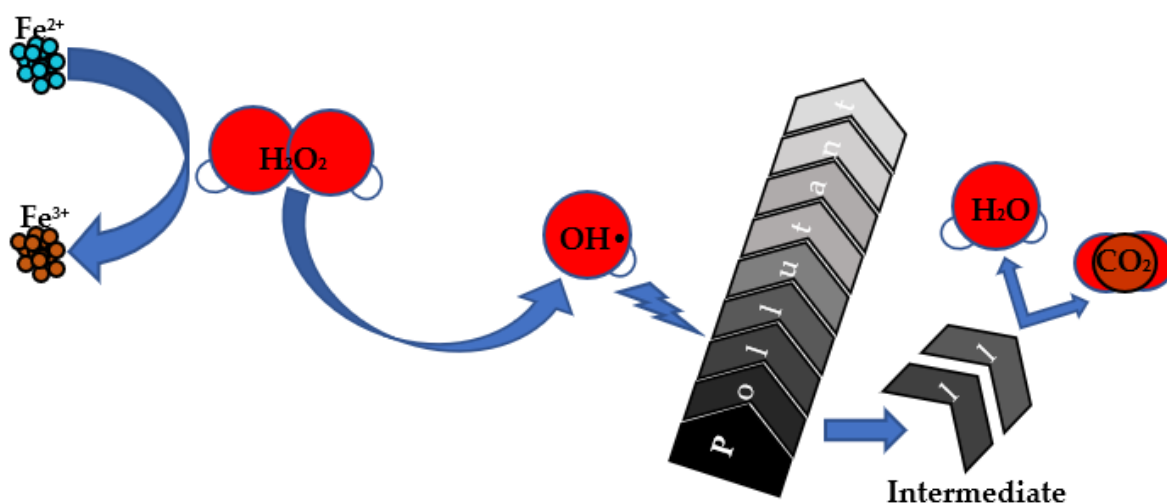
$$Fe^{2+} + H_2O_2 \rightarrow Fe^{3+} + OH^- + OH^{\bullet} \tag{1}$$

$$Fe^{3+} + H_2O_2 \rightarrow Fe^{2+} + H^+ + HO_2^{\bullet} \tag{2}$$
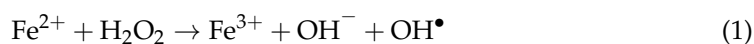
Figure 1. Scheme of the Fenton process. In general, the multiple reactions involved can be summarized by Equations (1) and (2) [40,41].

The Fenton reactions are based on the oxidation of Fe^{2+} to Fe^{3+}, which simultaneously generates the hydroxyl radical (Equation (1)), followed by the reduction of Fe^{3+} to Fe^{2+} (Equation (2)), which allows the regeneration of the catalyst. However, the reaction in which $OH^{\bullet}$ is produced is much faster than that of catalyst regeneration [42], leading to the accumulation of Fe^{3+} and therefore decreasing catalytic efficiency.

Among its main advantages are its operational simplicity, zero toxicity, mild reaction conditions (ambient temperature and atmospheric pressures), and high degradation efficiency [43–46]. However, there are still some important limitations to overcome such as the slow reduction rate of Fe^{3+} to Fe^{2+} resulting in high levels of sludge generation with iron content, the deactivation of the catalyst, and a narrow pH working range [47–51].

The pH level is one of the most important parameters because it limits degradation efficiency. At pH values below 3, H_2O_2 goes on to form oxonium ions ($H_3O_2^{+}$), which have less oxidative power than $OH^{\bullet}$, while as the pH rises above 3, colloidal ferric species such as ferric hydroxide are formed from dissolved iron, which produces high amounts of sludge [52].

Recently, numerous investigations have been carried out (see Table 1) focused on the optimization of Fenton conditions. Variables such as catalyst pollutant and H_2O_2 concentration have been evaluated, as well as the pH of the solution, to determine under what conditions the highest percentage of pollutant molecule degradation is reached.

Typically, the pH is a crucial factor in the Fenton process, hardly affecting catalyst stability and pollutant degradation. From this, numerous investigations have been carried out with different pH values found at important degradation levels of pollutants such as antibiotics, colorants, and industrial wastewater. It is known that the pH optimal value for the Fenton reaction is closer to 3 due to the stability of H_2O_2, $OH^{\bullet}$, and Fe^{3+}. In this sense, Rao et al. [53] treated complex recalcitrant wastewater using $FeSO_4 \cdot 7H_2O$ as a catalyst (typical Fenton catalyst) in a concentration of 50 mg L^{-1} and a pH value of 3 obtaining a degradation of 72% of DQO. On the other hand, Zhao et al. [54] removed a polymer quaternary ammonium salt using the same catalyst but using a pH of 2 and a Fenton catalyst concentration slightly lower (40 mg L^{-1}), achieving a percentage of elimination closer to 70%. Liu et al. [55] degraded a reference colorant for degradation tests, methylene blue, and analyzed the activation of the Fenton reaction under visible light irradiation using MoS_2-Fe (150 mg L^{-1}) as the Fenton catalyst at a pH value of 3, reaching a degradation of 65%. In turn, Qin et al. [56] achieved a 99.1% degradation level for a widely used antibiotic, amoxicillin, using 1 g L^{-1} of a core-shell structured $MnFe_2O_4$@C-NH_2 at a pH of 3 (Figure 2).

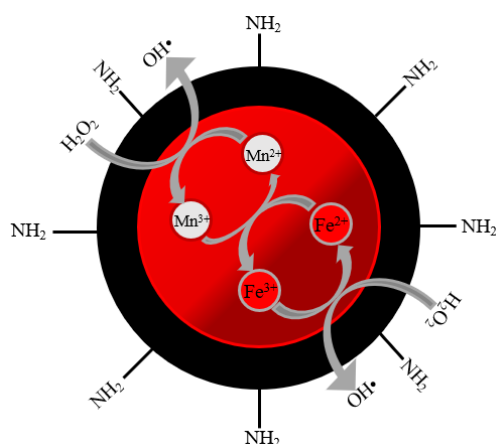**Figure 2.** Schematic of the OH$^\bullet$ generation by $MnFe_2O_4$@C-NH_2. Adapted from [56].

Other antibiotics tested at pH 3 have been sulfamerazine (40 mg L^{-1}), sulfathiazole (0.5 mg L^{-1}), azithromycin (0.1 mg L^{-1}), norfloxacin (50 mg L^{-1}), and sulfamethoxazole (0.01 mg L^{-1}), with removal percentages >65%, using as Fenton catalysts, CNTs-Fe_3O_4 (0.5 mg L^{-1}), dissolved iron from zero-valent iron nanoparticles (9 mg L^{-1}), $MnFe_3O_4$-HS (1000 mg L^{-1}), Fe_3O_4/Schwertmannita/carbon (50 mg L^{-1}) (Figure 3) and fresh powder from Fe^0, respectively [57–61]. On the other hand, Hommem et al. [62] studied a range of pHs from 3.5 to 4.5, for the degradation of amoxicillin (0.45 mg L^{-1}) using $FeSO_4 \cdot 7H_2O$ (0.095 mg L^{-1}) as catalysts, obtaining 100% degradation in all cases.

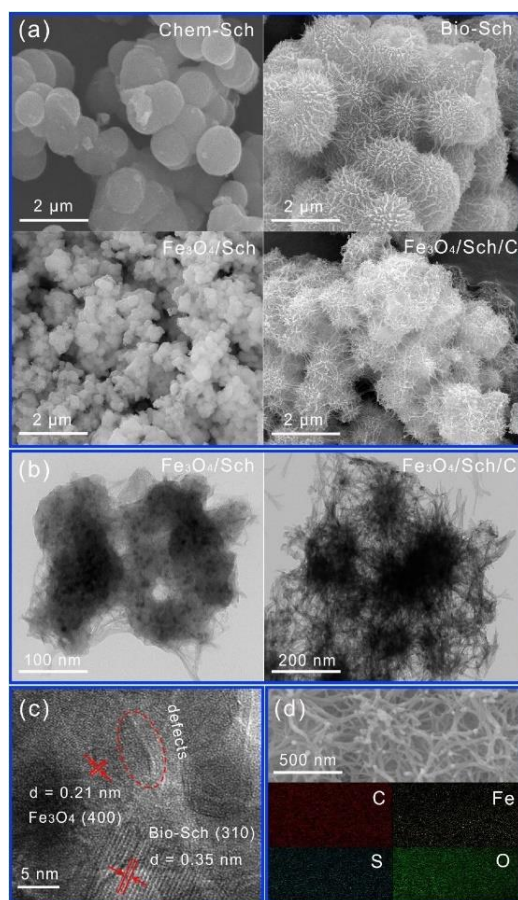**Figure 3.** (**a**) SEM images of Chem-Sch, Bio-Sch, Fe_3O_4/Sch, Fe_3O_4/Sch/C, (**b**) TEM of Fe_3O_4/Sch and Fe_3O_4/Sch/C, (**c**) HRTEM of Fe_3O_4/Sch/C, and (**d**) elemental mapping of different elements C, Fe, S, and O recorded from Fe_3O_4/Sch/C [60].

Other authors tried to increase the operating pH to facilitate the use of the Fenton process in a real application. Cheng et al. achieved a tetracycline hydrochloride degradation of 91.3% at a pH value of 4 using magnetic pullulan hydrogel as a Fenton catalyst (1250 mg L^{-1}) [63]. Similarly, Wang et al. [64] obtained a good tetracycline degradation (83%) at a pH value of 4.3 using iron loaded in graphitic carbon derived from microplastics. The highest pH values (5 to 5.5) tested also obtained good results: 100% degradation of carbamazepine and norfloxacin and 86.9% for ciprofloxacin using $LaCu_{0.5}Mn_{0.5}O_3$, $FeSO_4 \cdot 7H_2O$ with hydroxylamine (10 μM of Fe^{2+}), and δ-Fe_3OOH/MWCNTs as Fenton catalysts, respectively [65–67]. However, neutralization of the final effluent is still required, so the search for catalysts and conditions that allow the development of this process at a neutral pH value is preferred. In this way, several researchers have studied the degradation of different pollutants such as amoxicillin, sulfadiazine, tetracycline, sulfadiazine, and rifampicin metronidazole, among others, working at pHs of 6 to 7.5, and obtaining degradation higher that 90% using goethite, $Fe_2(SO_4)_3 \cdot H_2O$, single-atom iron fixed in porous carbon, copper-modified MgFe-CO_3 double-layered hydroxide, rGO@nFe/Pd, magnetic biocarbon, $CoFe_2O_4$-S, and $LaCu_{0.8}Mn_{0.2}O_3$ [68–75] as Fenton catalysts. Guo et al. [76] also achieved the total degradation of ofloxacin at the widest pH using GO–Fe_3O_4 in a discharge plasma system. Wang et al. [77] also obtained the total degradation of ofloxacin using Fe_3O_4@S-doped ZnO at a pH of 5.2 to 9.0. For their part, Sun et al. [78] worked in a wide range of pH values from 3 to 9, degrading 99% of sodium sulfadiazine with $FeCO_3$ [6000 mg L^{-1}].

Table 1. Operating conditions for some Fenton processes.

Catalyst	Catalyst Concentration	H_2O_2 Concentration	Pollutant	Pollutant Concentration	Solution pH	Percentage of Elimination	Ref.
$LaCu_{0.5}Mn_{0.5}O_3$	0.6 g L^{-1}	0.7 g L^{-1}	Carbamazepine (CZP)	15 mg L^{-1}	5.5	100%	[65]
ZnO dopped Fe_3O_4@S	0.25 g L^{-1}	5 mL L^{-1}	Ofloxacin (OFX)	10 mg L^{-1}	5.2–9.0	100%	[77]
$FeSO_4 \cdot 7H_2O$	50 mg L^{-1}	26.4 mM	Industrial wastewater (DQO)	850 mg L^{-1} (DQO)	3	72%	[53]
$FeSO_4 \cdot 7H_2O$	40 mg L^{-1}	23 mL L^{-1}	Hydroxyethylpoly-dialyldimethylammonium-acrylamide-acrylic-acrylate (PDM)	200 mg L^{-1}	2	69.3%	[54]
Siderite ($FeCO_3$)	6 g L^{-1}	100 mMol L^{-1}	sodium sulfadiazine	50 mg L^{-1}	9	99%	[78]
Goethite	-	460 mg L^{-1}	Amoxicillin	105 mg L^{-1}	6.5–7	83%	[68]
$MnFe_2O_4$@C-NH_2	1 g L^{-1}	3 mL L^{-1}	Amoxicillin	30 mg L^{-1}	3.0	99.1%	[56]
$Fe_2(SO_4)_3 \cdot xH_2O$	30 mg L^{-1}	-	Tetracycline	50 mg L^{-1}	6.0	90%	[69]
$Fe_2(SO_4) \cdot 7H_2O$	0.095 mg L^{-1}	2.35 mg L^{-1}	Amoxicillin	0.45 mg L^{-1}	3.5–4.5	100%	[62]
rGO–Fe_3O_4	0.23 g L^{-1}	-	Ofloxacin	20 mg L^{-1}	7.0–4.0	99.9%	[76]
MoS_2-Fe	150 mg L^{-1}	10 mMol L^{-1}	Methylene blue	25 mg L^{-1}	3	65%	[55]
CNTs–Fe_3O_4	0.5 g L^{-1}	24.5 mM	Sulfamerazine	40 mg L^{-1}	3	70%	[57]
Dissolved iron from zero valence iron nanoparticles (nZVI)	9 mg L^{-1}	34 mg L^{-1}	Sulfathiazole	0.5 mg L^{-1}	3	>96%	[58]
$Fe_2(SO_4) \cdot 7H_2O$ with hydroxylamine	10 μM de Fe^{2+}	1.0 mM	Norfloxacin	10 mg L^{-1}	5	100%	[66]
CuS@Fe_3O_4/Pt	-	-	Tetracycline	40 mg L^{-1}	-	78%	[79]
Single-atom iron fixed in porous carbon (Fe-ISA@CN)	100 mg L^{-1}	10 mM	Sulfadiazine	2 mg L^{-1}	6.5	96%	[70]
LDH–CuMgFe–CO_3	0.5 g L^{-1}	4 mMol L^{-1}	Sulfathiazole	0.15 mg L^{-1}	7.5	100%	[71]
rGO@nFe/Pd	200 mg L^{-1}	167 mMol	Rifampicin	50 mg L^{-1}	6.14	94.6%	[72]
$MnFe_2O_4$–HS	1 g L^{-1}	29.4 mM	Azithromycin	0.1 mg L^{-1}	3.0	92.6%	[59]
MagFePC (Hybrid)	250 mg L^{-1}	5 mL L^{-1}	Tetracycline	-	6.0	100%	[80]
Magnetic pullulan hydrogels	1.25 g L^{-1}	1.25 mL L^{-1}	Tetracycline hydrochloride	20 mg L^{-1}	4.0	91.3%	[63]

Table 1. *Cont.*

Catalyst	Catalyst Concentration	H_2O_2 Concentration	Pollutant	Pollutant Concentration	Solution pH	Percentage of Elimination	Ref.
Magnetic biocarbon	0.2 g L^{-1}	50 mM	Metronidazole	20 mg L^{-1}	6.0	97.4%	[73]
$CoFe_2O_4$–S	500 mg L^{-1}	5 mMol L^{-1}	Tetracycline	0.1 M	7.0	90%	[74]
COF (Photo-Fenton)	167 mg L^{-1}	50 mL L^{-1}	Rhodamine B	150 mg L^{-1}	4.4	41.2%	[81]
Fe_3O_4/Schwettmann/ Carbon	50 mg	45 μL	Norfloxacin	50 mg L^{-1}	3.0	100%	[60]
δ-Fe_3OOH/MWCNTs	235 mg L^{-1}	20.6 mMol	Ciprofloxacin	10 mg L^{-1}	5.3	86.9%	[67]
Fe^{2+}	5.0 mMol L^{-1} de Fe^{2+}	10 mmol L^{-1}	Antibiotic resistance gene (ARG)	$11.53 \text{ Log}_{10}\text{(copies) g}^{-1}$ dry sludge	3	66.86%	[82]
Fe–MPC	0.02 g L^{-1}	1.0 mM	Tetracycline	40 mg L^{-1}	4.3	83%	[64]
Fresh powder from Fe^0	-	-	Sulfamethoxazole	10 μg L^{-1}	3	100%	[61]
$LaCu_{0.8}Mn_{0.2}O_3$	0.2 g L^{-1}	$13.8 \times 10^{-3} \text{ mol L}^{-1}$	Paracetamol	50 mg L^{-1}	6.7	90%	[75]

Apart from the commonly mentioned conditions, relevance has been found in some unusual factors, such as the slow and continuous addition of diluted H_2O_2, which improved the stochiometric efficacy of the reaction compared to the concentrated reagent being added only once [83]. Similarly, a high concentration of H_2O_2 causes an unfavorable effect on the reaction by bringing $OH^\bullet$ to H_2O [84], which decreases the efficiency of the process.

Although high percentages of elimination have been achieved for some pollutants, it is important to note that those tests in which dissolved iron has been used in solution (conventional process) have an optimal pH value close to 3, which maintains the previously mentioned limitations.

In order to overcome its limitations, one of the variations in the conventional process is the use of chelating agents, which can allow the reaction to happen at a pH close to neutral; however, the possible harmful effects such as toxicity and contribution to total organic carbon remain to limit its use [85]. Therefore, the use of heterogeneous catalysts is proposed, where the reactive species are generated mainly on the surface of the catalyst [86], and not, as in the homogeneous process, where the reaction happens in the solution. This makes the recovery and reuse of the heterogeneous catalyst easier [87] and decreases the leaching of Fe^{3+} and, therefore, the generation of sludge. However, some heterogeneous catalysts, although they present minor leaching, behave as if they were homogeneous [88].

An ideal Fenton heterogeneous catalyst must have high catalytic activity and stability, and be easy to recover and reuse [89,90]. To supply this, different materials have been evaluated with iron in different oxidation states. Fe^0 has been reported as a possible heterogeneous Fenton catalyst when maintained in acidic conditions and in the presence of dissolved O_2 [91,92]. In the presence of oxygen, the in situ generation of H_2O_2 in zero-valent materials is possible, since the surface of the material can reduce O_2 using two electrons, accompanied by the generation of Fe^{2+} [93]. Iron oxides, possessing Fe in different oxidation states and being the most abundant minerals in the earth's crust, have been evaluated in the Fenton process. Among these, goethite [94], hematite [95], and magnetite [96] have been investigated. Among the mentioned iron oxides, Fe_3O_4 has aroused greater interest, due to its zero toxicity, effective catalytic activity (thanks to its Fe^{2+} species in its crystal structure), as well as its easy recovery and reuse due to its magnetic properties [97–100]. However, Fe_3O_4 presents a low catalytic activity, mainly due to the slow speed of the Fe^{3+}/Fe^{2+} cycle. Therefore, several strategies have been proposed to overcome this limitation, such as coating, use of materials as supports, adjuvants, etc. [101].

It has been found that the addition of different carbon materials can enhance the Fenton reaction because the presence of carboxyl, carbonyl, and quinone groups present in the carbon material surface accelerates the reduction of Fe^{3+} to Fe^{2+} (Figure 4) [102–106]. On the other hand, carbon materials have been also used as support of the Fenton catalyst. Sun et al. [107] prepared ferric hydroxyquinoline supported on active carbon fiber, which

enhanced the Fe^{3+}/Fe^{2+} cycle through the free electrons present in the carbon material. Yao et al. [108] supported copper ferrite on reduced graphene oxide finding that the presence of two metal ions improved the redox cycle of both ions Cu and Fe together, with a synergistic effect between the nanocube structure of the copper ferrite and the mesoporosity of the support. Kuśmierek et al. [109] and Cruz et al. [110] used organic xerogel as support for Fe/N and $CoFe_2O_4$ and, in both investigations, a catalytic improvement was observed and ascribed to a higher activation of H_2O_2 due to the coexistence of two differents atoms (Fe and N or Co and Fe) in a same matrix.
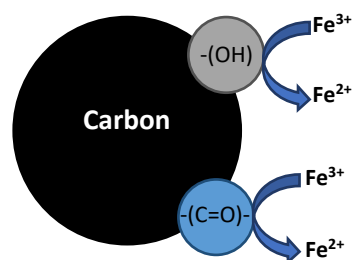

Figure 4. Effect of the addition of carbon in the promoted reduction of Fe^{3+} to Fe^2 [104].

This bimetallic synergism and the effect of the support were also observed by other authors. Zhang et al. [111] prepared Fe/Cu bimetallic-phase-supported montmorillonite using a two-step strategy of impregnation and calcination and found excellent efficiency in the removal of rhodamine B in comparison to single-metal-loaded montmorillonite. These results were ascribed to (i) the expansion of the montmorillonite pore size due to the insertion of Cu and Fe atoms making this clay more suitable as a Fenton catalyst, (ii) the electrons involved in the redox reaction of bimetallic active sites promote the rate of mutual oxidation reactions by enhancing the H_2O_2 conversion into oxidant radicals, and (iii) the leaching of the pure metal ions decreases due to the good stability of support. Li et al. [112] synthesized Fe–Mn/SAPO-18 zeolite catalysts by ion exchange, maintaining the zeolite structure. The author observed an enhanced degradation efficiency of methyl orange compared to the single-metal catalysts (Fe and Mn), which was also attributed to the synergistic effect of bimetal that improves $OH^\bullet$ radical generation and also promotes the formation of another active species, $HO_2^\bullet$. Similarly, Xu et al. [113] used sepiolite as support for Fe_3O_4 dispersion to be used as catalysts for the Fenton degradation of bisphenol A (BPA). The high surface area of the catalyst and the electron transfer and π-π interactions are responsible for the good BPA adsorption properties. Thus, the preconcentration of BFA by adsorption near the active site centers and the generation of hydroxyl radicals in the reaction of H_2O_2 and active sites make the Fenton degradation easier on the surface of Fe_3O_4-Sep. Ferroudj et al. [114] tried to analyze the catalyst's structure–activity relationships and the effect of Fe^{3+} doping in the Fenton degradation of methyl orange (MO) and reactive back 5 (RB5) by the synthesis of Fe^{3+} doped and undoped maghemite/silica microporous and mesoporous microspheres (γ-Fe_2O_3/SiO_2 MS). For that study, the authors concluded that porosity and Fe dispersion play an important role in the Fenton reaction. The creation of mesoporosity in the support enhances the reactants and products diffusion allowing a faster degradation of the tested dyes regarding its microporous counterpart, mainly for the RG5 molecule due to the biggest size. This degradation activity was improved after the doping of the silica framework with Fe^{3+}. Thus, the best results were obtained for the Fe-doped γ-Fe_2O_3/SiO_2 MS mesoporous catalyst. This material allows an almost complete degradation of MO in 25 min in contrast to the doped microporous catalyst, which achieved 92% of MO degradation in 1 h, and the undoped materials, which produces a much low degradation efficiency (63%) in 1 h. Similar results were obtained in the degradation of RB5.

The above-commented strategies to enhance the Fenton active-phase performances and the improvements achieved are collected and summarized in Table 2.

Table 2. Strategies and improvements in the development of electro-Fenton Catalysts.

Catalyst	Strategy	Improvement	Ref.
$Fe(NO_3)_3 \cdot 9H_2O$	Addition of MWCNT and complexation on the surface of the MWCNT through the surface groups.	• The reaction rate was 23 times higher than in traditional Fenton. • Faster Fe^{3+}/Fe^{2+} cycle (Demonstrated by the generation of $OH^\bullet$ and $HO_2^\bullet$, combined with an accelerated decomposition of the contaminant). • Better catalytic activity by MWCNT carboxylates groups. Accelerating the intermediate step from Fe-OOH to Fe^{2+}.	[102]
$FeCl_3 \cdot 6H_2O$	Addition of carbon materials (powdered activated carbon and carbon nanotubes).	• The reduction from Fe^{3+} to Fe^{2+} was accelerated. Due to the reducing power of carbon materials (especially carbonyl/quinone groups). • Carbon nanotubes had a lower rate of decomposition of H_2O_2 than powdered activated carbon.	[103]
$Fe(NO_3)_3 \cdot 9H_2O$	Addition of hydrothermally prepared carbon.	• Promoted the Fe^{3+}/Fe^{2+} cycle through the transfer of electrons from carbonaceous material to Fe^{3+}. • Hydroxyl groups on the surface of hydrothermal carbon strongly affect the reduction of Fe^{3+}.	[104]
$Fe_2O_3@FeB$	FeB coating to Fe_2O_3 core.	• An efficient Fe^{3+}/Fe^{2+} cycle was achieved, thanks to the oxidizing and constantly ceding electrons to Fe^{3+}. • The Fe^{2+} could also generate H_2O_2 in situ by the activation pathway of a single electron of O_2.	[115]
$FeCl_3 \cdot 6H_2O$	Addition of granular activated carbon.	• The formation of Fe^{2+} was accelerated, which improved the catalytic oxidation of the target contaminant.	[105]
Ferrihydrite	Addition of biocarbon and *S. oneidensis*.	• Faster Fe^{3+} reduction rate.	[106]
Montmorillonite (Fe/Cu-MMT)	Preparation of Fe–Cu bimetallic active sites intercalated on montmorillonite.	• The bleaching efficiency of the contaminant was higher, thanks to the electrons involved in the redox reaction of both metals, which promoted the rate of mutual oxidation. • A decrease in the leaching of pure metal ions of Fe and Cu, by presenting good stability with the support.	[111]
Fe–Mn/SAPO-18	Fe–Mn bimetallic active sites supported on SAPO-18.	• Improved degradation efficiency of the contaminant, compared to the single-metal catalysts (Fe and Mn) supported on the zeolite.	[112]
Fe_3O_4–Sep	Sepiolite support for Fe_3O_4 nanoparticles.	• Improved adsorption of the catalyst and, therefore, the in situ degradation of the contaminant on the surface of Fe_3O_4-Sep.	[113]
γ-Fe_2O_3–SiO_2	Mesoporosity creation and Fe^{3+} doping of maghemite/silica microspheres.	• The substitution of microporosity or mesoporosity led to a greater discoloration of the effluent to be treated.	[114]
QuFe@ACF	Active carbon fiber support for ferric hydroxyquinoline.	• Free electrons in the carbon fibers were able to drive electron transfer to ferric 8-hydroxyquinoline to promote the Fe^{3+}/Fe^{2+} cycle faster.	[107]
Fe-C	Fe-doped carbon xerogel.	• Improved dispersion of Fe^0 species.	[116]
CF/rGO	Reduced graphene oxide support for copper ferrite.	• The redox efficiency improved due to the two metal ions (Cu^{2+}/Cu^+ and Fe^{3+}/Fe^{2+}). • Synergistic effect between the nanotube structure of the copper ferrite together with the mesoporosity of the support.	[108]

Table 2. *Cont.*

Catalyst	Strategy	Improvement	Ref.
Fe–N/C	Carbon xerogel support for heteroatoms (Fe, N).	• Improved mass transfer to catalytic active sites. • Increased activation of H_2O_2 due to the coexistence of Fe and N.	[109]
$CoFe_2O_4$/NOM	Xerogel support from the natural organic matrix (NOM) for $CoFe_2O_4$.	• Increased surface area, increasing exposure to catalytically active sites. • Improved electron transfer between metal ion pairs, which increased the speed of the redox cycle (Co^{2+}/Co^{3+} and Fe^{2+}/Fe^{3+}).	[110]

As evidenced in the literature, supporting Fenton heterogeneous catalysts is an effective method to increase the speed of the Fe^{3+}/Fe^{2+} cycle, making it possible to enhance the efficiency of the process. In the same way, an interesting option is the use of metal-doped (e.g., N–Cu) or bimetallic active phases (e.g., Fe–Mn or Fe–Cu), which not only favor redox or Fenton reactions but also more complex reactions such as the oxygen reduction reaction (ORR) (e.g., nitrogen), which is very important for the electro-Fenton process, another variable of conventional Fenton that is addressed below.
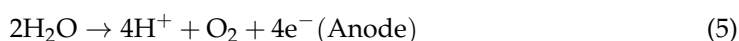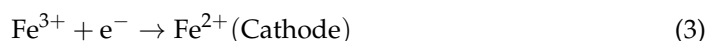
3. Electro-Fenton Process

Heterogeneous Fenton has been proven to be a process with considerable potential for treating a wide range of pollutants. However, the storage, transport, and handling of H_2O_2, as well as the high costs associated with the excess consumption of the reagent are a limitation of the process [117]. To overcome these problems, the heterogeneous electro-Fenton (HEF) has been proposed, where the main contributions are the in situ production of H_2O_2 through the ORR at the cathode, the reduction of Fe^{3+} in the same electrode to supply Fe^{2+} again and the improved generation of $OH^\bullet$ by the applied electricity [118–120].

This process has been successfully used for the degradation of different recalcitrant pollutants such as drugs, dyes, petroleum derivatives, etc. [121–124]. The mechanism of the electro-Fenton process is given by several stages, summarized in [125]:

1. Electrogeneration of H_2O_2 (cathodic reduction of O_2).
2. Production of $OH^\bullet$ (Fenton reaction).
3. Promotion of the formation of $OH^\bullet$ physisorbed on the surface of the electrode.
4. Regeneration of Fe^{2+} through the direct reduction of Fe^{3+} at the cathode.

In general, the reactions involved in the process can be summarized in Equations (3)–(6) [126–128]. However, it is necessary to pay special attention to the possible side reactions associated with the electrolysis of water that can decrease the performance of the catalytic activity of the process [129].

$$Fe^{3+} + e^- \rightarrow Fe^{2+} \, (Cathode) \tag{3}$$

$$O_2 + 2H^+ + 2e^- \rightarrow H_2O_2 \, (Cathode) \tag{4}$$

$$2H_2O \rightarrow 4H^+ + O_2 + 4e^- \, (Anode) \tag{5}$$

$$Fe^{2+} + H_2O_2 + H^+ \rightarrow Fe^{3+} + H_2O + OH^\bullet \tag{6}$$

One of the most important benefits of this process to highlight is the expansion of the working pH range with the removal of contaminants at a pH close to neutral as well as its improvement in levels of biodegradability and toxicity [130,131]. However, as evidenced by Equations (4) and (6), ORR is the limiting step of the process, so it is important to pay attention to the cathode used [132–134].

Traditionally, carbon materials have been used as cathodes due to their good conductivity, stability, and low cost. Thus, these carbon materials are presented as excellent candidates as high-performance cathode electrodes for electro-Fenton reactions for several reasons that are described in the following. Sun et al. [135] synthesized a family of porous biochars by the chemical activation of cellulose powder with $ZnCl_2$ and demonstrated that the carbonization temperature plays an important role in the catalytic performance in the EF oxidation of organic contaminants. While a high carbonization temperature favors the generation of water via the 4-electron pathway, a mild temperature of carbonization (400 °C) improved the generation of H_2O_2 via the 2-electron pathway. This different behavior is attributed to the surface chemistry of the carbon surface; mild carbonization temperatures provide an oxygen-functional-group-rich surface with a high C-O/C=O ratio, which enhances the H_2O_2 selectivity. In contrast, the use of higher carbonization temperatures (700 °C) guarantees a highly graphitic structure and created a carbon defect-rich porous structure highly selective to the 4-electron route. As a consequence, the biochar prepared at 550 °C presents a better catalytic performance as the cathode material for the EF degradation of several organic pollutants in presence of Fe (II), presenting a high H_2O_2 production rate (796.1 mg/g/h at −0.25 V vs. RHE at pH of 1) and achieving an almost complete removal (99%) of phenol after 1 h (at −0.25 V vs. RHE, pH = 3, [Fe (II)] = 0.5 mM, electrolyte: ((Na_2SO_4) = 0.1 M). Ergan et al. [136] also analyzed the effect of the thermal activation of activated carbon fibers in the H_2O_2 electrogeneration and EF efficiency. In this case, the effect of the carbonization time (from 1 h to 10 h) at 900 °C and also the carbonization atmosphere (CO_2 or N_2) was analyzed, observing that the best H_2O_2 production and dye (acid orange 7) degradation (92.9%) was obtained when the fibers were activated in an N_2 atmosphere for 5 h due to a superior hydrophobicity, crystallite size, and larger electroactive surface area. Ramírez-Pereda et al. [137] compared two types of carbon materials: carbon fibers (CF) and vitreous carbon (VC) as electrodes for the electrogeneration of H_2O_2. The authors found that the generation of H_2O_2 is enhanced using CF (96% of H_2O_2 production efficiency) in comparison to VC (54% of H_2O_2 production efficiency), which was attributed to possible competitive reactions. Xia et al. [138,139] analyzed the performance of a polyacrylonitrile-based carbon fiber brush (PAN–CFB) as a cathode electrode for ORR reduction to H_2O_2 and studied the effect of the electrochemical modification of its surface. For the unmodified PAN–CFB, the highest production of H_2O_2 (current efficiency > 90%) was observed at a potential of −0.9 V in an acidic medium, whereas for electrochemically modified PAN–CFB, it was obtained at −0.4 V. However, in a neutral medium (pH = 7), an electrochemically modified PAN–CFB cathode inefficiently generated H_2O_2 (41.2% of current efficiency) in comparison with unmodified PAN–CBF, which still retains the high current efficiency (>90%). This was explained based on the surface chemistry modification after the electrochemical modification treatment, which converts the N-containing groups from pyridinic-N to 2-pyridone—these newly ORR active sites were influenced by solution pH, leading to different pathways in acidic or neutral media. Gao et al. [140] synthesized porous carbon felt modified with polypyrrole (Ppy) and anthraquinone 2-sulfonate, which had a higher specific surface area with more active sites for ORR; in addition, the modification with Ppy decreases the charge transfer resistance. In turn, Chen et al. [141] showed that the adsorption capacity of the carbon-based cathode plays an important role in the EF degradation of tetracycline. For that, they activated carbon felt with KOH at different temperatures, finding that the surface area and the oxygen-containing functional groups on the surface increased in the KOH activation, which significantly enhanced the drug adsorption capacity (being the sample carbonized at 900 °C, which presents the highest adsorption capacity) and also produced the best tetracycline degradation. This highest degree of pollutant degradation (tetracycline 80% removal) was explained based on the 3D structure and good adsorption capacity of activated carbon felt, which creates a space where the organic pollutant is adsorbed and preconcentrated near the active sites in charge of generating the H_2O_2, and, consequently, exposed to a high concentration of hydroxyl radicals in the system of homogeneous catalysis. Wang et al. [142] obtained a complete

degradation of dimethyl phthalate using KOH-activated graphite felt at 900 °C. This high performance was attributed to the high surface area, the presence of oxygenated functional groups, and the more hydrophilic surface generated by the activation of the KOH.

Want et al. [143] pointed out the importance of electrode conductivity on its EF performance. For that, CNT and graphene-modified carbon felt were synthesized and the effect of this modification was analyzed in the degradation of azo-dye (RB5) by EF reaction. The modification of the carbon felt with CNT and graphene increases the degradation rate by 1.2 and 1.5 times than with the original carbon felt, respectively, giving degradation rates of 55.3% and 70.1%, respectively, which was attributed to the improved roughening of the smooth carbon felt fiber (specific surface area), conductivity, and corrosion resistance.

Since the ORR reaction is crucial for the H_2O_2 production, the improvement in the O_2 supply to the active sites seems to be a key factor for the improvement in the EF efficiency, together with, as described above, the preconcentration of the pollutant near the H_2O_2-producing active sites. In this sense, Özcan et al. [144] compared carbon felt with carbon sponge as cathode materials for the degradation of basic blue 3 (BB3) by EF process finding a faster BB3 degradation using the carbon sponge-based electrode, which was associated with the major H_2O_2 production. Sopaj et al. [145] also evaluated the performance of carbon sponges in comparison with carbon felt and stainless steel in sulfamethazine degradation. The highest production of H_2O_2, and, consequently, the highest degradation, was obtained using the carbon sponge instead of carbon felt, the classical cathode for the electro-Fenton process, and stainless steel. This improved catalytic performance of carbon sponge is attributed to the high specific surface are and porosity, which results in inadequate conditions for the mass transport of species of interest (O_2 and H_2O_2) throughout its 3D structure. Ganiyu et al. [146] also synthesized a carbon foam with high performance (total degradation and high mineralization) in the EF degradation of sulfanilamide, which was also attributed to the interconnected spherical cells' porous structure (Figure 5), with high-area B.E.T. that improved the diffusion of substances and gaseous oxygen in the pores and active sites of the cathode, together with an excellent hydrophobicity and conductivity. Nonetheless, it exhibited poor performance in the electro-regeneration of Fe^{2+} from the reduction of Fe^{3+}. This poor Fe^{2+} electro-regeneration of "gas diffuser materials" was also observed by Brillas et al. [147]. They demonstrated that H_2O_2 generation is important; however, it is not a uniquely important factor in the degradation of pollutants by EF. They analyzed the Fe(III)–EDDS-assisted EF degradation of butylated hydroxyanisole (BHA) using a carbon felt or an air-diffusion electrode as a cathode. They observed a much higher Fe(III) reduction efficiency in the novel Fe(III)–EDDS-assisted EF process in comparison with conventional EF. Moreover, the carbon felt resulted in a higher butylate hydroxyanisole degradation despite having an H_2O_2 generation lower than the air-diffusion cathode, which was attributed to the greater regeneration of Fe^{2+} observed using the carbon felt. To overcome this limitation, Chu et al. [148] used a dual cathode system: a gas diffusion electrode (GDE) to generate H_2O_2 by O_2 reduction and a graphite electrode for the regeneration of Fe^{2+} from Fe^{3+} and analyzed its performance as a conventional single-cathode system in the degradation of 4-nitrophenol. They observed that the dual cathode system led to a more effective degradation of 4-nitrophenol, even with a lower initial Fe^{2+} concentration attributed to the rapid change between the Fe^{3+}/Fe^{2+} couple in the dual cathode system. Since the main function of GDE is the electrogeneration of H_2O_2, the regeneration of Fe^{2+} by the cathodic reduction in the single-cathode system is very weak, whereas this regeneration was enhanced by the reduction at the graphite cathode in the dual-cathode system. Chu et al. [149] have also improved the reduction of Fe^{3+} of graphite by its modification with acidified carbon nanotubes, obtaining a degradation of 94.7% of p-nitrophenol. The acidification of the carbon nanotube enhanced the performance in the Fe^{3+} reduction in comparison with the unmodified graphite cathode.
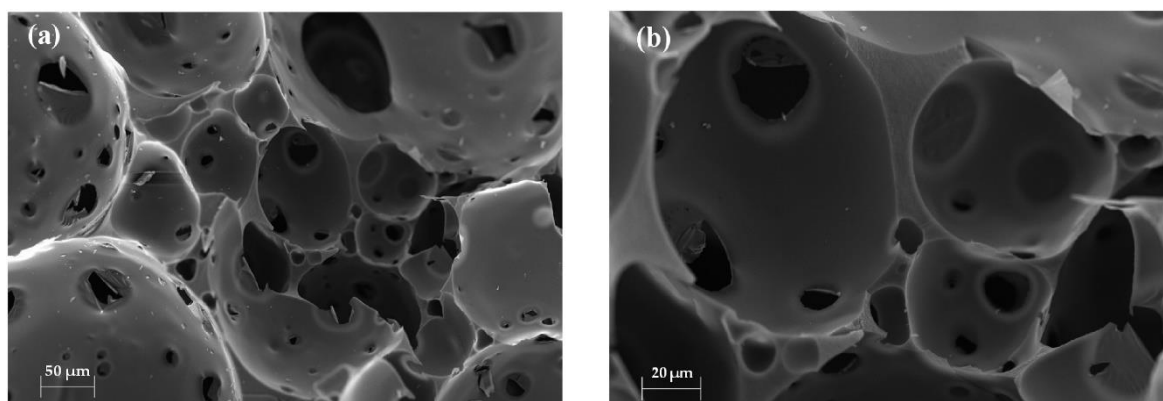
Figure 5. SEM images of carbon foam with low (**a**) and high magnification (**b**) [146].

Other advanced electrodes that improve the O_2-supply are gas diffusion electrodes (GDE) evaluated by different researchers. Zarei et al. [150] synthesized a three-dimensional graphene (3DG)-based carbon paper GDE for the removal of nalidixic acid. The nalidixic acid removal was 90%, which was attributed to a higher surface area with more irregularities and roughness than graphene oxide, allowing rapid diffusion of O_2 to achieve higher H_2O_2 production. On the other hand, Zhou et al. [151] used graphite felt, but in this case, as a floating cathode in which one side of a porous cathode is open to the air, and the other side is submerged in the aqueous solution instead of the traditionally submerged cathode. This novel strategy allows the creation of a three-phase boundary (O_2 gas, electrolyte, and cathode) allowing the usage of O_2 from both air and the electrolyte. This disposition is more energy-efficient and cost-effective in comparison with a GDE because avoids hydrophobic gas diffusion layer formation and the use of an air or O_2 pump. An ibuprofen degradation of 78.3%, with only 25.4% obtained in the conventional position. Liu et al. [152] used a GDE of graphene doped with N-doped carbon nanotubes as the cathode in the dimethyl phthalate removal (100%), finding that the graphene–nanotubes interaction significantly improve the ORR activity.

The hydrophobicity of the cathode ©s also so important in the EF reaction. Chu et al. [153] managed to completely degrade cefepime with a sandwich-like superhydrophobic carbon cathode composed of graphite, carbon nanotubes, and PTFE observing that the hydrophobicity of the electrode significantly affects the ORR to H_2O_2 (Figure 6). Moreover, the prepared superhydrophobic carbon cathode resulted in an excellent reduction of O_2 to H_2O_2, and, consequently, an excellent cefepime degradation, which is mainly dependent on the ·OH production via Fenton reactions. Karatas et al. [154] also attributed the excellent performance of a carbon black electrode for the full degradation of atrazine to the superhydrophobic character of the electrode obtained because this high hydrophobicity provides high H_2O_2 yield by supporting the mass transfer of oxygen molecules.

Another strategy to improve EF performance is the use of metallic-doped electrode materials. Huang et al. [155] prepared a graphite felt-based cathode by first doping the graphite felt with Fe–Mn, then with active carbon, carbon black, and PTFE, and used it for the degradation of ciprofloxacin (Figure 7). This modified graphite felt-based cathode showed a higher degradation efficiency (95.4%) and wider operational pH range than their unmodified counterpart, which was principally associated with the larger surface area and volume pore as well as more active sites. Various researchers have also proposed doping carbon materials for improving EF efficiency. Ma et al. [156] doped multiwalled carbon nanotubes with Ag and Cu foam and noted that the high Ag dispersion improves the ORR and Fe^{2+} regeneration. Dung et al. [157] synthesized cobalt ferrite-coated carbon felt for the degradation of tartrazine (97%), where it is noted that the presence of Co^{3+}/Co^{2+} and Fe^{3+}/Fe^{2+} pairs improve the pollutant degradation; additionally, an additional Fenton catalyst was not needed in this test because the cathode fulfilled both functions. Paz et al. [158] used doped Vulcan XC72 with tungsten oxide nanoparticles and showed an improvement

in the H_2O_2 production due to the surface being more acidic and hydrophilic. Fdez-Sanromán et al. [159] degraded 100% of pymetrozine with a cathode based on carbon felt and modified with carbon nanofibers doped with iron; the improvement was explained by the porous structure that was enhanced with the incorporated nanofibers, and it was also explained that the catalytic activity of a typical Fenton catalyst is more effective in the presence of iron.
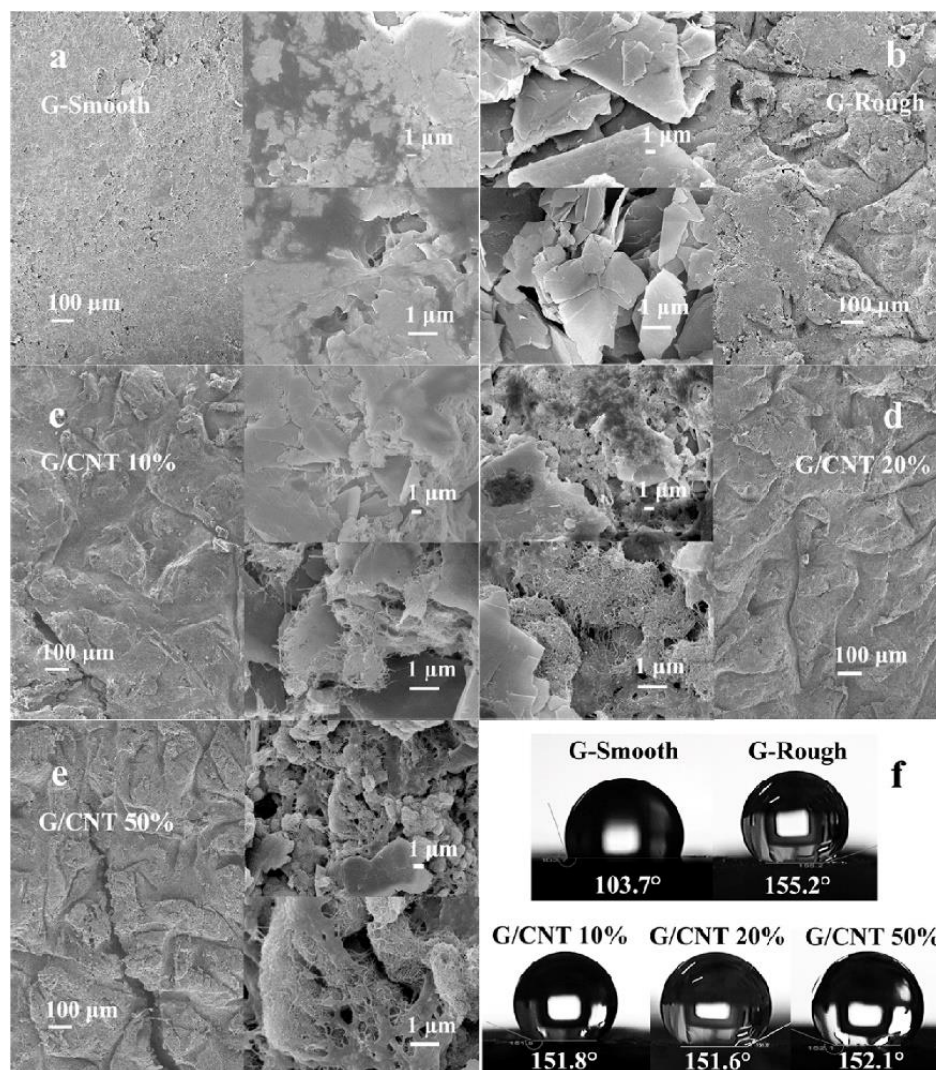

Figure 6. SEM images of "G-Smooth" cathode (**a**), "G-Rough" cathode (**b**), "G/CNT 10%" cathode (**c**), "G/CNT 20%" cathode (**d**), and "G/CNT 50%" cathode (**e**); Water contact angle images of the cathodes (**f**) [153].

In general, it could be summarized that the important parameters to take into account in the cathode preparation are the mesoporous structure that translates into the high surface area, the hydrophobicity that plays an important role in terms of the diffusivity of O_2 inside and outside of the electrode, as well as the regeneration of Fe^{2+} that happens in the electrode, and finally, the composition of the cathode, especially the presence of efficient nitrogenous groups toward ORR [160,161]. However, more in-depth research should be conducted, despite the extensive literature that supports the above. In this regard, Cordeiro stressed that graphite within a series of carbonaceous materials presented the smallest B.E.T. area and zero existence of oxygenated groups on the surface, and still showed the best efficiency of H_2O_2, which was associated with its laminar structure and low hydrophobicity leading to the faster release of H_2O_2 compared to more porous materials [162].
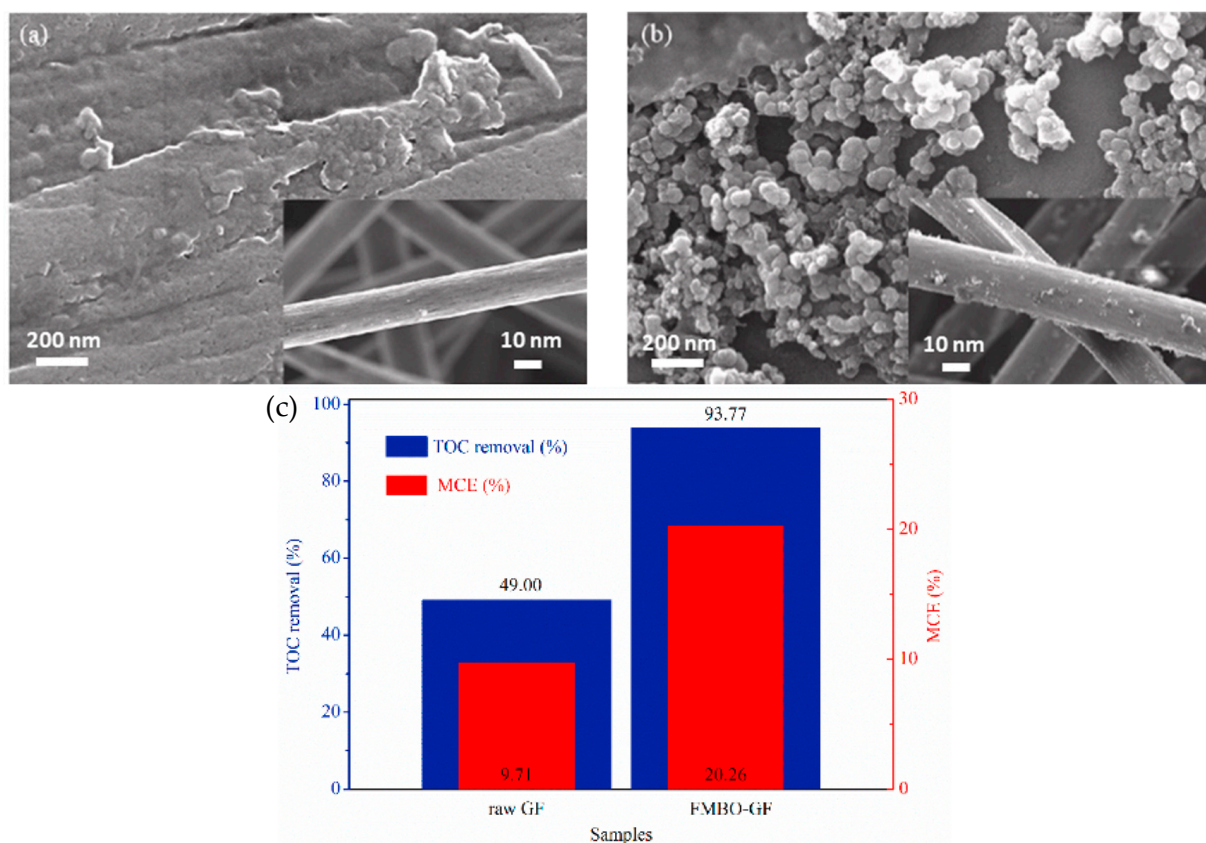
Figure 7. SEM images of (**a**) the unmodified graphite felt (raw GF) cathode, (**b**) the unmodified graphite felt (FMBO–GF) cathode, and (**c**) TOC removal efficiency and the mineralization current efficiency (MCE) of raw GF and FMBO–GF in 2 h under 25 mg/L initial pollutant concentration, pH 7, and 2 mA/cm^2 current density [155].

Another important parameter to consider in the cathode environment is the balance between the three reactants (oxygen, proton, and electron), which must have a molar rate of 2:1:2, respectively [163]. For this, it is important to start studying how to supply air/O_2, which is based on two types of aeration specifically.

1. Direct aeration in solution.
2. Aeration through a gas diffusing electrode (GDE).

Direct aeration in solution through bubbling is the traditional method; on the other hand, GDEs have the advantage that thanks to their porous structure and coexistence of the limits of three phases, they have solved the problems of low solubility and mass transfer of O_2 [164], which can accelerate ORR kinetics and gas-use efficiency, summarizing even better energy use. In general, GDEs can improve ORR mainly due to two main mechanisms [165].

1. The increase in the mass transfer of O_2 improves the contact of the gas with the catalyst and, therefore, the active sites for the ORR.
2. The increase in the mass transfer is not only in reference to O_2 but also between the catalyst and electrolyte, which promotes the release of H_2O_2 and active sites, improving the formation of the oxidizing species.

GDEs can be defined as porous electrodes in which the solid part is in contact with the gas phase, and then with the solution to be treated [166], which generates a three-phase interface in which the reactions of interest will happen. GDEs are mainly composed of a catalyst layer (in contact with the solution) and a diffuser (in contact with air or oxygen) (Figure 8) [167]. At this point, it is important to clarify that a very thick layer of catalyst can decrease the output rate of H_2O_2 to the solution, which can cause it to degrade on the

surface of the material. An alternative to adjusting the thickness of the layer or avoiding its limitation is to adjust the hydrophobicity of the catalyst [168].
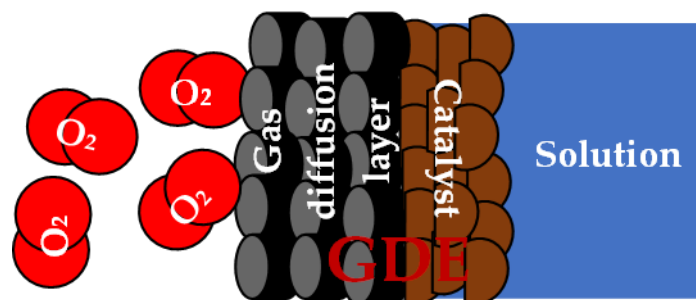

Figure 8. Schematic of a gas diffusion electrode adapted from [166].

As it has been pointed out, good results have been obtained in the EF degradation of a huge variety of emerging pollutants. However, since H_2O_2 production by the O_2 reduction at the cathode seems to be the limiting step, a deeper investigation into ORR is necessary to better understand how cathode variations benefit or affect the efficiency of the EF process.

4. Promising New Fenton Catalysts: Spinel Ferrites and Perovskites

Fenton catalysts with higher reaction rates are currently being sought to increase their overall efficiencies. Among these, spinel ferrites have attracted increasing interest in recent years due to their low cost, excellent catalytic activity, and magnetic properties that allow a facile separation and reutilization. In this section, the synthesis routes, advantages, and applications of spinel ferrites will be described.

There are different methods of synthesis within which the following stand out:

Chemical coprecipitation

Chemical coprecipitation is one of the most promising methods thanks to its ease of realization, as well as the possibility of mass production. It is mainly based on the co- precipitation of materials by a pH change. In general, this method consists of a mixture of precursors with the species of M^{2+} and M^{3+} (metal), to later precipitate the particles by the addition of a base (KOH, NaOH, or NH_4OH). It can be summarized in Equation (7) [169–172].

$$M^{2+} + 2Fe^{3+} + 8OH^- \rightarrow MFe_2O_4 + 4H_2O \tag{7}$$

4.1. Sol–Gel Method

This method is one of the most used for the synthesis of nanoparticles due to its relatively low cost, operational simplicity, and high homogeneity of the material obtained. It is based on a series of reactions, summarized in the hydrolysis of a metal alkoxide and the subsequent polycondensation of the hydroxyl groups formed, which produces a three-dimensional matrix [173–175], which must subsequently be subjected to thermal processes to improve the crystallinity of the nanoparticles.

4.2. Hydrothermal/Solvothermal

This process can be defined as a series of chemical reactions that occur in a closed system with one or more precursors in the presence of the solvent (water for the hydrothermal case), at a temperature above the boiling point of this [176]. This process has several advantages such as its operational simplicity, versatility, and low cost, among others [177,178]. An important advantage to highlight is the well-controlled diffusivity within the system [179], which allows good control of the structure and morphology of the synthesized particles.
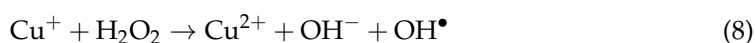
From these synthesis methods, it has been possible to obtain different new Fenton-type catalysts at the nanometer scale, with different coatings and supports [180–182] in order to improve the efficiency of the hetero-Fenton process. It has been established that in the

hetero-Fenton process, having a catalyst with a higher amount of transition-metal ions and a higher specific area leads to better Fenton activity [183,184]. Fe_3O_4 is currently being extensively investigated as a Fenton catalyst [185–187] due to its relatively high activity and easy magnetic separation. An essential advantage is the presence of Fe^{2+} and Fe^{3+} in a single material, due to its cubic structure where half of the Fe^{3+} ions occupied all of the tetrahedral sites and the Fe^{2+} ions are founded in the octahedral, allowing the presence of the two important species in Fenton processes. It has been reported in the literature that transition-metal ions occupying tetrahedral sites are catalytically inert, while those located at octahedral sites tend to determine catalytic activity, which is due to effect that the metal cations in these positions are found exclusively on the surface of the solid and thus take part in reactions to generate $OH^\bullet$ radicals [188]. It has been suggested that the activation of H_2O_2 in the presence of magnetite takes place on the surface of the solid, i.e., the Fe^{3+}-OH [189].

According to crystalline field theory, common metal cations have the following order of preference to occupy octahedral sites, $Cr^{3+} > Ni^{3+} > Cu^{3+} > Al^{3+} > Mg^{2+} > Fe^{2+} > Co^{2+} > Fe^{3+} > Mn^{2+} > Zn^{2+}$ [190]. The most studied are Fe, Mn, Cu, Ni, Zn, and Co [191,192].

Spinel ferrites have a general formula of $A^{2+}B^{3+}_2O^{-2}_4$ and a cubic lattice structure, where positions A and B are occupied by divalent and trivalent metal cations, according to the distribution of cations in the lattice, and the spinels can be normal, random, or inverse. In a normal spinel, tetrahedral sites are related to position A and octahedral sites to B. In a reverse spinel, tetrahedral sites are occupied by half of the B cations and the octahedral sites by all of the A cations. This distribution of cations is responsible for determining the magnetic properties of ferrites [193]. There are different types of spinel-structured materials; however, in this work, we will focus specifically on three of them: copper and cobalt ferrites and iron cobaltite.

Copper ferrite ($CuFe_2O_4$) is a well-known material with a reverse-spinel structure, which has a stable structure that reduces metals leaching, together with unique magnetic, electrical, physical, and chemical properties [194–197]. These properties make them a promising Fenton-type catalyst. Cu^+ ions have been reported to have the ability to generate $OH^\bullet$ radicals by a mechanism similar to that of Fe^{2+} according to Equations (8)–(10) [198].

$$Cu^+ + H_2O_2 \rightarrow Cu^{2+} + OH^- + OH^\bullet \tag{8}$$

$$Cu^{2+} + H_2O_2 \rightarrow Cu^+ + H^+ + HO_2^\bullet \tag{9}$$

$$Cu^{2+} + HO_2^\bullet \rightarrow Cu^+ + H^+ + O_2 \tag{10}$$

Feng et al. [199] synthesized $CuFe_2O_4$ nanoparticles to be used as a Fenton catalyst in the degradation of sulfanilamide. They suggest that CuO is more reactive and effective than Fe^{3+} for the activation of H_2O_2 and, which is more important, can work in a higher pH range than conventional iron oxides. Moreover, Zhang et al. [200] observed that the leaching of Cu^{2+} is 30 times lower in $CuFe_2O_4$ than with CuO. The promising performance of the copper spinel ferrite as a Fenton catalyst was pointed out by several authors. Suraj et al. [201] synthesized $CuFe_2O_4$ by the chemical coprecipitation method and used it as a heterogeneous Fenton catalyst for the treatment of pulp and paper wastewater, obtaining a 78% elimination of the chemical oxygen demand. Ding et al. [202] demonstrated that the morphology of the spinel is also very important. They synthesized hollow $CuFe_2O_4$ spheres with oxygen vacancies (Figure 9), which demonstrated greater degradation of ciprofloxacin than normal $CuFe_2O_4$ particles. This better performance of hollow spheres was attributed, among other factors, to the synergistic oxygen vacancies and confinement effects on the catalyst surface. The oxygen vacancies produce highly active electron-rich Cu^+ species, which enhanced the H_2O_2 activation and, thus, the hydroxyl radical generation. In turn, the hollow structure is responsible for concentrating the organic pollutants near the $^\bullet$OH-generator active sites, improving the organic pollutant molecules/$^\bullet$OH radicals

contact, and accelerating the degradation. According to Deyou et al. [203], the particle size and surface area are more important factors than a crystalline structure for improving the catalytic efficiency of $CuFe_2O_4$. López-Ramón et al. [204] evaluated the effect of calcination temperature on the catalytic activity of $CuFe_2O_4$ synthesized by the sol–gel method, finding that the calcination temperature has two opposite effects: the activity decreases with increasing temperature due to the increase in crystalline size and cubic-to-tetragonal transformation of ferrite and appearance of hematite; however, the metal leaching decreases with increasing calcination temperatures.
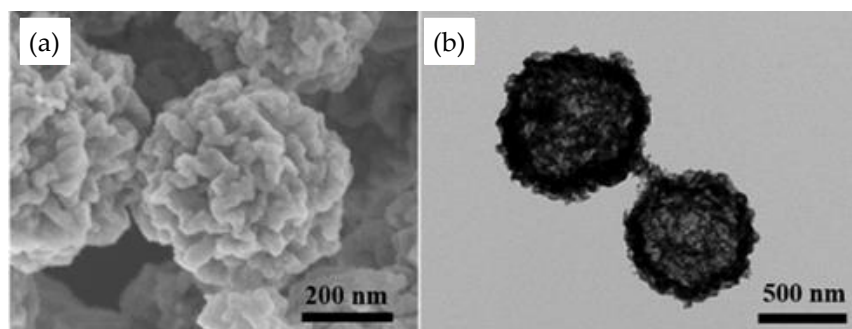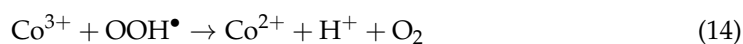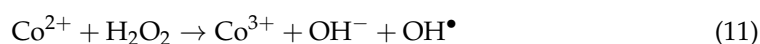

**Figure 9.** SEM (**a**) and TEM (**b**) of $CuFe_2O_4$ hollow spheres [202].

Cobalt ferrite ($CoFe_2O_4$), like other ferrites, has a high catalytic activity, stable crystal structure, low solubility, magnetic properties, as well as the ease of controlling the leaching of cobalt due to the strong interactions between metals, and the strong redox activity of Co with catalytic properties similar to those of noble metals (Pt, Ir, and Au) [205–208], which make it a promising material as a Fenton-like catalyst.

Feng et al. [209] synthesized monodispersed $CoFe_2O_4$ nanoparticles by a solvothermal method to evaluate them as a Fenton catalyst in the degradation of methylene blue, reaching a concentration decrease of 96.8%. The authors highlighted that the existence of Co^{2+} ions could favor the decomposition of H_2O_2 to $OH^\bullet$ and subsequently give way to different reactions, as evidenced in Equations (11)–(14).

$$Co^{2+} + H_2O_2 \rightarrow Co^{3+} + OH^- + OH^\bullet \tag{11}$$

$$OH^\bullet + H_2O_2 \rightarrow OOH^\bullet + H_2O_2 \tag{12}$$

$$Fe^{3+} + OOH^\bullet \rightarrow Fe^{2+} + H^+ + O_2 \tag{13}$$

$$Co^{3+} + OOH^\bullet \rightarrow Co^{2+} + H^+ + O_2 \tag{14}$$

Sing and Singhal [210] demonstrated that the transition-metal doping of cobalt ferrites is a promising method for tuning the physical characteristics of catalysts and thus, enhancing their catalytic and magnetic properties. For that, the authors synthesized a series of Ru-doped cobalt ferrite nanoparticles by the sol–gel method for the photo-Fenton degradation of red Remazol textile dye, achieving a degradation of approximately 90% within 120 min. The mechanism proposed is based on the photocatalytic and Fenton character of the Ru-modified ferrite. An electron-hole pair is created by the irradiation of cobalt ferrite nanoparticles with visible light. The photogenerated electrons are responsible for the $OH^\bullet$ generation from H_2O_2 and also the reduction of the Fe^{3+} cation on cobalt ferrite to Fe^{2+}, which further generates $OH^\bullet$ radicals in the reaction with hydrogen peroxide. Vinosha et al. [211] also analyzed the photo-Fenton performance of $CoFe_2O_4$ nanoparticles obtained by means of chemical coprecipitation, achieving almost total degradation of methylene blue (~99.3% in 75 min) under visible light irradiation. As an outstanding result, they proposed that the pH used in the synthesis was not an impact parameter that

affected the morphology of the catalyst; however, it significantly affects the particle size (a more alkaline (pH > 9) medium, larger crystallite size). It has been proposed that the reactions that lead to the formation of $CoFe_2O_4$ by the chemical coprecipitation method in an aqueous medium, are those presented in Equations (15) and (16) [212].

$$2Fe^{3+} + Co^{2+} \rightarrow Fe_2Co(OH)_8 \tag{15}$$

$$Fe_2Co(OH)_8 \rightarrow CoFe_2O_4 + 4H_2O \tag{16}$$
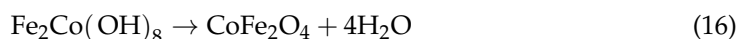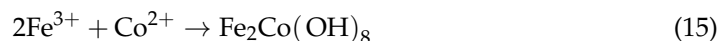
In turn, Iron cobaltite ($FeCo_2O_4$) has been also studied in environmental remediation and energy storage, thanks to its electrical properties and electrochemical performance [213]. In the energy storage field, Mohamed et al. demonstrated that iron cobaltite nanorods show a better capacity and lower overpotential as the cathode of lithium−O_2 batteries than other metal cobaltites (Mn, Ni, and Zn) [214] because the $FeCo_2O_4$ surface has the highest number of electropositive Co^{3+} active sites that improve the oxygen adsorption and Fe^{2+} in the tetrahedral site that favors the release of electrons to reduce oxygen. Yadav et al. [215] demonstrated that iron cobaltites are also efficient for supercapacitive and photocatalytic applications due to the valence states of the Fe^{3+}/Fe^{2+} and Co^{3+}/Co^{2+} species, which are considered active catalytic sites. These nanoflake-like iron cobaltites present a capacitance as high as 1230 F g^{-1} (5 mV s^{-1}) with a good rate capability and superior cycling stability and also show a good photocatalytic performance achieving up to 94.19% degradation of crystal violet dye under sunlight illumination. However, despite this, very little work has been carried out with reference to their evaluation as a Fenton-like catalyst [216,217]. Zhang et al. [216] synthesized nitrogen-containing carbon/$FeCo_2O_4$ composites and analyzed their performances as Fenton catalysts for the degradation of methylene blue obtaining almost 100% removal in 10 min without pH adjustment, which was attributed to the uniform distribution of bimetals and nitrogen doping, which ensured the exposure of sites with high catalytic activity. Zhao et al. [217] analyzed the behavior of $FeCo_2O_4/g–C_3N_4$ as a photo-Fenton catalyst in the degradation of rhodamine B (RhB), obtaining 98% degradation in 45 min, which was attributed to a synergetic interaction between photocatalytic and Fenton-like reactions and the effective separation of the photogenerated charges. Therefore, it is proposed that the use of iron cobaltite as a pristine catalyst (without doping or support) in the Fenton reaction may be promising for future applications.

In general, spinel ferrites turn out to be attractive materials for catalytic activities in Fenton processes, mainly because they manage to improve the generation reaction of Fe^{2+} and achieve a synergistic effect between metal ions with valences similar to those of iron involved in the process (M^{2+}, M^{3+}, M: Metal).

Perovskites are other types of materials with promising catalytic activity that can be synthesized by the abovementioned methods (Chemical coprecipitation, sol–gel, and hydro/solvothermal) [218–221]. Perovskites can be defined as a type of mixed oxide with different formulations, binary (ABO), ternary (AA'BO or ABB'O), and quaternary (AA'BB'O), where A and B are cations sites occupied by alkali metals, alkaline-earth metals or rare-earth metals and transition metals, respectively [222].

Some perovskites have been studied in different Fenton-type reactions, for example, Carrasco-Díaz et al. [75] removed paracetamol by Fenton reaction using $LaCu_{1−x}M_xO_3$ (M = Mn, Ti) as the catalyst and determined that the most active catalyst was the one that contained the highest amount of Cu^{2+} at the surface. Moreover, they found that the titanium and manganese species seem not to be responsible for the improvement of activity with respect to the sample $LaCuO_3$. Li et al. [223] synthetized a $Ca_{1−x}FeO_{3−\delta}$ perovskite and determined that the A-site cation can distort the FeO_6 octahedra in the perovskite and regulate the oxygen vacancies (OV) concentration; in this way, an A-site cation deficient of $Ca_{0.9}FeO_{3-\delta}$ results in an improved H_2O_2 activation for the degradation of tetracycline by a Fenton-like process. Similarly, Xie et al. [224] found that the copper incorporation in $LaCoO_3$ perovskite improved the electro-Fenton activity due to the enhancement of redox

activity and oxygen vacancies, but in this case, by the substitution of B-site elements, which synergistically promoted the activation of hydrogen peroxide to a hydroxyl radical ($\bullet$OH). On the other hand, Rusevova et al. [225] degraded phenol via heterogeneous Fenton-like reactions using iron-containing $LaFeO_3$, and $BiFeO_3$ perovskites, and made a comparison with data reported in the literature using, as a catalyst, nano-sized Fe(II, III) oxide particles, determining that the perovskites synthetized in this work had a higher catalytic activity. Zhao et al. [226] determined that $BiFeO_3$ supported in carbon aerogel (BFO/CA) with a three-dimensional (3D) structure improves the catalytic activity and stability of $BiFeO_3$, resulting in an interesting strategy for the development of advanced catalysts for its possible application in Fenton processes.

In summary, perovskites are materials similar to spinel ferrites, and the contribution of two different metal species (formation of OVs) can be of interest to the Fenton process.

5. Oxygen Reduction Reaction through Two Electrons (ORR 2e$^-$)

The oxygen reduction reaction (ORR) has attracted attention in recent years due to its applicability in various fields of industry, both in energy storage and water treatment processes [227–229]. However, this review is focused on ORR as a route for the electrogeneration of H_2O_2, a product that controls the efficiency of the electro-Fenton oxidation reaction.

In general, ORR involves two types of reactions [230]:

1.   Oxygen molecules that are converted directly into water (4e$^-$);
2.   Oxygen molecules that are initially reduced to peroxide and later to water (2e$^-$).

Analyzing the mechanism, it has been established that ORR 2e$^-$ takes place in two steps involving two single proton-coupled electron transfers; in the first, there is the transfer of electrons and generation of the HOO intermediate linked to the active site (*), while in the second, H_2O_2 is produced (Equations (17 and (18)).

$$O_2 + {}^* + H^+ + e^- \rightarrow OOH^* \tag{17}$$

$$OOH^* + H^+ + e^- \rightarrow H_2O_2 + {}^* \tag{18}$$
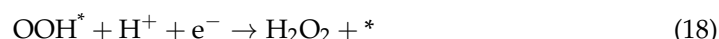
However, H_2O_2 types formed at the cathode can react in three ways [231]:

1.   Being electro-reduced to H_2O at the cathode (usually at porous cathodes);
2.   Being oxidized to O_2 at the anode via $HO_2\cdot$ as an intermediate;
3.   Disproportionate to O_2 and H_2O in a non-electrochemical reaction.

Therefore, the objective in the design of catalysts for the electroproduction of H_2O_2 by ORR is to synthesize materials capable of binding the OOH* intermediate with the appropriate strength; this is neither very strong nor weak to avoid the 4e$^-$ pathway predominating [232].

The most studied way of improving the performance of the ORR 2e$^-$ is the synthesis and optimization of the cathode materials, since, together with the generation of H_2O_2, the current efficiency and, therefore, the energy consumption needs can also be taken into account [233]. In general, an optimal catalyst for ORR 2e$^-$ must have good electrical conductivity, stability, and resistance to acid corrosion [234], properties associated with carbon-based materials [235]. Carbon materials have proven to have excellent properties for use as a cathode due to their high electrical conductivity, zero toxicity, low cost, high stability, and high catalytic activity [236–238]. However, although carbonaceous materials exhibit high selectivity toward H_2O_2 production, they have a slow kinetic toward this reaction, resulting in poor performance.

Different strategies to improve the electrochemical production of H_2O_2 have been recently studied and one of them consists of the deposition of other catalysts or metal oxides (MnO_2, V_2O_5, and CeO_2) on the surface of carbonaceous materials [155]. On the other hand, doping with heteroatoms such as oxygen (O), sulfur (S), nitrogen (N), and fluorine (F) is another strategy developed to increase the electrocatalytic performance of

carbon materials. The carbon lattice doping with heteroatoms introduces defects to the carbon structure, modifying their atomic and electronic structure and, thus, resulting in new promising materials for several energetic applications such as energy production and storage. However, the improvement mechanism of the introduction of these heteroatoms is still under debate by researchers worldwide. Some authors [239–243] found that the introduction of some oxygen functional groups can induce greater electrical conductivity and electrocatalytic activity thanks to the formation of a hydrophilic surface. Recently, different carbonaceous materials have been evaluated as ORR $2e^-$ catalysts, where the importance of the amount and type of oxygenated functional groups present on the surface of these has been evidenced, finding that a greater amount of carboxyl group translates into greater efficiency in H_2O_2 generation because it facilitates the displacement of the electron density of the active site, allowing a better interaction in the adsorption of O_2 [162,244]. In the same way, it has also been established that the higher the ratio of I_D/I_G in carbonaceous materials, the greater the production of H_2O_2 [245].

Zahoor et al. [246] indicated that the sp^2 electron configuration of graphite, graphene, and nanotubes are rich in π electrons which can be transferred without resistance in ORR; however, this electron flow is not enough to promote ORR. Thus, the heteroatom introduction (e.g., N) within its network induces π electron activation by bonding with the solitary electron pairs of N and providing negative charges. The carbon atoms adjacent to nitrogen have a high positive charge density, which increases the adsorption of oxygen and reactive intermediates, which results in enhanced ORR activity. Okamoto et al. [247] found by density-functional calculations that the adsorption of O_2 is more energetically favorable with the increase in the number of N around a C=C bond. Lagarreta-Mendoza et al. [248] proposed quantum phenomena for the explication of the ORR mechanism on N-doped carbon-based electrocatalysts, which consists of the hybridization change in carbon atoms in the graphene lattice, from sp^2 to sp^3. Nitrogen doping could induce a quantum tunnel phenomenon called nitrogen inversion, which consists of a process in which the lone pair of an sp^3 nitrogen atom migrates from one face of the atom, travels through the nucleus (quantum tunneling), and reappears on the other side. This inversion of nitrogen (due to network defects) allows the N atom to act as a "switch" that activates or stops the flow of electrons, generating active sites for ORR The heteroatom–carbon interaction induces the activation of the electron π when joining with the lone pairs of N so that later, the O_2 molecules are reduced into the carbons positively charged by the neighboring N. Additionally, it has been observed that the insertion of a single atom of N does not, apparently, have enough influence to alter the carbon, so a minimum of three atoms are necessary to cause small differences in the length of the C and N bonds [248]. As reported in the literature, N-pyrrolic is more likely to promote ORR $4e^-$ by increasing electron donation capacity, while N-pyridinic has more tendency for ORR $2e^-$ [249]. Wang et al. [250] investigated the ORR $2e^-$ activity of multiwalled carbon nanotubes (MWCNT) with different degrees of oxidation by oxidation with concentrated sulfate and potassium permanganate at 20 to 60 °C for 1 h. They observed that the presence of oxygen groups created after the oxidation treatment enhances the H_2O_2 generation, with the MWCNT always being oxidized and more active than the nonoxidized counterpart. Among the oxidized MWCNT, the sample prepared at middle conditions (40 °C and 1 h) present the best H_2O_2 selectivity which was explained by the composition of its outer and inner structure. After the oxidation treatment, the outer surface is damaged by the creation of a large number of defects together with the introduction of oxygen functional groups such as COOH and C-O-C that act as excellent active sites for the ORR $2e^-$, while the inner structure is maintained, ensuring its good electrical conductivity.

Similarly, it is reported that carbon doping with heteroatoms and transition metals can energetically optimize the charge and rotation density of carbon, helping to promote the activation and reduction of O_2 by weakening the O–O bond in the ORR process [251]. Some studies have found that N can change the mode of adsorption of O_2, while sulfur (S) affects the binding capacity of the OOH intermediate by varying the spin density [252,253]. Ting

Soo et al. [254] reviewed the electrochemical performance of modified graphene as an ORR electrocatalyst, and the spin density, charge, and energy gap were evaluated, finding that the microstructural properties of heteroatom-doped graphene and the high spin density or atomic charge density on adjacent carbon atoms are the key factors that contribute to the enhanced electrocatalytic activity. However, an over-dose of heteroatom doping has negative effects due to the formation of high-sized clusters that make electron transfer difficult. Zhang et al. [255] explained that any chemical species that is substituted for graphene can lead to a high asymmetry spin density and atomic charge density, which promotes ORR. However, by applying DFT calculations they demonstrated that ORR on N-doped graphene is a four-electron pathway. Conversely, Pei Su et al. [256] prepared N-doped graphene showing high H_2O_2 yield, selectivity, and low EEC. They also observed that the C=C and N-pyridinic bonds in N-graphene have the ability to enhance the onset potential, while the N-graphitic groups are responsible for the current disk obtained. Moreover, in EF reaction, they demonstrated that N-graphitic are responsible for the H_2O_2 generation, and N-pyridinic groups catalyze the OH$^\bullet$ radical productions from H_2O_2 (Figure 10). To further investigate the effect of the N-group amount and nature, Pei Su et al. [257] controlled the N-surface chemistry of N-doped graphene (N–GE) via pyrolysis temperatures (200, 300, 400, 550, 750, and 950 °C) in the catalytic activity, observing that the value of electrons transferred in the ORR was in the range of 2 to 2.5 for temperatures of 200 to 400 °C, and from 2.5 to 2.7 for further temperature increases. Thus, the sample pyrolyzed at 400 °C presented the highest active N content and H_2O_2 selectivity and achieved the highest phenol degradation (93.58%). They proposed that the conversion of graphite N and pyridinic-N in N–GE plays an important role in the oxygen reduction reaction (ORR) and OH$^\bullet$ conversion, while the conversion of pyridinic-N-oxide to pyridinic-N is critical for catalyst stability and sustainability.
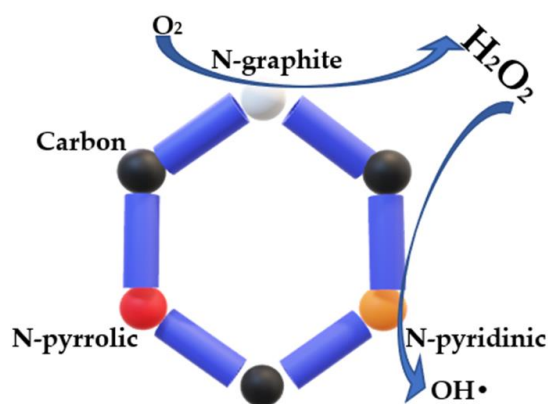

Figure 10. Schematic illustration of the effect of N-contained surface groups in the generation and activation of H_2O_2. Adapted from [256].

Qin et al. [258] and Xie et al. [259] evaluated N and O co-doped carbon material, highlighting the synergistic effect of the different species composed of the two atoms in question on the generation of H_2O_2. The pyridine-N groups combined with ether (C-O-C)/carboxyl (COOH) were highlighted, which presented lower adsorption energy of the intermediate *OOH, facilitating protonation toward H_2O_2. Some studies [260] have also pointed out that the -COOH and carbonyl (-C=O) groups are active for ORR 2e$^-$, and mainly the -COOH group.

Iglesias et al. [261] synthesized N-doped graphitized carbon nanohorns (N–CNH) via coating and controlled annealing of polydopamine (PDA) (Figure 11) and analyzed its use as an electrode material for OEE 2e$^-$. The excellent catalytic performance of N–CNH to perform ORR 2e$^-$ is explained based on the high surface area and accessible porosity of the CNH scaffold, a good distribution of different N-contained surface groups, and improved conductivity and easy electron transfer. The authors also highlight that the microporosity and the specific pyridinic/pyrrolic ratio are crucial factors affecting the ORR route. The

microporosity decreases the residence time of H_2O_2 on the material avoiding further reduction to H_2O_2. The relative types of N atoms also affect the electrocatalytic performance. However, the influence is dependent on the pH. At an acidic pH, protonation of the N-pyridinic occurs which compromises the ability to weaken the O–O bond producing H_2O_2 as the main product while at a neutral or alkaline pH, a reduction in selectivity toward H_2O_2 is observed because the formation of H_2O by the O–O breaking becomes progressively more available.
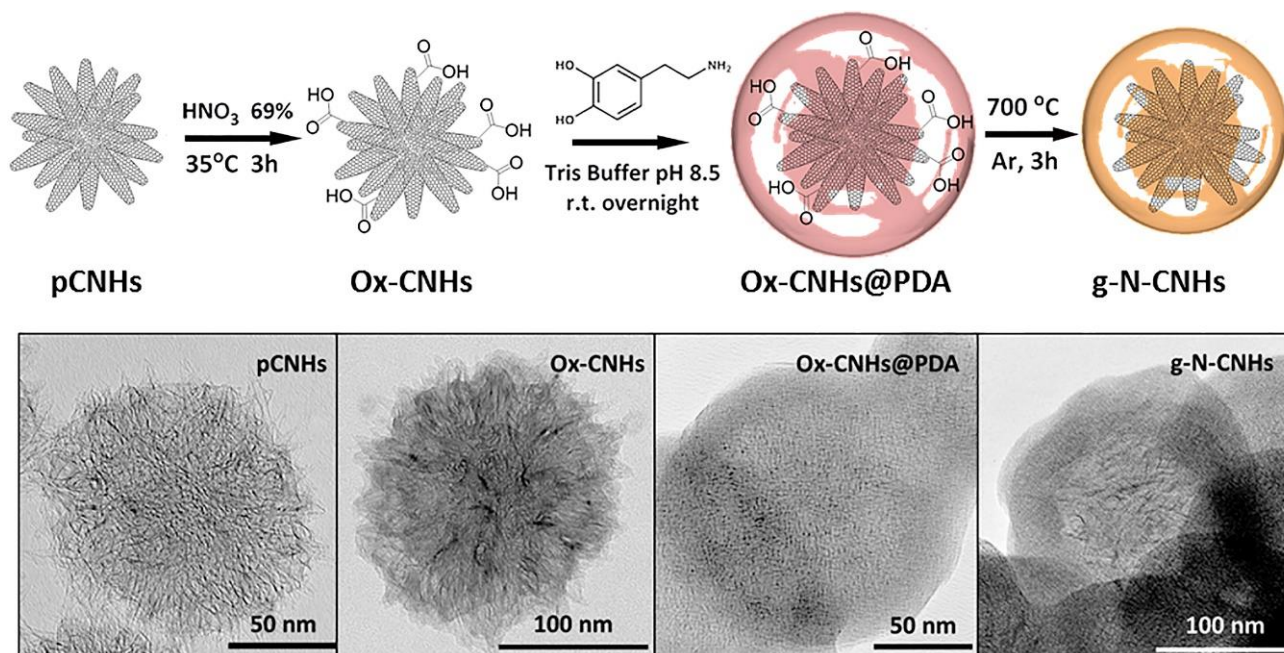

Figure 11. Synthesis of N-doped graphitized carbon nanohorns and TEM images at each stage of the synthesis [261].

Chen et al. [262] also demonstrated that porosity is so important in controlling the selectivity of the process. Chen et al. determined that activated carbon with abundant micropores and a high surface area is better for high ORR activity via 4e⁻, while carbon and graphite black with a smaller specific area tend to catalyze ORR via 2e⁻. Granules with more micropores facilitated the ORR process and caused a further reduction of H_2O_2, leading to less H_2O_2 generation. Similarly, Wenhui He et al. [263] analyzed the effect of the 3D hierarchical porosity on N-doped carbon on the catalytic performance. For that, they prepared N-doped carbon with hierarchical micro-, meso-, and macroporosity by the use of 3D macroporous templates and endogenous pore-generating agents with the assistance of KOH activation. It was concluded that the catalytic efficiency of nitrogen-doped species in ORR highly depends on their degree of exposure to the carbon matrix and that the hierarchical structure can strongly influence the rate of diffusion of O_2 and rapid release of H_2O_2.

In general, it can be concluded that there are some important requirements to obtain carbonaceous materials with high catalytic activity for ORR 2e⁻ such as high porosity (subject to further investigation), large surface area, presence of oxygenated groups, bonds C=C, N-pyridinic, and a greater amount of C atoms sp³ hybridization.

Zhang et al. [264] synthesized interface atomic domains (IAD) of C/N/O atoms (pyridine-N, C=O), from biomass tar by pyrolysis, oxidation, and doping. With this assured an ordered structure (by pyrolysis), with functional groups C=O (oxidation), which results as a host for the generation of N-pyridinic (doping). As a result, it was found that the material obtained had high selectivity for ORR 2e⁻ (N-pyridinic) and an excellent mass transfer of O_2 (C=O and ordered structure).

Another strategy is the doping of porous carbon materials with transition metals which can accelerate the redox reaction by the action of metal ions, thereby increasing the rate of electron transfer. Similarly, nonprecious metals have proven to have an excellent capacity for ORR [265]. It has been shown that compared to bare carbon, metal/carbon compounds have a noticeable improvement toward ORR [266]. Metal/carbon catalysts can adsorb O_2 in two ways, which translates into a greater or lesser efficiency toward reduction via 2 or 4 electrons [267–270].

1. Lateral adsorption leads to a longer bond length and therefore weakens the O=O bond, giving as a product, H_2O (Figure 12).
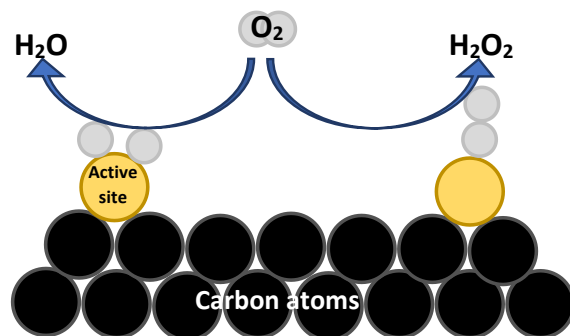

Figure 12. ORR pathways depend on the geometric structure of catalysts. Adapted from [271].

2. Adsorption at the end, where oxygen is adsorbed in the form of OOH, which can produce H_2O_2 and H_2O (Figure 12).

Thus, to obtain metal-doped materials selective to the electrogeneration of H_2O_2, the end-on adsorption of O_2 molecules on the catalyst surfaces need to be promoted. One strategy is the isolation of the active atomic metal sites [271]. For that, three pathways have been developed: (i) alloying an active metal with an inert metal that can induce geometric isolation of the active metal where the O_2 is end-on adsorbed; (ii) the partial poisoning of the active metal surface with an inert phase or molecules, e.g., the coating of Pt nanoparticles with amorphous carbon by CVD (Figure 13); and (iii) the synthesis of atomically dispersed catalysts.
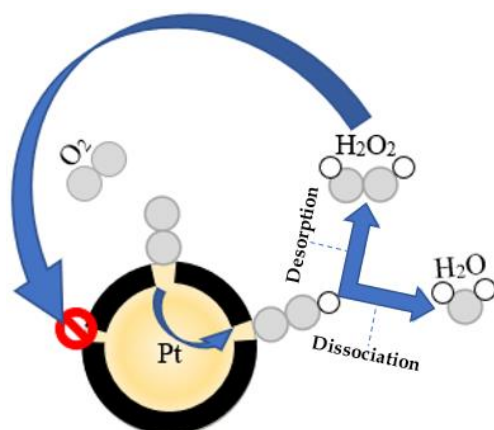

Figure 13. Effect of a carbon coating on Pt/C catalysts surface by acetylene CVD, and H_2O_2 selectivity depending on the CVD operation time for Pt/C catalysts. Adapted from [272].

Some nonprecious metals, used as a doping material in carbonaceous matrices, despite increasing costs, are offset by high dispersion in the matrix, which favors the production of H_2O_2 [273]. In general, although iron may be an ideal metal to regulate the binding energy of the intermediate *OOH with the carbon matrix, it has been shown that it has a strong tendency toward the route of $4e^-$ [274,275]. Co is one of the metals studied for ORR,

demonstrating greater selectivity toward two electrons compared to Fe [276]. On the other hand, Chen et al. [277] investigated the incorporation of Cu atoms in mesoporous N/O-codoped graphitic carbon catalysts with a tailored mesoporosity concluding that the H_2O_2 production depends on the number of C atoms bound to the O atom, which increases by doping with a tiny amount of N. However, the inclusion of copper significantly decreased the selectivity toward H_2O_2. Cu, having a strong binding with oxygen, quickly generates blockages of the active sites due to the O and OH species generated in the reaction [278]. In other studies, Zhang et al. [279] synthesized $Au@Cu_{2-x}S$-CNTs core-shell deficient in Cu and determined that the catalysts exhibited higher ORR activity and selectivity toward H_2O_2, associated with the Cu defects, which (from theoretical calculations) decreases the energy of reaction of OOH*. Wang et al. [280] probed that the nanostructure of the Cu active site is the key to the success of the catalyst; if the active site and host effect are optimally coordinated, it will certainly show considerable potential in the catalytic performance. For that, the authors designed electron-deficient and electron-rich Cu active sites by the regulation of nitrogenous ligand solvents and analyzed the effect in the capture and activation of the C≡C bond of acetylene. The results showed that the Cu sites, stabilized by N-pyrrolic, generate electron-deficient states that improve the activation capacity of acetylene and, thus, the catalytic activity (hydrochlorination). In turn, Hyo-Noh et al. [281] determined that Cu can strongly increase the chemical bonding with O (unfavorable for ORR $2e^-$) and thus bare Cu particles cannot catalyze the ORR at all, but this energy can be easily controlled by the coating with N-doped carbon shells (regulated through CO_2 treatment), resulting in ORR activity comparable to the Pt (111) surface.

Therefore, recently, the investigate into other types of metals has begun. Lenarda et al. [282] investigated different metal (Fe, Ni, Mn, and Co) nanoparticles embedded with an N-doped graphitic carbon and determined that the nature of the metal dictates the type of final surface N-group by obtaining different N-pyridinic/N-pyrrolic ratios, which is essential for H_2O_2 selectivity. The optimal ratio was obtained when Co was used.

Thus, Co is presented as a promising metal to increase the ORR activity without losing H_2O_2 selectivity. In a recent study, Gao et al. [283] prepared single-atom transition metals anchored in nitrogen-doped graphene citing that Co could be an active site for the ORR $2e^-$ pathway since the bond with the OOH* intermediate has optimized adsorption energy, neither too strong nor too weak, in addition to presenting a higher OOH* to O* reduction barrier than that achieved with iron and magnesium atoms. However, Cao et al. [284] evaluated Co nanoparticles supported on N-doped holey graphene aerogel in ORR, determining that the reaction pathway was given by a 4-electron process. Collman et al. [285] studied the geometric effect of cobalt on two different porphyrin structures (monomeric and dicobalt), where the monomeric consists of a Co atom surrounded by N, with which they were able to determine that the selectivity toward H_2O_2 is favored mainly by the isolated site above the electronic effects, since in both cases, the union of the OOH* is the same. In turn, Ferrara et al. [286] studied the effect of pyrolysis temperature against the selectivity of H_2O_2 in Co-encapsulated nanoparticles on a nitrogen-doped carbon matrix, determining that higher temperatures (>800 °C) lead to greater H_2O_2 selectivity, attributed to a larger degree of graphitization and pyrrolic N content. However, the N and O content progressively decreases with increasing pyrolysis temperature, leading to a lower ORR current density.

However, some of the problems of catalysts doped with nonprecious metals are related to their instability in selectivity toward H_2O_2 with pH. At acidic pHs, the $2e^-$ route is favored; however, at basic pHs, the $4e^-$ route is given. Therefore, the use of metal oxides such as magnetite has been proposed to improve the ORR $2e^-$ activity of catalysts based on carbonaceous materials [287].

With the above, and considering the other limitations associated with both the ORR $2e^-$ and Fenton reactions, the doping of carbonaceous materials with structures of the spinel ferrite type is proposed as a viable solution, where the desired bifunctionality is achieved, both for obtaining H_2O_2 and its subsequent decomposition (Fenton) to •OH.

This fact, together with the metal active site control and the spontaneous radical $^{\bullet}$OH production in controlled N-doped carbons, opens the gate to the design of new bifunctional catalysts for the simultaneous production of H_2O_2 and its conversion to $^{\bullet}$OH radicals for the electro-Fenton oxidation of organic pollutants in the water.

6. Bifunctional Electro-Fenton Catalyst for Direct $^{\bullet}$OH Formation

Despite the advances achieved in EF and ORR for the on-site production of H_2O_2, there are still some problems to overcome such as the secondary pollution related to the Fenton catalysts [288,289] and the requirement of two catalysts: one selective to the reduction of oxygen to H_2O_2 and another Fenton-type catalyst for the transformation of H_2O_2 to hydroxyl radicals. Recent efforts are being made to develop materials with dual functionality for the electroreduction of oxygen to H_2O_2 and Fenton catalysis. However, the preparation of heterogeneous EF catalysts with high selectivity and activity toward ORR via the two-electron pathway is challenging since the active sites for Fenton catalysis are mainly transition metals that usually catalyze oxygen reduction via the $4e^-$ route without the production of H_2O_2.

One strategy to develop bifunctional catalysts capable of generating and activating H_2O_2 is the doping of carbon materials with different heteroatoms or carbon structures. Li et al. [290] demonstrated that heteroatom-doped carbon materials can convert H_2O_2 to $^{\bullet}$OH radicals without the need for a Fenton metal catalyst. For that, the authors synthesized an O, F-codoped carbon bifunctional catalyst by the carbonization of polyvinylidene fluoride and proposed that the H_2O_2 generation depends principally on the ratio C-O/C=O (optimal value in 4), while the activation to $^{\bullet}$OH occurs on the semi-ionic C-F bonds obtaining a sulfamerazine degradation of 90.1% in 3 h during the metal-free EF process. A similar fact was observed by Yang et al. [291] using N-doped graphene. They found that the bifunctional effect is attributed to the presence of N-graphite, which influences the H_2O_2 generation and N-pyrrolic responsible for H_2O_2 activation. Similarly, Haider et al. [292] synthesized, in situ, an electrode from polyaniline-derived N-doped carbon nanofibers with bifunctional activity in EF, which was attributed to the content of C=C, oxygen groups, and N-graphitic, which enhanced the H_2O_2 generation and which can be further activated by N-pyridinic to generate the $^{\bullet}$OH radicals. In turn, Qin et al. [293] used it as a bifunctional metal-free cathode based on O-doped carbon nanotubes. They attributed the excellent metal-free EF behavior of this catalyst to the defects and the C-sp^3 that enhances the oxygen adsorption promoting the H_2O_2 production and to the -C=O active sites that are associated with the $^{\bullet}$OH production. Chen et al. [294] found that groups BC_3 and BC_2O present in a boride-activated carbon enhanced the oxygen adsorption and facilitated the desorption of $^{\bullet}$OOH, improving the H_2O_2 generation but also promoting the in situ conversion to $^{\bullet}$OH. Xie et al. [295] showed that the reduced graphene oxide could improve the H_2O_2 generation, while the MOF (MIL-88A) and carbon felt (MIL-88A/CF) could activate the H_2O_2 to OH$^{\bullet}$; thus the cathode rGO/MIL-88A/CF resulted in an excellent bifunctional catalyst.

The introduction of different metals in the carbon matrix for use as bifunctional catalysts has also been studied from simple immobilization to more complex structures such as core-shell. Zhang et al. [296] immobilized Fe_3O_4 in a gas diffusion electrode (GDE) and used it as a rotating cathode for the EF removal of tetracycline. They concluded that the rotating disk gas diffuser greatly enhanced the mass transfer providing a high efficiency in the H_2O_2 generation, whereas the Fe_3O_4 active phase was capable of dissociating the H_2O_2 to OH. Cui et al. [297] also developed a Fe_3O_4/MWCNTs/CB (carbon black) GDE, which has high performance in the production and activation of H_2O_2. The presence of CB enhanced the H_2O_2 production, whereas its activation to OH$^{\bullet}$ was ascribed to $\equiv$Fe(II) on the surface of Fe_3O_4/MWCNTs. Moreover, an improvement in the regeneration of Fe^{2+} was observed due to the high-speed charge channel of MWCNT (Figure 14). On the other hand, Hu et al. [298] synthesized a bifunctional catalyst based on Fe_3C and FeN nanoparticles encapsulated by porous graphitic layers and determined by density function calculations that the active sites for H_2O_2 generation were the Fe_3C, and the activation to OH$^{\bullet}$ depend

on FeN$_x$ sites. Cao et al. [299] designed and synthesized FeO$_x$ nanoparticles embedded into N-doped hierarchically porous carbon for its use as a bifunctional catalyst against phenol, sulfamethoxazole, atrazine, rhodamine B, and 2,4-dichlorophenol in neutral water solution. They found that the presence of N pyridinc and N-pyrrolic increased the H$_2$O$_2$ selectivity, and the FeO$_x$ nanoparticles could enhance the electron transfer to improve the OH$^\bullet$ production. Moreover, the Fe^{3+}/Fe^{2+} cycle could be enhanced by the strong interaction between N-doped porous carbon and FeO$_x$ NPs.

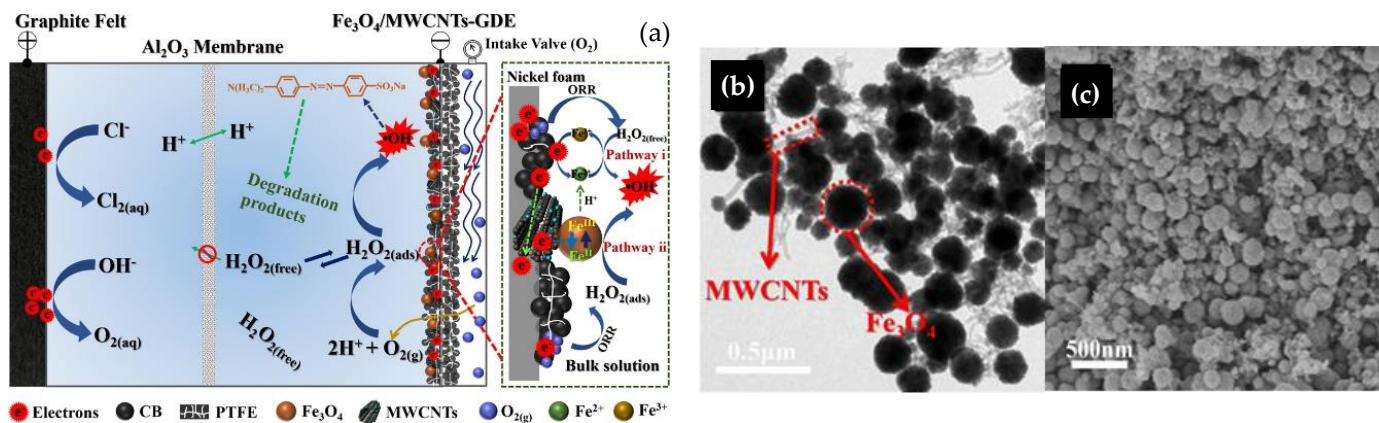**Figure 14.** (**a**) Possible heterogeneous EF catalytic mechanisms using Fe$_3$O$_4$/MWCNTs/CB GDE dual−composite. (**b**) TEM and (**c**) SEM images of Fe$_3$O$_4$/MWCNTs/CB composite [297].

Another proposal to improve the production and activation of H$_2$O$_2$ has been the use of catalysts with the presence of two or more different metal or metallic species that can moderate the activity of alone metals and thereby obtain better bifunctional activity. Ghasemi et al. [300] prepared a cathode with carbon nanotubes (CNTs) and CuFe nano-layered double hydroxide showing that the incorporation of CNTs improves the H$_2$O$_2$ generation, and the atoms of Cu and Fe were responsible for the generation of OH$^\bullet$. Cui et al. [301] used Cu/CuFe$_2$O$_4$ integrated graphite felt as a bifunctional cathode and attributed the H$_2$O$_2$ generation to Cu^0 and the OH$^\bullet$ production to primary Fe^{2+} ions. Moreover, the Fe^{3+}/Fe^{2+} redox cycles could be accelerated by the electron donation of Cu^0 and Fe^0, and even Cu$^+$. Similarly, Luo et al. [302] degraded 98.1% of tetracycline in 2 h using Cu-doped Fe@Fe$_2$O$_3$ core-shell nanoparticles loaded on nickel foam as a cathode, and determined that Cu^0 and Fe^0 react with O$_2$ producing H$_2$O$_2$; Fe^{2+} and Cu$^+$ are responsible for the $^\bullet$OH generation from the in situ generated H$_2$O$_2$. Moreover, they proposed that Fe^{2+} and Cu^{2+} additional EF active sites could be generated from the redox process between Cu$^+$ and Fe^{3+} and the replacement reaction between Cu^{2+} and Fe^0. Sun et al. [303] synthesized a nickel foam cathode co-modified with core-shell CoFe alloy/N-doped carbon (CoFe@NC) and carbon nanotubes (CNTs), where the production of H$_2$O$_2$ was attributed to CNTs and the activation to OH$^\bullet$ to CoFe@NC through Fe^{2+} and Co^{2+} oxidation to Fe^{3+} and Co^{3+}, which are again reduced by Co^0/Fe^0 and the electric field. Similarly, Yu et al. [304] determined that the carbon felt was the ORR catalyst selective to H$_2$O$_2$, and the Co and Fe atoms generated the OH (Co > Fe) in the cathode of CoFe-layered double hydroxide/carbon felt with bifunctional activity. Li et al. [305] prepared an electrode doped with Fe and Mn oxides coated with a carbon layer and determined that the carbon material was responsible for H$_2$O$_2$ generation, and the metals for OH$^\bullet$ production. It was also noted that the presence of Mn considerably improves the regeneration of Fe^{3+}/Fe^{2+} due to Mn that could transfer an electron to Fe to accelerate the cycle.

Bifunctional catalysts using a 3-electron ORR pathway have also been recently proposed as an improved alternative. Xiao et al. [306] reported a catalyst capable of directly generating $^\bullet$OH via a 3-electron pathway with FeCo alloy encapsulated by carbon aerogel. This performance was principally associated with the generation of H$_2$O$_2$ by the 2 electron ORR of the COOH group present in the graphite shell, followed by the reduction by one

electron toward $^\bullet OH$. This 3-electron pathway can be regulated by the electrons from the encapsulated metals.

7. Conclusions

This paper summarizes the different strategies for the design of catalysts with high performance toward Fenton processes and the ORR by the $2e^-$ route as a mechanism to improve the efficiency of the electro-Fenton process, finally focusing on the design of bifunctional electro-Fenton catalysts for the production and activation of H_2O_2.

The key to obtaining high efficiency of ORR $2e^-$ is the proper use of structures that allow the end-on adsorption of O_2, oxygenated functional groups on the surface of the catalyst, as well as the inclusion of doping atoms that allow synergistic effects toward the selectivity of H_2O_2. Although the strategies developed have been based on the amount of H_2O_2 produced and the ORR pathway, some research has opened a gate to the possibility that the morphology of the surface of the catalyst has a much greater impact than expected. Therefore, it is necessary to evaluate, in detail, not only the chemical composition but also other factors such as hydrophobicity, roughness, and/or porosity of the catalyst surface. In general, there are several parameters to consider in the search for an ideal catalyst for ORR $2e^-$, but the amount of N-pyridinic, hydrophobicity, roughness, and doping metal, are so far the most crucial.

As Fenton catalysts, different Fenton-type metals and bimetallic-based materials have been reviewed, raising spinel ferrites as an alternative of interest to provide the bifunctionality for carbonaceous materials, by improving selectivity toward ORR $2e^-$, maintaining the metal ions necessary for Fenton-type catalytic activity suitable for generating $OH^\bullet$ obtained from the H_2O_2 generated in the same structure of the catalyst.

Finally, bifunctional electro-Fenton catalysts are described for the production and activation of H_2O_2. The main strategies are focused on the use of heteroatom-doped carbon materials or carbon-encapsulated Fenton-type metals/carbon composites that moderate the metal's activity and provide an active site for H_2O_2 generation by the ORR $2e^-$ route, presenting metal sites for the activation of in situ generated H_2O_2 to $\cdot OH$ radicals required for the degradation of organic pollutants.

References

1. Li, L.; Zhao, X.; Liu, D.; Song, K.; Liu, Q.; He, Y. Occurrence and ecological risk assessment of PPCPs in typical inflow rivers of Taihu lake, China. *J. Environ. Manag.* **2021**, *285*, 112176. [CrossRef]
2. Archana, G.; Dhodapkar, R.; Kumar, A. Ecotoxicological risk assessment and seasonal variation of some pharmaceuticals and personal care products in the sewage treatment plant and surface water bodies (lakes). *Environ. Monit. Assess.* **2017**, *189*, 446. [CrossRef] [PubMed]
3. Luo, Y.; Guo, W.; Ngo, H.H.; Nghiem, L.D.; Hai, F.I.; Zhang, J.; Liang, S.; Wang, X.C. A review on the occurrence of micropollutants in the aquatic environment and their fate and removal during wastewater treatment. *Sci. Total Environ.* **2014**, *473–474*, 619–641. [CrossRef] [PubMed]
4. UNESCO. Emerging Pollutants in Water and Wastewater. 2020. Available online: https://en.unesco.org/emergingpollutantsin waterandwastewater (accessed on 1 July 2022).
5. Molina, C.B.; Sanz-Santos, E.; Boukhemkhem, A.; Bedia, J.; Belver, C.; Rodriguez, J.J. Removal of emerging pollutants in aqueous phase by heterogeneous Fenton and photo-Fenton with Fe_2O_3-TiO_2-clay heterostructures. *Environ. Sci. Pollut. Res.* **2020**, *27*, 38434–38445. [CrossRef] [PubMed]
6. Mailler, R.; Gasperi, J.; Coquet, Y.; Buleté, A.; Vulliet, E.; Deshayes, S.; Zedek, S.; Mirande-Bret, C.; Eudes, V.; Bressy, A.; et al. Removal of a wide range of emerging pollutants from wastewater treatment plant discharges by micro-grain activated carbon in fluidized bed as tertiary treatment at large pilot scale. *Sci. Total Environ.* **2016**, *542*, 983–996. [CrossRef]
7. González-Mira, A.; Torreblanca, A.; Hontoria, F.; Navarro, J.C.; Mañanós, E.; Varó, I. Effects of ibuprofen and carbamazepine on the ion transport system and fatty acid metabolism of temperature conditioned juveniles of Solea senegalensis. *Ecotoxicol. Environ. Saf.* **2018**, *148*, 693–701. [CrossRef] [PubMed]
8. Kazakova, J.; Villar-Navarro, M.; Ramos-Payán, M.; Aranda-Merino, N.; Román-Hidalgo, C.; Bello-López, M.Á.; Fernández-Torres, R. Monitoring of pharmaceuticals in aquatic biota (*Procambarus clarkii*) of the Doñana National Park (Spain). *J. Environ. Manag.* **2021**, *297*, 113314. [CrossRef]
9. Majumder, A.; Gupta, B.; Gupta, A.K. Pharmaceutically active compounds in aqueous environment: A status, toxicity and insights of remediation. *Environ. Res.* **2019**, *176*, 108542. [CrossRef]
10. Rashid, S.S.; Liu, Y.Q. Comparison of life cycle toxicity assessment methods for municipal wastewater treatment with the inclusion of direct emissions of metals, PPCPs and EDCs. *Sci. Total Environ.* **2021**, *756*, 143849. [CrossRef]
11. Chaturvedi, P.; Shukla, P.; Giri, B.S.; Chowdhary, P.; Chandra, R.; Gupta, P.; Pandey, A. Prevalence and hazardous impact of pharmaceutical and personal care products and antibiotics in environment: A review on emerging contaminants. *Environ. Res.* **2021**, *194*, 110664. [CrossRef]
12. Rodil, R.; Quintana, J.B.; Concha-Graña, E.; López-Mahía, P.; Muniategui-Lorenzo, S.; Prada-Rodríguez, D. Emerging pollutants in sewage, surface and drinking water in Galicia (NW Spain). *Chemosphere* **2012**, *86*, 1040–1049. [CrossRef]
13. An, W.; Duan, L.; Zhang, Y.; Zhou, Y.; Wang, B.; Yu, G. Pollution characterization of pharmaceutically active compounds (PhACs) in the northwest of Tai Lake Basin, China: Occurrence, temporal changes, riverine flux and risk assessment. *J. Hazard. Mater.* **2022**, *422*, 126889. [CrossRef] [PubMed]
14. Rodriguez-Mozaz, S.; Vaz-Moreira, I.; Varela Della Giustina, S.; Llorca, M.; Barceló, D.; Schubert, S.; Berendonk, T.U.; Michael-Kordatou, I.; Fatta-Kassinos, D.; Martinez, J.L.; et al. Antibiotic residues in final effluents of European wastewater treatment plants and their impact on the aquatic environment. *Environ. Int.* **2020**, *140*, 105733. [CrossRef]
15. Kümmerer, K. Antibiotics in the aquatic environment—A review—Part I. *Chemosphere* **2009**, *75*, 417–434. [CrossRef]
16. Gelband, H.; Miller-Petrie, M.; Pant, S.; Gandra, S.; Levinson, J.; Barter, D.; White, A.; Laxminarayan, R. The State of the World's Antibiotics 2015. In *Justice A Distance*; Center for Disease Dynamics, Economics & Policy: Washington, DC, USA, 2015; pp. 1–30. [CrossRef]
17. Bengtsson-Palme, J.; Kristiansson, E.; Larsson, D.G.J. Environmental factors influencing the development and spread of antibiotic resistance. *FEMS Microbiol. Rev.* **2018**, *42*, 68–80. [CrossRef] [PubMed]
18. Dong, J.; Yan, D.; Mo, K.; Chen, Q.; Zhang, J.; Chen, Y.; Wang, Z. Antibiotics along an alpine river and in the receiving lake with a catchment dominated by grazing husbandry. *J. Environ. Sci.* **2022**, *115*, 374–382. [CrossRef] [PubMed]
19. Wilke, C. Many of the World's Rivers are Flush with Dangerous Levels of Antibiotics 2019. *Science News*, 14 June 2019.
20. Gros, M.; Catalán, N.; Mas-Pla, J.; Čelić, M.; Petrović, M.; Farré, M.J. Groundwater antibiotic pollution and its relationship with dissolved organic matter: Identification and environmental implications. *Environ. Pollut.* **2021**, *289*, 117927. [CrossRef]
21. Wang, K.; Zhuang, T.; Su, Z.; Chi, M.; Wang, H. Antibiotic residues in wastewaters from sewage treatment plants and pharmaceutical industries: Occurrence, removal and environmental impacts. *Sci. Total Environ.* **2021**, *788*, 147811. [CrossRef]
22. Qian, M.; Yang, L.; Chen, X.; Li, K.; Xue, W.; Li, Y.; Zhao, H.; Cao, G.; Guan, X.; Shen, G. The treatment of veterinary antibiotics in swine wastewater by biodegradation and Fenton-like oxidation. *Sci. Total Environ.* **2020**, *710*, 136299. [CrossRef]
23. Jafarisani, M.; Cheshme Khavar, A.H.; Mahjoub, A.R.; Luque, R.; Rodríguez-Padrón, D.; Satari, M.; Gharravi, A.M.; Khastar, H.; Kazemi, S.S.; Masoumikarimi, M. Enhanced visible-light-driven photocatalytic degradation of emerging water contaminants by a modified zinc oxide-based photocatalyst; In-vivo and in-vitro toxicity evaluation of wastewater and PCO-treated water. *Sep. Purif. Technol.* **2020**, *243*, 116430. [CrossRef]

24. Ata, R.; Yıldız Töre, G. Characterization and removal of antibiotic residues by NFC-doped photocatalytic oxidation from domestic and industrial secondary treated wastewaters in Meric-Ergene Basin and reuse assessment for irrigation. *J. Environ. Manag.* **2019**, *233*, 673–680. [CrossRef] [PubMed]

25. Zha, S.; Cheng, Y.; Gao, Y.; Chen, Z.; Megharaj, M.; Naidu, R. Nanoscale zero-valent iron as a catalyst for heterogeneous Fenton oxidation of amoxicillin. *Chem. Eng. J.* **2014**, *255*, 141–148. [CrossRef]

26. Wang, A.; Zhang, Y.; Han, S.; Guo, C.; Wen, Z.; Tian, X.; Li, J. Electro-Fenton oxidation of a β-lactam antibiotic cefoperazone: Mineralization, biodegradability and degradation mechanism. *Chemosphere* **2021**, *270*, 129486. [CrossRef] [PubMed]

27. Wang, C.; Lin, C.Y.; Liao, G.Y. Degradation of antibiotic tetracycline by ultrafine-bubble ozonation process. *J. Water Process Eng.* **2020**, *37*, 101463. [CrossRef]

28. Baaloudj, O.; Assadi, I.; Nasrallah, N.; El Jery, A.; Khezami, L.; Assadi, A.A. Simultaneous removal of antibiotics and inactivation of antibiotic-resistant bacteria by photocatalysis: A review. *J. Water Process Eng.* **2021**, *42*, 102089. [CrossRef]

29. Baran, W.; Adamek, E.; Jajko, M.; Sobczak, A. Removal of veterinary antibiotics from wastewater by electrocoagulation. *Chemosphere* **2018**, *194*, 381–389. [CrossRef]

30. Salas, G. Tratamiento por Oxidación Avanzada (Reacción Fenton) de Aguas Residuales de la Industria Textil. *Rev. Peru. Quim. Ing. Quim.* **2010**, *12*, 30–38.

31. Fenton, H.J. Oxidation of Tartaric Acid in presence of Iron. *J. Chem. Soc. Trans.* **1894**, *65*, 899–910. [CrossRef]

32. Huang, Y.; Liu, H.; Liu, S.; Li, C.; Yuan, S. Glucose oxidase modified Fenton reactions for in-situ ROS generation and potential application in groundwater remediation. *Chemosphere* **2020**, *253*, 126648. [CrossRef]

33. Ramos, J.M.P.; Pereira-Queiroz, N.M.; Santos, D.H.S.; Nascimento, J.R.; de Carvalho, C.M.; Tonholo, J.; Zanta, C.L.P.S. Printing ink effluent remediation: A comparison between electrochemical and Fenton treatments. *J. Water Process Eng.* **2019**, *31*, 100803. [CrossRef]

34. Usman, M.; Ho, Y.S. A bibliometric study of the Fenton oxidation for soil and water remediation. *J. Environ. Manag.* **2020**, *270*, 110886. [CrossRef] [PubMed]

35. Wong, K.T.; Jang, S.B.; Choong, C.E.; won Kang, C.; Lee, G.C.; Song, J.Y.; Yoon, Y.; Jang, M. In situ Fenton remediation for diesel contaminated clayey zone assisted by thermal plasma blasting: Synergism and cost estimation. *Chemosphere* **2022**, *286*, 131574. [CrossRef] [PubMed]

36. Jain, B.; Singh, A.K.; Kim, H.; Lichtfouse, E.; Sharma, V.K. Treatment of organic pollutants by homogeneous and heterogeneous Fenton reaction processes. *Environ. Chem. Lett.* **2018**, *16*, 947–967. [CrossRef]

37. Sharma, M.; Mohapatra, T.; Ghosh, P. Hydrodynamics, mass and heat transfer study for emerging heterogeneous Fenton process in multiphase fluidized-bed reactor system for wastewater treatment—A review. *Chem. Eng. Res. Des.* **2021**, *171*, 48–62. [CrossRef]

38. Yu, G.H.; Kuzyakov, Y. Fenton chemistry and reactive oxygen species in soil: Abiotic mechanisms of biotic processes, controls and consequences for carbon and nutrient cycling. *Earth-Sci. Rev.* **2021**, *214*, 103525. [CrossRef]

39. Gligorovski, S.; Strekowski, R.; Barbati, S.; Vione, D. Environmental Implications of Hydroxyl Radicals ($^{\bullet}$OH). *Chem. Rev.* **2015**, *115*, 13051–13092. [CrossRef] [PubMed]

40. Amir, J.; Rojas, A.; Fernando, L.; Giraldo, G.; Trujillo, J.M. Empleo del reactivo de Fenton para la degradación del colorante Tartrazina. *Lasallista Investig.* **2009**, *6*, 27–34.

41. Zhang, X.; Zhang, Y.; Yu, Z.; Wei, X.; Wu, W.D.; Wang, X.; Wu, Z. Facile synthesis of mesoporous anatase/rutile/hematite triple heterojunctions for superior heterogeneous photo-Fenton catalysis. *Appl. Catal. B Environ.* **2020**, *263*, 118335. [CrossRef]

42. Song, W.; Cheng, M.; Ma, J.; Ma, W.; Chen, C.; Zhao, J. Decomposition of hydrogen peroxide driven by photochemical cycling of iron species in clay. *Environ. Sci. Technol.* **2006**, *40*, 4782–4787. [CrossRef]

43. Wang, N.; Zheng, T.; Zhang, G.; Wang, P. A review on Fenton-like processes for organic wastewater treatment. *J. Environ. Chem. Eng.* **2016**, *4*, 762–787. [CrossRef]

44. Ochando-Pulido, J.M.; Pimentel-Moral, S.; Verardo, V.; Martinez-Ferez, A. A focus on advanced physico-chemical processes for olive mill wastewater treatment. *Sep. Purif. Technol.* **2017**, *179*, 161–174. [CrossRef]

45. Babuponnusami, A.; Muthukumar, K. A review on Fenton and improvements to the Fenton process for wastewater treatment. *J. Environ. Chem. Eng.* **2014**, *2*, 557–572. [CrossRef]

46. Bokare, A.D.; Choi, W. Review of iron-free Fenton-like systems for activating H_2O_2 in advanced oxidation processes. *J. Hazard. Mater.* **2014**, *275*, 121–135. [CrossRef] [PubMed]

47. Fernández, L.; González-Rodríguez, J.; Gamallo, M.; Vargas-Osorio, Z.; Vázquez-Vázquez, C.; Piñeiro, Y.; Rivas, J.; Feijoo, G.; Moreira, M.T. Iron oxide-mediated photo-Fenton catalysis in the inactivation of enteric bacteria present in wastewater effluents at neutral pH. *Environ. Pollut.* **2020**, *266*, 115181. [CrossRef] [PubMed]

48. Wang, L.; Zhang, Y.; Qian, J. Graphene aerogel-based catalysts in Fenton-like reactions for water decontamination: A short review. *Chem. Eng. J. Adv.* **2021**, *8*, 100171. [CrossRef]

49. Dinçer, A.R.; Çifçi, D.İ.; Cinkaya, D.D.; Dülger, E.; Karaca, F. Treatment of organic peroxide containing wastewater and water recovery by fenton-adsorption and fenton-nanofiltration processes. *J. Environ. Manag.* **2021**, *299*, 113557. [CrossRef] [PubMed]

50. Hu, C.; Huang, D.; Zeng, G.; Cheng, M.; Gong, X.; Wang, R.; Xue, W.; Hu, Z.; Liu, Y. The combination of Fenton process and Phanerochaete chrysosporium for the removal of bisphenol A in river sediments: Mechanism related to extracellular enzyme, organic acid and iron. *Chem. Eng. J.* **2018**, *338*, 432–439. [CrossRef]

51. Soufi, A.; Hajjaoui, H.; Elmoubarki, R.; Abdennouri, M.; Qourzal, S.; Barka, N. Spinel ferrites nanoparticles: Synthesis methods and application in heterogeneous Fenton oxidation of organic pollutants—A review. *Appl. Surf. Sci. Adv.* **2021**, *6*, 100145. [CrossRef]

52. Cheng, M.; Zeng, G.; Huang, D.; Lai, C.; Xu, P.; Zhang, C.; Liu, Y. Hydroxyl radicals based advanced oxidation processes (AOPs) for remediation of soils contaminated with organic compounds: A review. *Chem. Eng. J.* **2016**, *284*, 582–598. [CrossRef]

53. Rao, S.N.; Shrivastava, S. Treatment of complex recalcitrant wastewater using Fenton process. *Mater. Today Proc.* **2020**, *29*, 1161–1165. [CrossRef]

54. Zhao, X.; Chen, L.; Ma, H.; Ma, J.; Gao, D. Effective removal of polymer quaternary ammonium salt by biodegradation and a subsequent Fenton oxidation process. *Ecotoxicol. Environ. Saf.* **2020**, *188*, 109919. [CrossRef] [PubMed]

55. Liu, C.; Yi, H.; Yang, B.; Jia, F.; Song, S. Activation of Fenton reaction by controllable oxygen incorporation in MoS_2-Fe under visible light irradiation. *Appl. Surf. Sci.* **2021**, *566*, 150674. [CrossRef]

56. Qin, H.; Cheng, H.; Li, H.; Wang, Y. Degradation of ofloxacin, amoxicillin and tetracycline antibiotics using magnetic core–shell $MnFe_2O_4$@C-NH$_2$ as a heterogeneous Fenton catalyst. *Chem. Eng. J.* **2020**, *396*, 125304. [CrossRef]

57. Liu, Y.; Zhang, X.; Deng, J.; Liu, Y. A novel CNTs-Fe_3O_4 synthetized via a ball-milling strategy as efficient fenton-like catalyst for degradation of sulfonamides. *Chemosphere* **2021**, *277*, 130305. [CrossRef]

58. Fornazaria, A.L.; Labriola, V.F.; Da Silva, B.F.; Castro, L.F.; Perussi, J.R.; Vieira, E.M.; Azevedo, E.B. Coupling Zero-Valent Iron and Fenton processes for degrading sulfamethazine, sulfathiazole, and norfloxacin. *J. Environ. Chem. Eng.* **2021**, *9*, 105761. [CrossRef]

59. Qin, H.; Yang, Y.; Shi, W.; She, Y.; Wu, S. Heterogeneous Fenton degradation of azithromycin antibiotic in water catalyzed by amino/thiol-functionalized $MnFe_2O_4$ magnetic nanocatalysts. *J. Environ. Chem. Eng.* **2021**, *9*, 106184. [CrossRef]

60. Li, T.; Chen, Y.; Wang, X.; Liang, J.; Zhou, L. Modifying organic carbon in Fe_3O_4-loaded schwertmannite to improve heterogeneous Fenton activity through accelerating Fe(II) generation. *Appl. Catal. B Environ.* **2021**, *285*, 119830. [CrossRef]

61. Goswami, A.; Jiang, J.Q.; Petri, M. Treatability of five micro-pollutants using modified Fenton reaction catalysed by zero-valent iron powder (Fe(0)). *J. Environ. Chem. Eng.* **2021**, *9*, 105393. [CrossRef]

62. Homem, V.; Alves, A.; Santos, L. Amoxicillin degradation at ppb levels by Fenton's oxidation using design of experiments. *Sci. Total Environ.* **2010**, *408*, 6272–6280. [CrossRef]

63. Cheng, S.; Zhang, C.; Li, J.; Pan, X.; Zhai, X.; Jiao, Y.; Li, Y.; Dong, W.; Qi, X. Highly efficient removal of antibiotic from biomedical wastewater using Fenton-like catalyst magnetic pullulan hydrogels. *Carbohydr. Polym.* **2021**, *262*, 117951. [CrossRef]

64. Wang, C.; Sun, R.; Huang, R.; Wang, H. Superior fenton-like degradation of tetracycline by iron loaded graphitic carbon derived from microplastics: Synthesis, catalytic performance, and mechanism. *Sep. Purif. Technol.* **2021**, *270*, 118773. [CrossRef]

65. Del Álamo, A.C.; González, C.; Pariente, M.I.; Molina, R.; Martínez, F. Fenton-like catalyst based on a reticulated porous perovskite material: Activity and stability for the on-site removal of pharmaceutical micropollutans in a hospital wastewater. *Chem. Eng. J.* **2020**, *401*, 126113. [CrossRef]

66. Wang, C.; Yu, G.; Chen, H.; Wang, J. Degradation of norfloxacin by hydroxylamine enhanced fenton system: Kinetics, mechanism and degradation pathway. *Chemosphere* **2021**, *270*, 129408. [CrossRef]

67. Salari, M.; Rakhshandehroo, G.R.; Nikoo, M.R.; Zerafat, M.M.; Mooselu, M.G. Optimal degradation of Ciprofloxacin in a heterogeneous Fenton-like process using (δ-FeOOH)/MWCNTs nanocomposite. *Environ. Technol. Innov.* **2021**, *23*, 101625. [CrossRef]

68. Karimnezhad, H.; Navarchian, A.H.; Tavakoli Gheinani, T.; Zinadini, S. Amoxicillin removal by Fe-based nanoparticles immobilized on polyacrylonitrile membrane: Individual nanofiltration or Fenton reaction, vs. engineered combined process. *Chem. Eng. Res. Des.* **2020**, *153*, 187–200. [CrossRef]

69. Chen, P.; Sun, F.; Wang, W.; Tan, F.; Wang, X.; Qiao, X. Facile one-pot fabrication of ZnO_2 particles for the efficient Fenton-like degradation of tetracycline. *J. Alloys Compd.* **2020**, *834*, 155220. [CrossRef]

70. Yang, W.; Hong, P.; Yang, D.; Yang, Y.; Wu, Z.; Xie, C.; He, J.; Zhang, K.; Kong, L.; Liu, J. Enhanced Fenton-like degradation of sulfadiazine by single atom iron materials fixed on nitrogen-doped porous carbon. *J. Colloid Interface Sci.* **2021**, *597*, 56–65. [CrossRef]

71. de Melo Costa-Serge, N.; Gonçalves, R.G.L.; Rojas-Mantilla, H.D.; Santilli, C.V.; Hammer, P.; Nogueira, R.F.P. Fenton-like degradation of sulfathiazole using copper-modified MgFe-CO_3 layered double hydroxide. *J. Hazard. Mater.* **2021**, *413*, 125388. [CrossRef]

72. Liu, L.; Xu, Q.; Owens, G.; Chen, Z. Fenton-oxidation of rifampicin via a green synthesized rGO@nFe/Pd nanocomposite. *J. Hazard. Mater.* **2021**, *402*, 123544. [CrossRef]

73. Yi, Y.; Luo, J.; Fang, Z. Magnetic biochar derived from Eichhornia crassipes for highly efficient Fenton-like degradation of antibiotics: Mechanism and contributions. *J. Environ. Chem. Eng.* **2021**, *9*, 106258. [CrossRef]

74. Gao, Y.; Zhu, W.; Liu, J.; Lin, P.; Zhang, J.; Huang, T.; Liu, K. Mesoporous sulfur-doped $CoFe_2O_4$ as a new Fenton catalyst for the highly efficient pollutants removal. *Appl. Catal. B Environ.* **2021**, *295*, 120273. [CrossRef]

75. Carrasco-Díaz, M.R.; Castillejos-López, E.; Cerpa-Naranjo, A.; Rojas-Cervantes, M.L. Efficient removal of paracetamol using $LaCu_{1-x}M_xO_3$ (M = Mn, Ti) perovskites as heterogeneous Fenton-like catalysts. *Chem. Eng. J.* **2016**, *304*, 408–418. [CrossRef]

76. Guo, H.; Li, Z.; Xie, Z.; Song, J.; Xiang, L.; Zhou, L.; Li, C.; Liao, L.; Li, J.; Wang, H. Accelerated Fenton reaction for antibiotic ofloxacin degradation in discharge plasma system based on graphene-Fe_3O_4 nanocomposites. *Vacuum* **2021**, *185*, 110022. [CrossRef]

77. Wang, X.; Jin, H.; Wu, D.; Nie, Y.; Tian, X.; Yang, C.; Zhou, Z.; Li, Y. Fe₃O₄@S-doped ZnO: A magnetic, recoverable, and reusable Fenton-like catalyst for efficient degradation of ofloxacin under alkaline conditions. *Environ. Res.* **2020**, *186*, 109626. [CrossRef]

78. Sun, F.; Liu, H.; Wang, H.; Shu, D.; Chen, T.; Zou, X.; Huang, F.; Chen, D. A novel discovery of a heterogeneous Fenton-like system based on natural siderite: A wide range of pH values from 3 to 9. *Sci. Total Environ.* **2020**, *698*, 134293. [CrossRef]

79. Ma, E.; Wang, K.; Hu, Z.; Wang, H. Dual-stimuli-responsive CuS-based micromotors for efficient photo-Fenton degradation of antibiotics. *J. Colloid Interface Sci.* **2021**, *603*, 685–694. [CrossRef]

80. Gu, W.; Huang, X.; Tian, Y.; Cao, M.; Zhou, L.; Zhou, Y.; Lu, J.; Lei, J.; Zhou, Y.; Wang, L.; et al. High-efficiency adsorption of tetracycline by cooperation of carbon and iron in a magnetic Fe/porous carbon hybrid with effective Fenton regeneration. *Appl. Surf. Sci.* **2021**, *538*, 147813. [CrossRef]

81. Liao, Q.; Wang, D.; Ke, C.; Zhang, Y.; Han, Q.; Zhang, Y.; Xi, K. Metal-free Fenton-like photocatalysts based on covalent organic frameworks. *Appl. Catal. B Environ.* **2021**, *298*, 120548. [CrossRef]

82. Luo, L.; Wang, G.; Wang, Z.; Ma, J.; He, Y.; He, J.; Wang, L.; Liu, Y.; Xiao, H.; Xiao, Y.; et al. Optimization of Fenton process on removing antibiotic resistance genes from excess sludge by single-factor experiment and response surface methodology. *Sci. Total Environ.* **2021**, *788*, 147889. [CrossRef]

83. Teel, A.L.; Warberg, C.R.; Atkinson, D.A.; Watts, R.J. Comparison of mineral and soluble iron Fenton's catalysts for the treatment of trichloroethylene. *Water Res.* **2001**, *35*, 977–984. [CrossRef]

84. Lewis, S.; Lynch, A.; Bachas, L.; Hampson, S.; Ormsbee, L.; Bhattacharyya, D. Chelate-modified fenton reaction for the degradation of trichloroethylene in aqueous and two-phase systems. *Environ. Eng. Sci.* **2009**, *26*, 849–859. [CrossRef]

85. Bello, M.M.; Abdul Raman, A.A.; Asghar, A. A review on approaches for addressing the limitations of Fenton oxidation for recalcitrant wastewater treatment. *Process Saf. Environ. Prot.* **2019**, *126*, 119–140. [CrossRef]

86. Huang, C.; Zhang, C.; Huang, D.; Wang, D.; Tian, S.; Wang, R.; Yang, Y.; Wang, W.; Qin, F. Influence of surface functionalities of pyrogenic carbonaceous materials on the generation of reactive species towards organic contaminants: A review. *Chem. Eng. J.* **2021**, *404*, 127066. [CrossRef]

87. Dumesic, J.A.; Huber, G.W.; Boudart, M. Principles of Heterogeneous Catalysis. In *Handbook of Heterogeneous Catalysis*; Wiley: Hoboken, NJ, USA, 2008. [CrossRef]

88. Expósito, E.; Sánchez-Sánchez, C.M.; Montiel, V. Mineral Iron Oxides as Iron Source in Electro-Fenton and Photoelectro-Fenton Mineralization Processes. *J. Electrochem. Soc.* **2007**, *154*, E116. [CrossRef]

89. Bai, Z.; Yang, Q.; Wang, J. Degradation of sulfamethazine antibiotics in Fenton-like system using Fe₃O₄ magnetic nanoparticles as catalyst. *Environ. Prog. Sustain. Energy* **2017**, *36*, 1743–1753. [CrossRef]

90. Xie, W.; Huang, Z.; Zhou, F.; Li, Y.; Bi, X.; Bian, Q.; Sun, S. Heterogeneous fenton-like degradation of amoxicillin using MOF-derived Fe0 embedded in mesoporous carbon as an effective catalyst. *J. Clean. Prod.* **2021**, *313*, 127754. [CrossRef]

91. Furia, F.; Minella, M.; Gosetti, F.; Turci, F.; Sabatino, R.; Di Cesare, A.; Corno, G.; Vione, D. Elimination from wastewater of antibiotics reserved for hospital settings, with a Fenton process based on zero-valent iron. *Chemosphere* **2021**, *283*, 131170. [CrossRef]

92. Rodriguez-Rodriguez, J.; Ochando-Pulido, J.M.; Martinez-Ferez, A. The effect of pH in tannery wastewater by Fenton vs. Heterogeneous Fenton process. *Chem. Eng. Trans.* **2019**, *73*, 205–210. [CrossRef]

93. He, J.; Yang, X.; Men, B.; Wang, D. Interfacial mechanisms of heterogeneous Fenton reactions catalyzed by iron-based materials: A review. *J. Environ. Sci.* **2016**, *39*, 97–109. [CrossRef]

94. Liu, G.; Zhang, Y.; Yu, H.; Jin, R.; Zhou, J. Acceleration of goethite-catalyzed Fenton-like oxidation of ofloxacin by biochar. *J. Hazard. Mater.* **2020**, *397*, 122783. [CrossRef]

95. Huang, X.; Hou, X.; Zhao, J.; Zhang, L. Hematite facet confined ferrous ions as high efficient Fenton catalysts to degrade organic contaminants by lowering H₂O₂ decomposition energetic span. *Appl. Catal. B Environ.* **2016**, *181*, 127–137. [CrossRef]

96. Yang, S.; Xiong, Y.; Ge, Y.; Zhang, S. Heterogeneous Fenton oxidation of nitric oxide by magnetite: Kinetics and mechanism. *Mater. Lett.* **2018**, *218*, 257–261. [CrossRef]

97. Liu, W.; Zhou, J.; Liu, D.; Liu, S.; Liu, X.; Xiao, S. Enhancing electronic transfer by magnetic iron materials and metal-organic framework via heterogeneous Fenton-like process and photocatalysis. *Mater. Sci. Semicond. Process* **2021**, *135*, 106096. [CrossRef]

98. Hassani, A.; Karaca, M.; Karaca, S.; Khataee, A.; Açışlı, Ö.; Yılmaz, B. Preparation of magnetite nanoparticles by high-energy planetary ball mill and its application for ciprofloxacin degradation through heterogeneous Fenton process. *J. Environ. Manag.* **2018**, *211*, 53–62. [CrossRef]

99. Gholizadeh, A.M.; Zarei, M.; Ebratkhahan, M.; Hasanzadeh, A. Phenazopyridine degradation by electro-Fenton process with magnetite nanoparticles-activated carbon cathode, artificial neural networks modeling. *J. Environ. Chem. Eng.* **2021**, *9*, 104999. [CrossRef]

100. Gonçalves, R.G.L.; Lopes, P.A.; Resende, J.A.; Pinto, F.G.; Tronto, J.; Guerreiro, M.C.; de Oliveira, L.C.A.; de Castro Nunes, W.; Neto, J.L. Performance of magnetite/layered double hydroxide composite for dye removal via adsorption, Fenton and photo-Fenton processes. *Appl. Clay Sci.* **2019**, *179*, 105152. [CrossRef]

101. Rial, J.B.; Ferreira, M.L. Challenges of dye removal treatments based on IONzymes: Beyond heterogeneous Fenton. *J. Water Process Eng.* **2021**, *41*, 102065. [CrossRef]

102. Yang, Z.; Yu, A.; Shan, C.; Gao, G.; Pan, B. Enhanced Fe(III)-mediated Fenton oxidation of atrazine in the presence of functionalized multi-walled carbon nanotubes. *Water Res.* **2018**, *137*, 37–46. [CrossRef]

103. Seo, J.; Lee, H.J.; Lee, H.; Kim, H.E.; Lee, J.Y.; Kim, H.S.; Lee, C. Enhanced production of reactive oxidants by Fenton-like reactions in the presence of carbon materials. *Chem. Eng. J.* **2015**, *273*, 502–508. [CrossRef]

104. Qin, Y.; Zhang, L.; An, T. Hydrothermal Carbon-Mediated Fenton-like Reaction Mechanism in the Degradation of Alachlor: Direct Electron Transfer from Hydrothermal Carbon to Fe(III). *ACS Appl. Mater. Interfaces* **2017**, *9*, 17115–17124. [CrossRef]

105. Bach, A.; Semiat, R. The role of activated carbon as a catalyst in GAC/iron oxide/H_2O_2 oxidation process. *Desalination* **2011**, *273*, 57–63. [CrossRef]

106. Kappler, A.; Wuestner, M.L.; Ruecker, A.; Harter, J.; Halama, M.; Behrens, S. Biochar as an Electron Shuttle between Bacteria and Fe(III) Minerals. *Environ. Sci. Technol. Lett.* **2014**, *1*, 339–344. [CrossRef]

107. Sun, L.; Yao, Y.; Wang, L.; Mao, Y.; Huang, Z.; Yao, D.; Lu, W.; Chen, W. Efficient removal of dyes using activated carbon fibers coupled with 8-hydroxyquinoline ferric as a reusable Fenton-like catalyst. *Chem. Eng. J.* **2014**, *240*, 413–419. [CrossRef]

108. Yao, T.; Qi, Y.; Mei, Y.; Yang, Y.; Aleisa, R.; Tong, X.; Wu, J. One-step preparation of reduced graphene oxide aerogel loaded with mesoporous copper ferrite nanocubes: A highly efficient catalyst in microwave-assisted Fenton reaction. *J. Hazard. Mater.* **2019**, *378*, 105. [CrossRef]

109. Kuśmierek, K.; Kiciński, W.; Norek, M.; Polański, M.; Budner, B. Oxidative and adsorptive removal of chlorophenols over Fe-, N- and S-multi-doped carbon xerogels. *J. Environ. Chem. Eng.* **2021**, *9*, 105568. [CrossRef]

110. Cruz, D.R.S.; de Jesus, G.K.; Santos, C.A.; Silva, W.R.; Wisniewski, A.; Cunha, G.C.; Romão, L.P.C. Magnetic nanostructured material as heterogeneous catalyst for degradation of AB210 dye in tannery wastewater by electro-Fenton process. *Chemosphere* **2021**, *280*, 130675. [CrossRef] [PubMed]

111. Zhang, X.; Guo, Y.; Shi, S.; Liu, E.; Li, T.; Wei, S.; Li, Y.; Li, Y.; Sun, G.; Zhao, Z. Efficient and stable iron-copper montmorillonite heterogeneous Fenton catalyst for removing Rhodamine B. *Chem. Phys. Lett.* **2021**, *776*, 138673. [CrossRef]

112. Li, X.; Tian, Z.; Liang, K.; Wang, Y. Enhanced photo-Fenton degradation performance over multi-metal co-supported SAPO-18 zeolites by promoted active species yield. *J. Photochem. Photobiol. A Chem.* **2019**, *379*, 79–87. [CrossRef]

113. Xu, X.; Chen, W.; Zong, S.; Ren, X.; Liu, D. Magnetic clay as catalyst applied to organics degradation in a combined adsorption and Fenton-like process. *Chem. Eng. J.* **2019**, *373*, 140–149. [CrossRef]

114. Ferroudj, N.; Beaunier, P.; Davidson, A.; Abramson, S. Fe^{3+}-doped ordered mesoporous γ-Fe_2O_3/SiO_2 microspheres as a highly efficient magnetically separable heterogeneous Fenton catalyst. *Microporous Mesoporous Mater.* **2021**, *326*, 111373. [CrossRef]

115. Wei, K.; Liu, X.; Cao, S.; Cui, H.; Zhang, Y.; Ai, Z. Fe_2O_3@FeB composites facilitate heterogeneous Fenton process by efficient Fe(III)/Fe(II) cycle and in-situ H_2O_2 generation. *Chem. Eng. J. Adv.* **2021**, *8*, 100165. [CrossRef]

116. Carrasco-Díaz, M.R.; Castillejos-López, E.; Cerpa-Naranjo, A.; Rojas-Cervantes, M.L. On the textural and crystalline properties of Fe-carbon xerogels. Application as Fenton-like catalysts in the oxidation of paracetamol by H_2O_2. *Microporous Mesoporous Mater.* **2017**, *237*, 282–293. [CrossRef]

117. Asghar, A.; Raman, A.A.A.; Daud, W.M.A.W. Advanced oxidation processes for in-situ production of hydrogen peroxide/hydroxyl radical for textile wastewater treatment: A review. *J. Clean. Prod.* **2015**, *87*, 826–838. [CrossRef]

118. Yazici Guvenc, S.; Dincer, K.; Varank, G. Performance of electrocoagulation and electro-Fenton processes for treatment of nanofiltration concentrate of biologically stabilized landfill leachate. *J. Water Process Eng.* **2019**, *31*, 100863. [CrossRef]

119. Tian, Y.; Zhou, M.; Pan, Y.; Cai, J.; Ren, G. Pre-magnetized Fe0 as heterogeneous electro-Fenton catalyst for the degradation of p-nitrophenol at neutral pH. *Chemosphere* **2020**, *240*, 124962. [CrossRef] [PubMed]

120. Huang, L.Z.; Zhu, M.; Liu, Z.; Wang, Z.; Hansen, H.C.B. Single sheet iron oxide: An efficient heterogeneous electro-Fenton catalyst at neutral pH. *J. Hazard. Mater.* **2019**, *364*, 39–47. [CrossRef]

121. Midassi, S.; Bedoui, A.; Bensalah, N. Efficient degradation of chloroquine drug by electro-Fenton oxidation: Effects of operating conditions and degradation mechanism. *Chemosphere* **2020**, *260*, 127558. [CrossRef]

122. Elbatea, A.A.; Nosier, S.A.; Zatout, A.A.; Hassan, I.; Sedahmed, G.H.; Abdel-Aziz, M.H.; El-Naggar, M.A. Removal of reactive red 195 from dyeing wastewater using electro-Fenton process in a cell with oxygen sparged fixed bed electrodes. *J. Water Process Eng.* **2021**, *41*, 102042. [CrossRef]

123. Senthilnathan, J.; Younis, S.A.; Kwon, E.E.; Surenjan, A.; Kim, K.H.; Yoshimura, M. An efficient system for electro-Fenton oxidation of pesticide by a reduced graphene oxide-aminopyrazine@3DNi foam gas diffusion electrode. *J. Hazard. Mater.* **2020**, *400*, 123323. [CrossRef]

124. McQuillan, R.V.; Stevens, G.W.; Mumford, K.A. Assessment of the electro-Fenton pathway for the removal of naphthalene from contaminated waters in remote regions. *Sci. Total Environ.* **2021**, *762*, 143155. [CrossRef]

125. Poza-Nogueiras, V.; Rosales, E.; Pazos, M.; Sanromán, M.Á. Current advances and trends in electro-Fenton process using heterogeneous catalysts—A review. *Chemosphere* **2018**, *201*, 399–416. [CrossRef] [PubMed]

126. Matyszczak, G.; Krzyczkowska, K.; Fidler, A. A novel, two-electron catalysts for the electro-Fenton process. *J. Water Process Eng.* **2020**, *36*, 101242. [CrossRef]

127. Liang, J.; Xiang, Q.; Lei, W.; Zhang, Y.; Sun, J.; Zhu, H.; Wang, S. Ferric iron reduction reaction electro-Fenton with gas diffusion device: A novel strategy for improvement of comprehensive efficiency in electro-Fenton. *J. Hazard. Mater.* **2021**, *412*, 125195. [CrossRef] [PubMed]

128. Zhang, C.; Zhou, M.; Yu, X.; Ma, L.; Yu, F. Modified iron-carbon as heterogeneous electro-Fenton catalyst for organic pollutant degradation in near neutral pH condition: Characterization, degradation activity and stability. *Electrochim. Acta* **2015**, *160*, 254–262. [CrossRef]

129.　Zhu, W.; Li, Y.; Gao, Y.; Wang, C.; Zhang, J.; Bai, H.; Huang, T. A new method to fabricate the cathode by cyclic voltammetric electrodeposition for electro-Fenton application. *Electrochim. Acta* **2020**, *349*, 136415. [CrossRef]

130.　Ganzenko, O.; Trellu, C.; Oturan, N.; Huguenot, D.; Péchaud, Y.; van Hullebusch, E.D.; Oturan, M.A. Electro-Fenton treatment of a complex pharmaceutical mixture: Mineralization efficiency and biodegradability enhancement. *Chemosphere* **2020**, *253*, 126659. [CrossRef]

131.　Robles, I.; Becerra, E.; Barrios, J.A.; Maya, C.; Jiménez, B.; Rodríguez-Valadez, F.J.; Rivera, F.; García-Espinoza, J.D.; Godínez, L.A. Inactivation of helminth eggs in an electro-Fenton reactor: Towards full electrochemical disinfection of human waste using activated carbon. *Chemosphere* **2020**, *250*, 126260. [CrossRef]

132.　Wang, Y.; Liu, Y.; Liu, T.; Song, S.; Gui, X.; Liu, H.; Tsiakaras, P. Dimethyl phthalate degradation at novel and efficient electro-Fenton cathode. *Appl. Catal. B Environ.* **2014**, *156–157*, 1–7. [CrossRef]

133.　Zhao, K.; Quan, X.; Chen, S.; Yu, H.; Zhang, Y.; Zhao, H. Enhanced electro-Fenton performance by fluorine-doped porous carbon for removal of organic pollutants in wastewater. *Chem. Eng. J.* **2018**, *354*, 606–615. [CrossRef]

134.　Liu, Y.; Chen, S.; Quan, X.; Yu, H.; Zhao, H.; Zhang, Y. Efficient Mineralization of Perfluorooctanoate by Electro-Fenton with H_2O_2 Electro-generated on hierarchically Porous Carbon. *Environ. Sci. Technol.* **2015**, *49*, 12528–12533. [CrossRef]

135.　Sun, C.; Chen, T.; Huang, Q.; Duan, X.; Zhan, M.; Ji, L.; Li, X.; Wang, S.; Yan, J. Biochar cathode: Reinforcing electro-Fenton pathway against four-electron reduction by controlled carbonization and surface chemistry. *Sci. Total Environ.* **2021**, *754*, 142136. [CrossRef] [PubMed]

136.　Ergan, B.T.; Gengec, E. Dye degradation and kinetics of online Electro-Fenton system with thermally activated carbon fiber cathodes. *J. Environ. Chem. Eng.* **2020**, *8*, 104217. [CrossRef]

137.　Ramírez-Pereda, B.; Álvarez-Gallegos, A.; Rangel-Peraza, J.G.; Bustos-Terrones, Y.A. Kinetics of Acid Orange 7 oxidation by using carbon fiber and reticulated vitreous carbon in an electro-Fenton process. *J. Environ. Manag.* **2018**, *213*, 279–287. [CrossRef]

138.　Xia, G.; Lu, Y.; Xu, H. An energy-saving production of hydrogen peroxide via oxygen reduction for electro-Fenton using electrochemically modified polyacrylonitrile-based carbon fiber brush cathode. *Sep. Purif. Technol.* **2015**, *156*, 553–560. [CrossRef]

139.　Xia, G.; Lu, Y.; Xueli, G.; Gao, C.; Xu, H. Electro-Fenton Degradation of Methylene Blue Using Polyacrylonitrile-Based Carbon Fiber Brush Cathode. *CLEAN Soil Ai Water* **2014**, *43*, 229–236. [CrossRef]

140.　Gao, Y.; Zhu, W.; Li, Y.; Li, J.; Yun, S.; Huang, T. Novel porous carbon felt cathode modified by cyclic voltammetric electrodeposited polypyrrole and anthraquinone 2-sulfonate for an efficient electro-Fenton process. *Int. J. Hydrogen Energy* **2021**, *46*, 9707–9717. [CrossRef]

141.　Chen, S.; Tang, L.; Feng, H.; Zhou, Y.; Zeng, G.; Lu, Y.; Yu, J.; Ren, X.; Peng, B.; Liu, X. Carbon felt cathodes for electro-Fenton process to remove tetracycline via synergistic adsorption and degradation. *Sci. Total Environ.* **2019**, *670*, 921–931. [CrossRef]

142.　Wang, Y.; Liu, Y.; Wang, K.; Song, S.; Tsiakaras, P.; Liu, H. Preparation and characterization of a novel KOH activated graphite felt cathode for the electro-Fenton process. *Appl. Catal. B Environ.* **2015**, *165*, 360–368. [CrossRef]

143.　Want, Y.-T.; Tu, C.-H.; Lin, Y.-S. Application of Graphene and Carbon Nanotubes on Carbon Felt Electrodes for the Electro-Fenton System. *Materials* **2019**, *12*, 1698. [CrossRef]

144.　Özcan, A.; Şahin, Y.; Savaş Koparal, A.; Oturan, M.A. Carbon sponge as a new cathode material for the electro-Fenton process: Comparison with carbon felt cathode and application to degradation of synthetic dye basic blue 3 in aqueous medium. *J. Electroanal. Chem.* **2008**, *616*, 71–78. [CrossRef]

145.　Sopaj, F.; Oturan, N.; Pinson, J.; Podvorica, F.I.; Oturan, M.A. Effect of cathode material on electro-Fenton process efficiency for electrocatalytic mineralization of the antibiotic sulfamethazine. *Chem. Eng. J.* **2020**, *384*, 123249. [CrossRef]

146.　Ganiyu, S.O.; de Araújo, M.J.G.; de Araújo Costa, E.C.T.; Santos, J.E.L.; dos Santos, E.V.; Martínez-Huitle, C.A.; Pergher, S.B.C. Design of highly efficient porous carbon foam cathode for electro-Fenton degradation of antimicrobial sulfanilamide. *Appl. Catal. B Environ.* **2021**, *283*, 119652. [CrossRef]

147.　Ye, Z.; Brillas, E.; Centellas, F.; Cabot, P.L.; Sirés, I. Electro-Fenton process at mild pH using Fe(III)-EDDS as soluble catalyst and carbon felt as cathode. *Appl. Catal. B Environ.* **2019**, *257*, 117907. [CrossRef]

148.　Chu, Y.Y.; Qian, Y.; Wang, W.J.; Deng, X.L. A dual-cathode electro-Fenton oxidation coupled with anodic oxidation system used for 4-nitrophenol degradation. *J. Hazard. Mater.* **2012**, *199–200*, 179–185. [CrossRef]

149.　Chu, Y.; Su, H.; Lv, R.; Zhang, X. Enhanced electro-reduction of Fe^{3+} to Fe^{2+} by acidified carbon nanotube-modified graphite cathode and its application in a novel Fenton process for p-nitrophenol degradation. *J. Water Process Eng.* **2021**, *40*, 101912. [CrossRef]

150.　Zarei, M.; Beheshti Nahand, F.; Khataee, A.; Hasanzadeh, A. Removal of nalidixic acid from aqueous solutions using a cathode containing three-dimensional graphene. *J. Water Process Eng.* **2019**, *32*, 100978. [CrossRef]

151.　Zhou, W.; Meng, X.; Rajic, L.; Xue, Y.; Chen, S.; Ding, Y.; Kou, K.; Wang, Y.; Gao, J.; Qin, Y.; et al. "Floating" cathode for efficient H_2O_2 electrogeneration applied to degradation of ibuprofen as a model pollutant. *Electrochem. Commun.* **2018**, *96*, 37–41. [CrossRef]

152.　Liu, T.; Wang, K.; Song, S.; Brouzgou, A.; Tsiakaras, P.; Wang, Y. New Electro-Fenton Gas Diffusion Cathode based on Nitrogen-doped Graphene@Carbon Nanotube Composite Materials. *Electrochim. Acta* **2016**, *194*, 228–238. [CrossRef]

153.　Chu, Y.; Su, H.; Liu, C.; Zheng, X. Fabrication of sandwich-like super-hydrophobic cathode for the electro-Fenton degradation of cefepime: H_2O_2 electro-generation, degradation performance, pathway and biodegradability improvement. *Chemosphere* **2022**, *286*, 131669. [CrossRef]

154. Karatas, O.; Gengec, N.A.; Gengec, E.; Khataee, A.; Kobya, M. High-performance carbon black electrode for oxygen reduction reaction and oxidation of atrazine by electro-Fenton process. *Chemosphere* **2021**, *287*, 132370. [CrossRef]

155. Huang, A.; Zhi, D.; Zhou, Y. A novel modified Fe–Mn binary oxide graphite felt (FMBO-GF) cathode in a neutral electro-Fenton system for ciprofloxacin degradation. *Environ. Pollut.* **2021**, *286*, 117310. [CrossRef] [PubMed]

156. Ma, B.; Lv, W.; Li, J.; Yang, C.; Tang, Q.; Wang, D. Promotion removal of aniline with electro-Fenton processes utilizing carbon nanotube 3D morphology modification of an Ag-loaded copper foam cathode. *J. Water Process Eng.* **2021**, *43*, 102295. [CrossRef]

157. Dung, N.T.; Duong, L.T.; Hoa, N.T.; Thao, V.D.; Ngan, L.V.; Huy, N.N. A comprehensive study on the heterogeneous electro-Fenton degradation of tartrazine in water using $CoFe_2O_4$/carbon felt cathode. *Chemosphere* **2022**, *287*, 132141. [CrossRef] [PubMed]

158. Paz, E.C.; Aveiro, L.R.; Pinheiro, V.S.; Souza, F.M.; Lima, V.B.; Silva, F.L.; Hammer, P.; Lanza, M.R.V.; Santos, M.C. Evaluation of H_2O_2 electrogeneration and decolorization of Orange II azo dye using tungsten oxide nanoparticle-modified carbon. *Appl. Catal. B Environ.* **2018**, *232*, 436–445. [CrossRef]

159. Fdez-Sanromán, A.; Acevedo-García, V.; Pazos, M.; Sanromán, M.Á.; Rosales, E. Iron-doped cathodes for electro-Fenton implementation: Application for pymetrozine degradation. *Electrochim. Acta* **2020**, *338*, 135768. [CrossRef]

160. Li, L.; Hu, H.; Teng, X.; Yu, Y.; Zhu, Y.; Su, X. Electrogeneration of H_2O_2 using a porous hydrophobic acetylene black cathode for electro-Fenton process. *Chem. Eng. Process. Process Intensif.* **2018**, *133*, 34–39. [CrossRef]

161. Yu, F.; Tao, L.; Cao, T. High yield of hydrogen peroxide on modified graphite felt electrode with nitrogen-doped porous carbon carbonized by zeolitic imidazolate framework-8 (ZIF-8) nanocrystals. *Environ. Pollut.* **2019**, *255*, 113119. [CrossRef]

162. Cordeiro-Junior, P.J.; Kronka, M.S.; Goulart, L.A.; Veríssimo, N.C.; Mascaro, L.H.; dos Santos, M.C.; Bertazzoli, R.; de Vasconcelos Lanza, M.R. Catalysis of oxygen reduction reaction for H_2O_2 electrogeneration: The impact of different conductive carbon matrices and their physicochemical properties. *J. Catal.* **2020**, *392*, 56–68. [CrossRef]

163. An, J.; Li, N.; Zhao, Q.; Qiao, Y.; Wang, S.; Liao, C.; Zhou, L.; Li, T.; Wang, X.; Feng, Y. Highly efficient electro-generation of H_2O_2 by adjusting liquid-gas-solid three phase interfaces of porous carbonaceous cathode during oxygen reduction reaction. *Water Res.* **2019**, *164*, 114933. [CrossRef] [PubMed]

164. Ridruejo, C.; Alcaide, F.; Álvarez, G.; Brillas, E.; Sirés, I. On-site H_2O_2 electrogeneration at a CoS_2-based air-diffusion cathode for the electrochemical degradation of organic pollutants. *J. Electroanal. Chem.* **2018**, *808*, 364–371. [CrossRef]

165. Li, D.; Zheng, T.; Liu, Y.; Hou, D.; Yao, K.K.; Zhang, W.; Song, H.; He, H.; Shi, W.; Wang, L.; et al. A novel Electro-Fenton process characterized by aeration from inside a graphite felt electrode with enhanced electrogeneration of H_2O_2 and cycle of Fe^{3+}/Fe^{2+}. *J. Hazard. Mater.* **2020**, *396*, 122591. [CrossRef] [PubMed]

166. Kubannek, F.; Turek, T.; Krewer, U. Modeling Oxygen Gas Diffusion Electrodesfor Various Technical Applications. *Chem. Ing. Tech.* **2019**, *91*, 720–733. [CrossRef]

167. Wang, J.; Li, C.; Rauf, M.; Luo, H.; Sun, X.; Jiang, Y. Gas diffusion electrodes for H_2O_2 production and their applications for electrochemical degradation of organic pollutants in water: A review. *Sci. Total Environ.* **2021**, *759*, 143459. [CrossRef]

168. Murawski, E.; Kananizadeh, N.; Lindsay, S.; Rao, A.M.; Popat, S.C. Decreased gas-diffusion electrode porosity due to increased electrocatalyst loading leads to diffusional limitations in cathodic H_2O_2 electrosynthesis. *J. Power Sources* **2021**, *481*, 228992. [CrossRef]

169. Jiang, W.; Yang, H.C.; Yang, S.Y.; Horng, H.E.; Hung, J.C.; Chen, Y.C.; Hong, C.Y. Preparation and properties of superparamagnetic nanoparticles with narrow size distribution and biocompatible. *J. Magn. Magn. Mater.* **2004**, *283*, 210–214. [CrossRef]

170. Lin, C.-C.; Lai, Y.-P.; Wu, K.-Y. A high-productivity process for mass-producing Fe_3O_4 nanoparticles by co-precipitation in a rotating packed bed. *Powder Technol.* **2021**, *395*, 369–376. [CrossRef]

171. Lin, C.C.; Lee, C.Y. Adsorption of ciprofloxacin in water using Fe_3O_4 nanoparticles formed at low temperature and high reactant concentrations in a rotating packed bed with co-precipitation. *Mater. Chem. Phys.* **2020**, *240*, 122049. [CrossRef]

172. Rao, M.N.; Sultana, R.; Kota, S.H. Hazardous Waste. *Solid Hazard. Waste Manag.* **2017**, *1*, 159–207. [CrossRef]

173. Praveen, P.; Viruthagiri, G.; Mugundan, S.; Shanmugam, N. Structural, optical and morphological analyses of pristine titanium di-oxide nanoparticles—Synthesized via sol—Gel route. *Spectrochim. Acta Part A Mol. Biomol. Spectrosc.* **2014**, *117*, 622–629. [CrossRef]

174. Dubey, R.S. Temperature-dependent phase transformation of TiO_2 nanoparticles synthesized by sol-gel method. *Mater. Lett.* **2018**, *215*, 312–317. [CrossRef]

175. Zanurin, A.; Johari, N.A.; Alias, J.; Ayu, H.M.; Redzuan, N.; Izman, S. Research progress of sol-gel ceramic coating: A review. *Mater. Today Proc.* **2021**, *48*, 1849–1854. [CrossRef]

176. Demazeau, G. Solvothermal and hydrothermal processes: The main physico-chemical factors involved and new trends. *Res. Chem. Intermed.* **2010**, *37*, 107–123. [CrossRef]

177. Krajian, H.; Abdallah, B.; Kakhia, M.; Alkafri, N. Hydrothermal growth method for the deposition of ZnO films: Structural, chemical and optical studies. *Microelectron. Reliab.* **2021**, *125*, 114352. [CrossRef]

178. Dem, L.N.; Lyutin, V.I. Status of hydrothermal growth of bulk ZnO: Latest issues and advantages. *J. Cryst. Growth* **2008**, *310*, 993–999. [CrossRef]

179. Yadav, S.; Sharma, A. Importance and challenges of hydrothermal technique for synthesis of transition metal oxides and composites as supercapacitor electrode materials. *J. Energy Storage* **2021**, *44*, 103295. [CrossRef]

180. Guo, X.; Wang, K.; Xu, Y. Tartaric acid enhanced $CuFe_2O_4$-catalyzed heterogeneous photo-Fenton-like degradation of methylene blue. *Mater. Sci. Eng. B* **2019**, *245*, 75–84. [CrossRef]

181. He, H.; Lu, J. Highly photocatalytic activities of magnetically separable reduced graphene oxide-CoFe$_2$O$_4$ hybrid nanostructures in dye photodegradation. *Sep. Purif. Technol.* **2017**, *172*, 374–381. [CrossRef]

182. Boepple, M.; Zhu, Z.; Hu, X.; Weimar, U.; Barsan, N. Impact of heterostructures on hydrogen sulfidesensing: Example of core-shell CuO/CuFe$_2$O$_4$ nanostructures. *Sens. Actuators B Chem.* **2020**, *321*, 128523. [CrossRef]

183. Liu, X.; Li, S.; Akinwolemiwa, B.; Hu, D.; Wu, T.; Peng, C. Low-crystalline transition metal oxide / hydroxide on MWCNT by Fenton-reaction-inspired green synthesis for lithium ion battery and OER electrocatalysis. *Electrochim. Acta* **2021**, *387*, 138559. [CrossRef]

184. Cheng, Z.; Li, S.; Thang, T.; Gao, X.; Luo, S.; Guo, M. Biochar loaded on MnFe$_2$O$_4$ as Fenton catalyst for Rhodamine B removal: Characterizations, catalytic performance, process optimization and mechanism. *Colloids Surf. A Physicochem. Eng. Asp.* **2021**, *631*, 127651. [CrossRef]

185. Zhou, T.; Huang, X.; Zhai, T.; Ma, K.; Zhang, H. Fabrication of novel three-dimensional Fe$_3$O$_4$ -based particles electrodes with enhanced electrocatalytic activity for Berberine removal. *Chemosphere* **2022**, *287*, 132397. [CrossRef] [PubMed]

186. Yang, R.; Peng, Q.; Yu, B.; Shen, Y.; Cong, H. Yolk-shell Fe$_3$O$_4$@MOF-5 nanocomposites as a heterogeneous Fenton-like catalyst for organic dye removal. *Sep. Purif. Technol.* **2021**, *267*, 118620. [CrossRef]

187. Zhu, X.; Zhang, L.; Zou, G.; Chen, Q.; Guo, Y.; Liang, S.; Hu, L.; North, M.; Xie, H. Carboxylcellulose hydrogel confined-Fe$_3$O$_4$ nanoparticles catalyst for Fenton-like degradation of Rhodamine B. *Int. J. Biol. Macromol.* **2021**, *180*, 792–803. [CrossRef]

188. Jacobs, J.P.; Maltha, A.; Reinjtjes, J.; Drimal, J.; Ponec, V. Brongersm The surface of catalytically active spinels. *Catalysis* **1994**, *147*, 294–300. [CrossRef]

189. So, H.L.; Lin, K.Y.; Chu, W. Triclosan removal by heterogeneous Fenton-like process: Studying the kinetics and surface chemistry of Fe$_3$O$_4$ as catalyst. *J. Environ. Chem. Eng.* **2019**, *7*, 103432. [CrossRef]

190. Miller, A. Distribution of Cations in Spinels. *Appl. Phys.* **1959**, *30*, S24–S25. [CrossRef]

191. Han, X.; Liu, S.; Huo, X.; Cheng, F.; Zhang, M.; Guo, M. Facile and large-scale fabrication of (Mg,Ni)(Fe,Al)$_2$O$_4$ heterogeneous photo-Fenton-like catalyst from saprolite laterite ore for effective removal of organic contaminants. *J. Hazard. Mater.* **2020**, *392*, 122295. [CrossRef]

192. Wang, Y.; Tian, D.; Chu, W.; Li, M.; Lu, X. Nanoscaled magnetic CuFe$_2$O$_4$ as an activator of peroxymonosulfate for the degradation of antibiotics norfloxacin. *Sep. Purif. Technol.* **2019**, *212*, 536–544. [CrossRef]

193. Amulya, M.A.S.; Nagaswarupa, H.P.; Kumar, M.R.A.; Ravikumar, C.R.; Kusuma, K.B.; Prashantha, S.C. Evaluation of bifunctional applications of CuFe$_2$O$_4$ nanoparticles synthesized by a sonochemical method. *J. Phys. Chem. Solids* **2021**, *148*, 109756. [CrossRef]

194. Gao, J.; Wu, S.; Han, Y.; Tan, F.; Shi, Y.; Liu, M.; Li, X. 3D mesoporous CuFe$_2$O$_4$ as a catalyst for photo-Fenton removal of sulfonamide antibiotics at near neutral pH. *J. Colloid Interface Sci.* **2018**, *524*, 409–416. [CrossRef]

195. Saravanakumar, B.; Ramachandran, S.P.; Ravi, G.; Ganesh, V.; Guduru, R.K.; Yuvakkumar, R. Electrochemical performances of monodispersed spherical CuFe$_2$O$_4$ nanoparticles for pseudocapacitive applications. *Vacuum* **2019**, *168*, 108798. [CrossRef]

196. Wu, X.; Xia, F.; Nan, Z. Facile synthesis of double-mesoporous-shelled hollow spheres of Cu–CuFe$_2$O$_4$/SiO$_2$ composite as excellent Fenton catalyst. *Mater. Chem. Phys.* **2020**, *242*, 122490. [CrossRef]

197. Li, J.; Ren, Y.; Ji, F.; Lai, B. Heterogeneous catalytic oxidation for the degradation of p-nitrophenol in aqueous solution by persulfate activated with CuFe$_2$O$_4$ magnetic nano-particles. *Chem. Eng. J.* **2017**, *324*, 63–73. [CrossRef]

198. Fontecha-Cámara, M.A.; Moreno-Castilla, C.; López-Ramón, M.V.; Álvarez, M.A. Mixed iron oxides as Fenton catalysts for gallic acid removal from aqueous solutions. *Appl. Catal. B Environ.* **2016**, *196*, 207–215. [CrossRef]

199. Feng, Y.; Liao, C.; Shih, K. Copper-promoted circumneutral activation of H$_2$O$_2$ by magnetic CuFe$_2$O$_4$ spinel nanoparticles: Mechanism, stoichiometric efficiency, and pathway of degrading sulfanilamide. *Chemosphere* **2016**, *154*, 573–582. [CrossRef]

200. Zhang, T.; Zhu, H.; Croue, J. Production of Sulfate Radical from Peroxymonosulfate Induced by a Magnetically Separable CuFe$_2$O$_4$ Spinel in Water: Efficiency, Stability, and Mechanism. *Environ. Sci. Technol.* **2013**, *47*, 2784–2791. [CrossRef]

201. Suraj, P.; Kumar, V.; Thakur, C.; Ghosh, P. Taguchi optimization of COD removal by heterogeneous Fenton process using copper ferro spinel catalyst in a fixed bed reactor—RTD, kinetic and thermodynamic study. *J. Environ. Chem. Eng.* **2019**, *7*, 102859. [CrossRef]

202. Ding, R.; Li, W.; He, C.; Wang, Y.; Liu, X.; Zhou, G.; Mu, Y. Oxygen vacancy on hollow sphere CuFe$_2$O$_4$ as an efficient Fenton-like catalysis for organic pollutant degradation over a wide pH range. *Appl. Catal. B Environ.* **2021**, *291*, 120069. [CrossRef]

203. Yu, D.; Ni, H.; Wang, L.; Wu, M.; Yang, X. Nanoscale-con fined precursor of CuFe$_2$O$_4$ mediated by hyperbranched polyamide as an unusual heterogeneous Fenton catalyst for efficient dye degradation. *J. Clean. Prod.* **2018**, *186*, 146–154. [CrossRef]

204. López-Ramón, M.V.; Álvarez, M.A.; Moreno-Castilla, C.; Fontecha-Cámara, M.A.; Yebra-Rodríguez, Á.; Bailón-García, E. Effect of calcination temperature of a copper ferrite synthesized by a sol-gel method on its structural characteristics and performance as Fenton catalyst to remove gallic acid from water. *J. Colloid Interface Sci.* **2018**, *511*, 193–202. [CrossRef]

205. Xu, M.; Li, J.; Yan, Y.; Zhao, X.; Yan, J.; Zhang, Y.; Lai, B. Catalytic degradation of sulfamethoxazole through peroxymonosulfate activated with expanded graphite loaded CoFe$_2$O$_4$ particles. *Chem. Eng. J.* **2019**, *369*, 403–413. [CrossRef]

206. Guo, X.; Li, H.; Zhao, S. Fast degradation of Acid Orange II by bicarbonate-activated hydrogen peroxide with a magnetic S-modified CoFe$_2$O$_4$ catalyst. *Taiwan Inst. Chem. Eng.* **2015**, *55*, 90–100. [CrossRef]

207. Yao, Y.; Yang, Z.; Zhang, D.; Peng, W.; Sun, H.; Wang, S. Magnetic CoFe$_2$O$_4$-Graphene Hybrids: Facile Synthesis, Characterization, and Catalytic Properties. *Ind. Eng. Chem. Res.* **2012**, *51*, 6044–6051. [CrossRef]

208. Hong, P.; Li, Y.; He, J.; Saeed, A.; Zhang, K. Rapid degradation of aqueous doxycycline by surface $CoFe_2O_4/H_2O_2$ system: Behaviors, mechanisms, pathways and DFT calculation. *Appl. Surf. Sci.* **2020**, *526*, 146557. [CrossRef]

209. Feng, X.; Mao, G.Y.; Bu, F.X.; Cheng, X.L.; Jiang, D.M.; Jiang, J.S. Controlled synthesis of monodisperse $CoFe_2O_4$ nanoparticles by the phase transfer method and their catalytic activity on methylene blue discoloration with H_2O_2. *Magn. Magn. Mater.* **2013**, *343*, 126–132. [CrossRef]

210. Singh, S.; Singhal, S. Transition metal doped cobalt ferrite nanoparticles: Efficient photocatalyst for photodegradation of textile dye. *Mater. Today Proc.* **2019**, *14*, 453–460. [CrossRef]

211. Vinosha, P.A.; Das, S.J. Investigation on the role of pH for the structural, optical and magnetic properties of cobalt ferrite nanoparticles and its effect on the photo-fenton activity. *Mater. Today Proc.* **2018**, *5*, 8662–8671. [CrossRef]

212. Kachi, W.; Al-Shammari, A.M.; Zainal, I.G. Cobalt Ferrite Nanoparticles: Preparation, characterization and salinized with 3-aminopropyl triethoxysilane. *Energy Procedia* **2019**, *157*, 1353–1365. [CrossRef]

213. Sun, Z.; Liu, X.; Dong, X.; Zhang, X.; Tan, Y.; Yuan, F.; Zheng, S.; Li, C. Synergistic activation of peroxymonosulfate via in situ growth $FeCo_2O_4$ nanoparticles on natural rectorite: Role of transition metal ions and hydroxyl groups. *Chemosphere* **2021**, *263*, 127965. [CrossRef]

214. Mohamed, S.G.; Tsai, Y.Q.; Chen, C.J.; Tsai, Y.T.; Hung, T.F.; Chang, W.S.; Liu, R.S. Ternary Spinel MCo_2O_4 (M = Mn, Fe, Ni, and Zn) Porous Nanorods as Bifunctional Cathode Materials for Lithium-O_2 Batteries. *Appl. Mater. Interfaces* **2015**, *7*, 12038–12046. [CrossRef]

215. Yadav, A.A.; Hunge, Y.M.; Kulkarni, S.B. Synthesis of multifunctional $FeCo_2O_4$ electrode using ultrasonic treatment for photo-catalysis and energy storage applications. *Ultrason. Sonochem.* **2019**, *58*, 104663. [CrossRef] [PubMed]

216. Zhang, T.; Ma, Q.; Zhou, M.; Li, C.; Sun, J.; Shi, W.; Ai, S. Degradation of methylene blue by a heterogeneous Fenton reaction catalyzed by $FeCo_2O_4$-N-C nanocomposites derived by ZIFs. *Powder Technol.* **2021**, *383*, 212–219. [CrossRef]

217. Zhao, L.; Yang, D.; Ma, L.; Feng, X.; Ding, H. An efficient heterogeneous catalyst of $FeCo_2O_4/g$-C_3N_4 composite for catalytic peroxymonosulfate oxidation of organic pollutants under visible light. *Colloids Surf. A* **2021**, *610*, 125725. [CrossRef]

218. Shan, Z.; Ma, F.; You, S.; Shan, L.; Kong, D.; Guo, H.; Cui, C. Enhanced visible light photo-Fenton catalysis by lanthanum-doping $BiFeO_3$ for norfloxacin degradation. *Environ. Res.* **2023**, *216*, 114588. [CrossRef]

219. Chen, X.; Qiao, J.; Wang, Z.; Sun, W.; Sun, K. Layered perovskites with exsolved Co-Fe nanoalloy as highly active and stable anodes for direct carbon solid oxide fuel cells. *J. Alloys Compd.* **2023**, *940*, 168872. [CrossRef]

220. Torregrosa-Rivero, V.; Sánchez-Adsuar, M.-S.; Illán-Gómez, M.J. Exploring the effect of using carbon black in the sol-gel synthesis of $BaMnO_3$ and $BaMn_{0.7}Cu_{0.3}O_3$ perovskite catalysts for CO oxidation. *Catal. Today* 2023, *in press*. [CrossRef]

221. Nguyen, A.T.; Phung, V.D.; Mittova, V.O.; Ngo, H.D.; Vo, T.N.; Le Thi, M.L.; Nguyen, V.H.; Mittova, I.Y.; Le, M.L.P.; Ahn, Y.N.; et al. Fabricating nanostructured $HoFeO_3$ perovskite for lithium-ion battery anodes via co-precipitation. *Scr. Mater.* **2022**, *207*, 114259. [CrossRef]

222. Alrozi, R.; Zubir, N.A.; Bakar, N.F.A.; Ladewig, B.P.; Motuzas, J.; Bakar, N.H.H.A.; Wang, D.K.; da Costa, J.C.D. Functional role of B-site substitution on the reactivity of $CaMFeO_3$ (M = Cu, Mo, Co) perovskite catalysts in heterogeneous Fenton-like degradation of organic pollutant. *J. Taiwan Inst. Chem. Eng.* **2023**, *143*, 104675. [CrossRef]

223. Li, J.; Ma, W.; Zhong, D.; Li, K.; Ma, J.; Zhang, S.; Du, X. Oxygen vacancy concentration modulation of perovskite-based heterogeneous catalysts for Fenton-like oxidation of tetracycline. *J. Clean. Prod.* **2022**, *362*, 132469. [CrossRef]

224. Xie, L.; Liu, X.; Chang, J.; Zhang, C.; Li, Y.; Zhang, H.; Zhan, S.; Hu, W. Enhanced redox activity and oxygen vacancies of perovskite triggered by copper incorporation for the improvement of electro-Fenton activity. *Chem. Eng. J.* **2022**, *428*, 131352. [CrossRef]

225. Rusevova, K.; Köferstein, R.; Rosell, M.; Richnow, H.H.; Kopinke, F.D.; Georgi, A. $LaFeO_3$ and $BiFeO_3$ perovskites as nanocatalysts for contaminant degradation in heterogeneous Fenton-like reactions. *Chem. Eng. J.* **2014**, *239*, 322–331. [CrossRef]

226. Zhao, H.; Cao, J.; Lv, H.; Wang, Y.; Zhao, G. 3D nano-scale perovskite-based composite as Fenton-like system for efficient oxidative degradation of ketoprofen. *Catal. Commun.* **2013**, *41*, 87–90. [CrossRef]

227. Ho, J.H.; Li, Y.; Dai, Y.; Kim, T.; Wang, J.; Ren, J.; Yun, H.S.; Liu, X. Ionothermal synthesis of N-doped carbon supported $CoMn_2O_4$ nanoparticles as ORR catalyst in direct glucose alkaline fuel cell. *Int. J. Hydrogen Energy* **2021**, *46*, 20503–20515. [CrossRef]

228. Estrada-Arriaga, E.B.; Guadarrama-Pérez, O.; Silva-Martínez, S.; Cuevas-Arteaga, C.; Guadarrama-Pérez, V.H. Oxygen reduction reaction (ORR) electrocatalysts in constructed wetland-microbial fuel cells: Effect of different carbon-based catalyst biocathode during bioelectricity production. *Electrochim. Acta* **2021**, *370*, 137745. [CrossRef]

229. Gao, X.; He, L.; Yu, H.; Xie, F.; Yang, Y.; Shao, Z. The non-precious metal ORR catalysts for the anion exchange membrane fuel cells application: A numerical simulation and experimental study. *Int. J. Hydrogen Energy* **2020**, *45*, 23353–23367. [CrossRef]

230. Liu, H.; Yang, D.H.; Wang, X.Y.; Zhang, J.; Han, B.H. N-doped graphitic carbon shell-encapsulated FeCo alloy derived from metal–polyphenol network and melamine sponge for oxygen reduction, oxygen evolution, and hydrogen evolution reactions in alkaline media. *J. Colloid Interface Sci.* **2021**, *581*, 362–373. [CrossRef] [PubMed]

231. Zhou, W.; Meng, X.; Gao, J.; Alshawabkeh, A.N. Hydrogen peroxide generation from O_2 electroreduction for environmental remediation: A state-of-the-art review. *Chemosphere* **2019**, *225*, 588–607. [CrossRef]

232. Melchionna, M.; Fornasiero, P.; Prato, M. The Rise of Hydrogen Peroxide as the Main Product by Metal-Free Catalysis in Oxygen Reductions. *Adv. Mater.* **2019**, *31*, 1802920. [CrossRef]

233. Yu, F.; Wang, Y.; Ma, H. Enhancing the yield of H_2O_2 from oxygen reduction reaction performance by hierarchically porous carbon modified active carbon fiber as an effective cathode used in electro-Fenton. *J. Electroanal. Chem.* **2019**, *838*, 57–65. [CrossRef]

234. Zhao, Q.; An, J.; Wang, X.; Li, N. In-situ hydrogen peroxide synthesis with environmental applications in bioelectrochemical systems: A state-of-the-art review. *Int. J. Hydrogen Energy* **2020**, *46*, 3204–3219. [CrossRef]

235. Candia-Onfray, C.; Bollo, S.; Yáñez, C.; Escalona, N.; Marco, J.F.; Menéndez, N.; Salazar, R.; Recio, F.J. Nanostructured Fe-N-C pyrolyzed catalyst for the H_2O_2 electrochemical sensing. *Electrochim. Acta* **2021**, *387*, 138468. [CrossRef]

236. Liu, Y.; Quan, X.; Fan, X.; Wang, H.; Chen, S. High-yield electrosynthesis of hydrogen peroxide from oxygen reduction by hierarchically porous carbon. *Angew. Chem. Int. Ed.* **2015**, *54*, 6837–6841. [CrossRef] [PubMed]

237. Qiu, Z.; Ge, X.; Huang, N.; Zhou, S.; Zhang, J.; Xuan, J. Polyethylene oxide-polypropylene oxide -polyethylene oxide derived porous carbon materials with different molecular weights as ORR catalyst in alkaline electrolytes. *Int. J. Hydrogen Energy* **2021**, *46*, 2952–2959. [CrossRef]

238. Inozemtseva, A.I.; Kataev, E.Y.; Frolov, A.S.; Amati, M.; Gregoratti, L.; Beranová, K.; Dieste, V.P.; Escudero, C.; Fedorov, A.; Tarasov, A.V.; et al. On the catalytic and degradative role of oxygen-containing groups on carbon electrode in non-aqueous ORR. *Carbon N. Y.* **2021**, *176*, 632–641. [CrossRef]

239. Wang, X.; Sun, G.; Routh, P.; Kim, D.H.; Huang, W.; Chen, P. Heteroatom-doped graphene materials: Syntheses, properties and applications. *Chem. Soc. Rev.* **2014**, *43*, 7067–7098. [CrossRef]

240. Eisenberg, D.; Stroek, W.; Geels, N.J.; Tanase, S.; Ferbinteanu, M.; Teat, S.J.; Mettraux, P.; Yan, N.; Rothenberg, G. A rational synthesis of hierarchically porous, N-doped carbon from Mg-based MOFs: Understanding the link between nitrogen content and oxygen reduction electrocatalysis. *Phys. Chem. Chem. Phys.* **2016**, *18*, 20778–20783. [CrossRef]

241. Shibuya, R.; Kondo, T.; Nakamura, J. Active sites in nitrogen-doped carbon materials for oxygen reduction reaction. *Carbon-Based Met. Catal. Des. Appl.* **2018**, *1–2*, 227–249. [CrossRef]

242. Zhou, W.; Rajic, L.; Meng, X.; Nazari, R.; Zhao, Y.; Wang, Y.; Gao, J.; Qin, Y.; Alshawabkeh, A.N. Efficient H_2O_2 electrogeneration at graphite felt modified via electrode polarity reversal: Utilization for organic pollutants degradation. *Chem. Eng. J.* **2019**, *364*, 428–439. [CrossRef]

243. Zhu, J.; Xiao, X.; Zheng, K.; Li, F.; Ma, G.; Yao, H.; Wang, X.; Chen, Y. KOH-treated reduced graphene oxide: 100% selectivity for H_2O_2 electroproduction. *Carbon* **2019**, *153*, 6–11. [CrossRef]

244. Wu, K.H.; Wang, D.; Lu, X.; Zhang, X.; Xie, Z.; Liu, Y.; Su, B.J.; Chen, J.M.; Su, D.S.; Qi, W.; et al. Highly Selective Hydrogen Peroxide Electrosynthesis on Carbon: In Situ Interface Engineering with Surfactants. *Chem* **2020**, *6*, 1443–1458. [CrossRef]

245. Xu, H.; Guo, H.; Chai, C.; Li, N.; Lin, X.; Xu, W. Anodized graphite felt as an efficient cathode for in-situ hydrogen peroxide production and Electro-Fenton degradation of rhodamine B. *Chemosphere* **2022**, *286*, 131936. [CrossRef]

246. Zahoor, A.; Christy, M.; Hwang, Y.J.; Lim, Y.R.; Kim, P.; Nahm, K.S. Improved electrocatalytic activity of carbon materials by nitrogen doping. *Appl. Catal. B Environ.* **2014**, *147*, 633–641. [CrossRef]

247. Okamoto, Y. First-principles molecular dynamics simulation of O_2 reduction on nitrogen-doped carbon. *Appl. Surf. Sci.* **2009**, *256*, 335–341. [CrossRef]

248. Legarreta-Mendoza, A.; Flores-Holguín, N.; Lardizabal-Gutiérrez, D. A proposal based on quantum phenomena for the ORR mechanism on nitrogen-doped carbon-based electrocatalysts. *Int. J. Hydrogen Energy* **2019**, *44*, 12374–12380. [CrossRef]

249. Zhu, Y.; Qiu, S.; Deng, F.; Ma, F.; Zheng, Y. Degradation of sulfathiazole by electro-Fenton using a nitrogen-doped cathode and a BDD anode: Insight into the H_2O_2 generation and radical oxidation. *Sci. Total Environ.* **2020**, *722*, 137853. [CrossRef] [PubMed]

250. Wang, Y.; Yi, M.; Wang, K.; Song, S. Enhanced electrocatalytic activity for H_2O_2 production by the oxygen reduction reaction: Rational control of the structure and composition of multi-walled carbon nanotubes. *Chin. J. Catal.* **2019**, *40*, 523–533. [CrossRef]

251. Yu, Y.; You, S.; Du, J.; Zhang, P.; Dai, Y.; Liu, M.; Jiang, B.; Ren, N.; Zou, J. Ti^{3+}-self-doped TiO_2 with multiple crystal-phases anchored on acid-pickled ZIF-67-derived Co_3O_4@N-doped graphitized-carbon as a durable catalyst for oxygen reduction in alkaline and acid media. *Chem. Eng. J.* **2021**, *403*, 126441. [CrossRef]

252. Li, Z.; Wang, W.; Zhou, M.; He, B.; Ren, W.; Chen, L.; Xu, W.; Hou, Z.; Chen, Y. In-situ self-templated preparation of porous core–shell Fe_{1-x}S@N, S co-doped carbon architecture for highly efficient oxygen reduction reaction. *J. Energy Chem.* **2021**, *54*, 310–317. [CrossRef]

253. Zhu, Y.; Deng, F.; Qiu, S.; Ma, F.; Zheng, Y.; Lian, R. Enhanced electro-Fenton degradation of sulfonamides using the N, S co-doped cathode: Mechanism for H_2O_2 formation and pollutants decay. *J. Hazard. Mater.* **2021**, *403*, 123950. [CrossRef]

254. Soo, L.T.; Loh, K.S.; Mohamad, A.B.; Daud, W.R.W.; Wong, W.Y. An overview of the electrochemical performance of modified graphene used as an electrocatalyst and as a catalyst support in fuel cells. *Appl. Catal. A Gen.* **2015**, *497*, 198–210. [CrossRef]

255. Zhang, L.; Xia, Z. Mechanisms of oxygen reduction reaction on nitrogen-doped graphene for fuel cells. *J. Phys. Chem. C* **2011**, *115*, 11170–11176. [CrossRef]

256. Su, P.; Zhou, M.; Lu, X.; Yang, W.; Ren, G.; Cai, J. Electrochemical catalytic mechanism of N-doped graphene for enhanced H_2O_2 yield and in-situ degradation of organic pollutant. *Appl. Catal. B Environ.* **2019**, *245*, 583–595. [CrossRef]

257. Su, P.; Zhou, M.; Song, G.; Du, X.; Lu, X. Efficient H_2O_2 generation and spontaneous [rad]OH conversion for in-situ phenol degradation on nitrogen-doped graphene: Pyrolysis temperature regulation and catalyst regeneration mechanism. *J. Hazard. Mater.* **2020**, *397*, 122681. [CrossRef] [PubMed]

258. Qin, M.; Fan, S.; Wang, L.; Gan, G.; Wang, X.; Cheng, J.; Hao, Z.; Li, X. Oxygen and nitrogen co-doped ordered mesoporous carbon materials enhanced the electrochemical selectivity of O_2 reduction to H_2O_2. *J. Colloid Interface Sci.* **2020**, *562*, 540–549. [CrossRef] [PubMed]

259. Xie, Y.; Li, Y.; Huang, Z.; Zhang, J.; Jia, X.; Wang, X.S.; Ye, J. Two types of cooperative nitrogen vacancies in polymeric carbon nitride for efficient solar-driven H_2O_2 evolution. *Appl. Catal. B Environ.* **2020**, *265*, 118581. [CrossRef]

260. Zhou, W.; Xie, L.; Gao, J.; Nazari, R.; Zhao, H.; Meng, X.; Sun, F.; Zhao, G.; Ma, J. Selective H_2O_2 electrosynthesis by O-doped and transition-metal-O-doped carbon cathodes via O_2 electroreduction: A critical review. *Chem. Eng. J.* **2021**, *410*, 128368. [CrossRef]

261. Iglesias, D.; Giuliani, A.; Melchionna, M.; Marchesan, S.; Criado, A.; Nasi, L.; Bevilacqua, M.; Tavagnacco, C.; Vizza, F.; Prato, M.; et al. N-Doped Graphitized Carbon Nanohorns as a Forefront Electrocatalyst in Highly Selective O_2 Reduction to H_2O_2. *Chem* **2018**, *4*, 106–123. [CrossRef]

262. Chen, J.Y.; Li, N.; Zhao, L. Three-dimensional electrode microbial fuel cell for hydrogen peroxide synthesis coupled to wastewater treatment. *J. Power Sources* **2014**, *254*, 316–322. [CrossRef]

263. He, W.; Jiang, C.; Wang, J.; Lu, L. High-Rate Oxygen Electroreduction over Graphitic-N Species Exposed on 3D Hierarchically Porous Nitrogen-Doped Carbons. *Angew. Chem.* **2014**, *53*, 9503–9507. [CrossRef]

264. Zhang, T.; Wu, J.; Wang, Z.; Wei, Z.; Liu, J.; Gong, X. Transfer of molecular oxygen and electrons improved by the regulation of C-N/C=O for highly efficient 2e-ORR. *Chem. Eng. J.* **2022**, *433*, 133591. [CrossRef]

265. Chen, D.; Zhu, J.; Mu, X.; Cheng, R.; Li, W.; Liu, S.; Pu, Z.; Lin, C.; Mu, S. Nitrogen-Doped carbon coupled $FeNi_3$ intermetallic compound as advanced bifunctional electrocatalyst for OER, ORR and zn-air batteries. *Appl. Catal. B Environ.* **2020**, *268*, 118729. [CrossRef]

266. Gao, Y.; Zhu, W.; Wang, C.; Zhao, X.; Shu, M.; Zhang, J.; Bai, H. Enhancement of oxygen reduction on a newly fabricated cathode and its application in the electro-Fenton process. *Electrochim. Acta* **2020**, *330*, 135206. [CrossRef]

267. Teng, Z.; Cai, W.; Sim, W.; Zhang, Q.; Wang, C.; Su, C.; Ohno, T. Applied Catalysis B: Environmental Photoexcited single metal atom catalysts for heterogeneous photocatalytic H_2O_2 production: Pragmatic guidelines for predicting charge separation. *Appl. Catal. B Environ.* **2021**, *282*, 119589. [CrossRef]

268. Yeager, E. Dioxygen electrocatalysis: Mechanisms in relation to catalyst structure. *J. Mol. Catal.* **1986**, *38*, 5–25. [CrossRef]

269. Chan, A.W.; Hoffmann, R.; Ho, W. Theoretical aspects of photoinitiated chemisorption, dissociation, and desorption of O_2 on Pt(111). *Langmuir* **1992**, *8*, 1111–1119. [CrossRef]

270. Viswanathan, V.; Hansen, H.A.; Rossmeisl, J.; Norskov, J. Unifying the 2e$^-$ and 4e$^-$ reduction of oxygen on metal surfaces. *J. Phys. Chem. Lett.* **2012**, *3*, 2948–2951. [CrossRef] [PubMed]

271. Kim, J.H.; Kim, Y.T.; Joo, S.H. Electrocatalyst design for promoting two-electron oxygen reduction reaction: Isolation of active site atoms. *Curr. Opin. Electrochem.* **2020**, *21*, 109–116. [CrossRef]

272. Choi, C.H.; Kwon, H.C.; Yook, S.; Shin, H.; Kim, H.; Choi, M. Hydrogen peroxide synthesis via enhanced two-electron oxygen reduction pathway on carbon-coated pt surface. *J. Phys. Chem. C* **2014**, *118*, 30063–30070. [CrossRef]

273. Perry, S.C.; Mavrikis, S.; Wang, L.; León, C.P. De Future perspectives for the advancement of electrochemical hydrogen peroxide production. *Curr. Opin. Electrochem.* **2021**, *30*, 100792. [CrossRef]

274. Huang, Y.; Liu, W.; Kan, S.; Liu, P.; Hao, R.; Hu, H.; Zhang, J.; Liu, H.; Liu, M.; Liu, K. Tuning morphology and structure of Fe–N–C catalyst for ultra-high oxygen reduction reaction activity. *Int. J. Hydrogen Energy* **2020**, *45*, 6380–6390. [CrossRef]

275. Daniel, G.; Kosmala, T.; Dalconi, M.C.; Nodari, L.; Badocco, D.; Pastore, P.; Lorenzetti, A.; Granozzi, G.; Durante, C. Upcycling of polyurethane into iron-nitrogen-carbon electrocatalysts active for oxygen reduction reaction. *Electrochim. Acta* **2020**, *362*, 137200. [CrossRef]

276. Zhang, J.; Song, L.H.; Zhao, C.F.; Yin, X.P.; Zhao, Y.F. Co, N co-doped porous carbons as high-performance oxygen reduction electrocatalysts. *Xinxing Tan Cailiao/N. Carbon Mater.* **2021**, *36*, 209–218. [CrossRef]

277. Chen, E.; Bevilacqua, M.; Tavagnacco, C.; Montini, T.; Yang, C.M.; Fornasiero, P. High surface area N/O co-doped carbon materials: Selective electrocatalysts for O_2 reduction to H_2O_2. *Catal. Today* **2020**, *356*, 132–140. [CrossRef]

278. Chen, J.; Wang, Z.; Mao, J.; Liu, C.; Chen, Y.; Lu, Z.; Feng, S.P. Bimetallic Ag–Cu nanosheets assembled flower-like structure for oxygen reduction reaction. *J. Alloys Compd.* **2021**, *856*, 157379. [CrossRef]

279. Zhang, A.; Liu, Y.; Wu, J.; Zhu, J.; Cheng, S.; Wang, Y.; Hao, Y.; Zeng, S. Electrocatalytic selectivity to H_2O_2 enabled by two-electron pathway on Cu-deficient $Au@Cu_2$-xS-CNTs electrocatalysts. *Chem. Eng. J.* **2023**, *454*, 140317. [CrossRef]

280. Wang, B.; Jin, C.; Shao, S.; Yue, Y.; Zhang, Y.; Wang, S.; Chang, R.; Zhang, H.; Zhao, J.; Li, X. Electron-deficient Cu site catalyzed acetylene hydrochlorination. *Green Energy Environ.* 2022, 1–13, *in press.* [CrossRef]

281. Noh, S.H.; Seo, M.H.; Ye, X.; Makinose, Y.; Okajima, T.; Matsushita, N.; Han, B.; Ohsaka, T. Design of an active and durable catalyst for oxygen reduction reactions using encapsulated Cu with N-doped carbon shells (Cu@N-C) activated by CO_2 treatment. *J. Mater. Chem. A* **2015**, *3*, 22031–22034. [CrossRef]

282. Lenarda, A.; Bevilacqua, M.; Tavagnacco, C.; Nasi, L.; Criado, A.; Vizza, F.; Melchionna, M.; Prato, M.; Fornasiero, P. Selective Electrocatalytic H_2O_2 Generation by Cobalt@N-Doped Graphitic Carbon Core–Shell Nanohybrids. *ChemSusChem* **2019**, *12*, 1664–1672. [CrossRef]

283. Gao, J.; Yang, H.; Gao, J.; Yang, H.; Huang, X.; Hung, S.; Cai, W.; Jia, C. Enabling Direct H_2O_2 Production in Acidic Media through Rational Design of Transition Metal Single Atom Catalyst Enabling Direct H_2O_2 Production in Acidic Media through Rational Design of Transition Metal Single Atom Catalyst. *Chem* **2019**, *6*, 658–674. [CrossRef]

284. Cao, K.W.; Huang, H.; Li, F.M.; Yao, H.C.; Bai, J.; Chen, P.; Jin, P.J.; Deng, Z.W.; Zeng, J.H.; Chen, Y. Co nanoparticles supported on three-dimensionally N-doped holey graphene aerogels for electrocatalytic oxygen reduction. *J. Colloid Interface Sci.* **2020**, *559*, 143–151. [CrossRef]

285. Coliman, J.P.; Denisevich, P.; Konai, Y.; Marrocco, M.; Koval, C.; Anson, F.C. Electrode Catalysis of the Four-Electron Reduction of Oxygen to Water by Dicobalt Face-to-Face Porphyrins. *J. Am. Chem. Soc.* **1980**, *102*, 6027–6036. [CrossRef]

286. Ferrara, M.; Bevilacqua, M.; Melchionna, M.; Criado, A.; Crosera, M.; Tavagnacco, C.; Vizza, F.; Fornasiero, P. Exploration of cobalt@N-doped carbon nanocomposites toward hydrogen peroxide (H_2O_2) electrosynthesis: A two level investigation through the RRDE analysis and a polymer-based electrolyzer implementation. *Electrochim. Acta* **2020**, *364*, 137287. [CrossRef]

287. Cheng, X.; Dou, S.; Qin, G.; Wang, B.; Yan, P.; Taylor, T.; Yang, X. Rational design of highly selective nitrogen-doped Fe_2O_3-CNTs catalyst towards H_2O_2 generation in alkaline media. *Int. J. Hydrogen Energy* **2020**, *45*, 6128–6137. [CrossRef]

288. Yue, D.; Qian, X.; Kan, M.; Fang, M.; Jia, J.; Yang, X.; Zhao, Y. A metal-free visible light active photo-electro-Fenton-like cell for organic pollutants degradation. *Appl. Catal. B Environ.* **2018**, *229*, 211–217. [CrossRef]

289. Hartmann, M.; Kullmann, S.; Keller, H. Wastewater treatment with heterogeneous Fenton-type catalysts based on porous materials. *J. Mater. Chem.* **2010**, *20*, 9002–9017. [CrossRef]

290. Li, Y.; Cao, W.X.; Zuo, X.J. O- and F-doped porous carbon bifunctional catalyst derived from polyvinylidene fluoride for sulfamerazine removal in the metal-free electro-Fenton process. *Environ. Res.* **2022**, *212*, 113508. [CrossRef]

291. Yang, W.; Zhou, M.; Oturan, N.; Li, Y.; Su, P.; Oturan, M.A. Enhanced activation of hydrogen peroxide using nitrogen doped graphene for effective removal of herbicide 2,4-D from water by iron-free electrochemical advanced oxidation. *Electrochim. Acta* **2019**, *297*, 582–592. [CrossRef]

292. Haider, M.R.; Jiang, W.L.; Han, J.L.; Sharif, H.M.A.; Ding, Y.C.; Cheng, H.Y.; Wang, A.J. In-situ electrode fabrication from polyaniline derived N-doped carbon nanofibers for metal-free electro-Fenton degradation of organic contaminants. *Appl. Catal. B Environ.* **2019**, *256*, 117774. [CrossRef]

293. Qin, X.; Zhao, K.; Quan, X.; Cao, P.; Chen, S.; Yu, H. Highly efficient metal-free electro-Fenton degradation of organic contaminants on a bifunctional catalyst. *J. Hazard. Mater.* **2021**, *416*, 125859. [CrossRef]

294. Chen, X.; Wang, L.; Sun, W.; Yang, Z.; Jin, J.; You, D.; Liu, G. Enhanced electrochemical advanced oxidation on boride activated carbon: The influences of boron groups. *Electrochim. Acta* **2021**, *400*, 139462. [CrossRef]

295. Xie, F.; Gao, Y.; Zhang, J.; Bai, H.; Zhang, J.; Li, Z.; Zhu, W. A novel bifunctional cathode for the generation and activation of H_2O_2 in electro-Fenton: Characteristics and mechanism. *Electrochim. Acta* **2022**, *430*, 141099. [CrossRef]

296. Zhang, Y.; Gao, M.; Wang, S.G.; Zhou, W.; Sang, Y.; Wang, X.H. Integrated electro-Fenton process enabled by a rotating Fe_3O_4/gas diffusion cathode for simultaneous generation and activation of H_2O_2. *Electrochim. Acta* **2017**, *231*, 694–704. [CrossRef]

297. Cui, L.; Huang, H.; Ding, P.; Zhu, S.; Jing, W.; Gu, X. Cogeneration of H_2O_2 and [rad]OH via a novel Fe_3O_4/MWCNTs composite cathode in a dual-compartment electro-Fenton membrane reactor. *Sep. Purif. Technol.* **2020**, *237*, 116380. [CrossRef]

298. Hu, J.; Wang, S.; Yu, J.; Nie, W.; Sun, J.; Wang, S. Duet Fe_3C and FeNxSites for H_2O_2Generation and Activation toward Enhanced Electro-Fenton Performance in Wastewater Treatment. *Environ. Sci. Technol.* **2021**, *55*, 1260–1269. [CrossRef]

299. Cao, P.; Quan, X.; Zhao, K.; Chen, S.; Yu, H.; Niu, J. Selective electrochemical H_2O_2 generation and activation on a bifunctional catalyst for heterogeneous electro-Fenton catalysis. *J. Hazard. Mater.* **2020**, *382*, 121102. [CrossRef]

300. Ghasemi, M.; Khataee, A.; Gholami, P.; Soltani, R.D.C.; Hassani, A.; Orooji, Y. In-situ electro-generation and activation of hydrogen peroxide using a CuFeNLDH-CNTs modified graphite cathode for degradation of cefazolin. *J. Environ. Manag.* **2020**, *267*, 110629. [CrossRef]

301. Cui, L.; Li, Z.; Li, Q.; Chen, M.; Jing, W.; Gu, X. $Cu/CuFe_2O_4$ integrated graphite felt as a stable bifunctional cathode for high-performance heterogeneous electro-Fenton oxidation. *Chem. Eng. J.* **2020**, 127666. [CrossRef]

302. Luo, T.; Feng, H.; Tang, L.; Lu, Y.; Tang, W.; Chen, S.; Yu, J.; Xie, Q.; Ouyang, X.; Chen, Z. Efficient degradation of tetracycline by heterogeneous electro-Fenton process using Cu-doped $Fe@Fe_2O_3$: Mechanism and degradation pathway. *Chem. Eng. J.* **2020**, *382*, 122970. [CrossRef]

303. Sun, X.; Qi, H.; Sun, Z. Bifunctional nickel foam composite cathode co-modified with CoFe@NC and CNTs for electrocatalytic degradation of atrazine over wide pH range. *Chemosphere* **2022**, *286*, 131972. [CrossRef]

304. Yu, D.; He, J.; Wang, Z.; Pang, H.; Li, L.; Zheng, Y.; Chen, Y.; Zhang, J. Mineralization of norfloxacin in a CoFe–LDH/CF cathode-based heterogeneous electro-fenton system: Preparation parameter optimization of the cathode and conversion mechanisms of H_2O_2 to ·OH. *Chem. Eng. J.* **2021**, *417*, 129240. [CrossRef]

305. Li, Y.; Wang, C.; Pan, S.; Zhao, X.; Liu, N. Mn doping improves in-situ H_2O_2 generation and activation in electro-Fenton process by Fe/Mn@CC cathode using high-temperature shock technique. *Chemosphere* **2022**, *307*, 136074. [CrossRef] [PubMed]

306. Xiao, F.; Wang, Z.; Fan, J.; Majima, T.; Zhao, H.; Zhao, G. Selective Electrocatalytic Reduction of Oxygen to Hydroxyl Radicals via 3-Electron Pathway with FeCo Alloy Encapsulated Carbon Aerogel for Fast and Complete Removing Pollutants. *Angew. Chem. Int. Ed.* **2021**, *60*, 10375–10383. [CrossRef] [PubMed]